Full-Duplex MU-MIMO Systems Under the Effects of Non-ideal Transceivers: Performance Analysis and Power Allocation Optimization

by

EMAD SALEH

Department of Electrical and Computer Engineering

A thesis submitted in partial fulfillment of the requirements
for the degree of Doctor of Philosophy (Ph.D.)

The Faculty of Graduate Studies

Lakehead University

Thunder Bay, Ontario, Canada

May 2023

Examining Committee Membership

The following served on the Examining Committee for this thesis. The decision of the Examining Committee is by majority vote.

External Examiner: Musbah Shaat

Centre Tecnològic de Telecomunicacions de Catalunya (CTTC), Spain

Internal Members: Waleed Ejaz

Assistant Professor, Dept. of Electrical Engineering,

Lakehead University, Canada

Apparao Dekka

Assistant Professor, Dept. of Electrical Engineering,

Lakehead University, Canada

Supervisors: Salama Ikki

Professor, Dept. of Electrical Engineering,

Lakehead University, Canada

Malek Alsmadi

Professor, School of Engineering Technology,

Confederation College, Canada

Declaration

I hereby declare that I am the sole author of this thesis. This is a true copy of the thesis, including any required final revisions, as accepted by my examiners.

I understand that my thesis may be made electronically available to the public.

Dedication

I would like to dedicate this work to my beloved mother

To the spirit of my dear father

To the spirit of my beloved sister Suhad

To the spirit of my dear cousin Rami

To my spouse

To my brothers

To my sisters

To my daughter Tala

To my sons Mohammed, Ibrahim and Monir

Acknowledgements

First and foremost, glory is to Allah, we cannot count your praise, you are as you praised yourself. I am grateful to Almighty Allah (Subhanahu Wa Taala) for granting me the light, faith and strength to accomplish the Ph.D. degree.

I would like to express my sincere gratitude to my supervisors, Prof. Salama Ikki and Dr. Malek Alsmadi, for their guidance, advice, recommendations and support. Your encouragement, motivation, immense knowledge, and patience made this work possible and saw the light.

I am also grateful to Dr. Musbah Shaat, Dr. Waleed Ejaz and Dr. Apparao Dekka for serving on my thesis committee and providing valuable comments that have improved my thesis. Once again I would like to thank Dr. Waleed Ejaz and Dr. Apparao Dekka for serving on my seminar and comprehensive exam committees and providing constructive feedback that helped improve this thesis.

Last but not least, my family is my priority and the most important in my life, my sincere appreciation and respect to all of you, especially my parents. I would like to say that you are the main source of inspiration in my life. I want to express my most sincere appreciation to my mother for her heartfelt prayer, endless love, encouragement, daily support, and countless sacrifices for our family and me. Thank you for being proud of me. I would like to express my deepest gratitude to my spouse, this work could not have been accomplished without your eternal love, encouragement, support, patience and sacrifice. I am also thankful to my brothers, sisters, uncles and aunts for their love, prayer and continuous support that they have provided to me throughout my study. Without your love and encouragement, I would not have finished this thesis. Thanks also to my mother-in-law and my in-laws for their help and prayer. Finally, thanks to our lovely kids, Tala, Mohammed, Ibrahim and Monir for being so cute and filling our life with love and hope. My special thanks are extended to all my relatives and friends.

Abstract

Modern Technologies, particularly connectivity, increasingly support many facets of everyday life. The next generation of wireless communication systems aims to provide new advanced services and support new demands. These services are required to serve a massive number of devices and achieve higher spectral and energy efficiency, ultra-low latency, and reliable communication. The research community around the globe is still working on finding novel technologies to meet these requirements. Full duplex (FD) communications have been recognized as one of the promising wireless transmission candidates and game-changers for the future of wireless communication and networking technologies, thanks to their ability to greatly improve spectral efficiency (SE) and dramatically enhance energy efficiency (EE). In this thesis, first, the influence of hardware impairment (HWI) on single-input single-output (SISO) FD access point (AP) is studied. More precisely, the SE and EE when the system's terminals have impaired transceivers are analyzed. Optimization problem for EE maximization is formulated to fulfill quality of service (QoS) and power budget constraints. An algorithm to solve the optimization problem by using the fractional programming theory and Karush–Kuhn–Tucker (KKT) conditions technique is proposed. The results unveil that excellent power allocation is crucial in FD communication networks and the proposed algorithm outperforms the maximum power transmission scheme. The results also reveal that HWIs degrade both SE and EE performance. Moreover, at high power region, no further improvements can be obtained by increasing the transmission power. This study assumes that all fading channels demonstrate Nakagami-m distribution.

Second, the effect of HWI on multiple-input multiple-output (MIMO) FD systems is studied. Closed-form expressions for the lower bounds of the average uplink (UL) and downlink (DL) achievable rates are derived. Different power allocation optimization problems to maximize the average FD SE and EE, while satisfying the QoS and power budget constraints are formulated. Moreover, the max-min objective functions are considered to assure fairness between users. These problems are solved using different optimization techniques, including the Dinkelbach approach, transformation, and the KKT conditions. Also, the SE algorithm is refined and a simpler solution is presented. This study also assumes

that all fading channels follow Nakagami-m distributions, where other scenarios can be considered special cases. Besides, a special case of Nakagami-m when $m = 1$ which results in Rayleigh fading channels is studied.

Third, the study is extended to involve more practical scenarios, where the imperfect channel state information (CSI) and multi-user scenarios are considered. Because the application of FD communication alongside space-division multiple access (SDMA) and MIMO techniques assures a more efficient utilization of the limited wireless frequency spectrum available and an improvement in SE. This study outlines a framework for FD communication systems considering practical conditions, such as imperfect CSI and HWI. The performance of FD multi-user multiple-input multiple-output (MU-MIMO) systems is analyzed, specifically studying the effects of practical channel estimation errors and HWI on the SE performance of the FD MU-MIMO systems. The linear detectors/precoders of maximum ratio combining (MRC)/maximum ratio transmission (MRT) and zero-forcing reception (ZFR)/zero-forcing transmission (ZFT) are considered at the base station (BS) for receiving and transmitting. Moreover, linear minimum mean square error (LMMSE) and least square (LS) error estimation are used to estimate the UL/DL channels at the BS. Mathematical derivations for the lower bound of UL and DL SEs are presented in the context of imperfect CSI and HWI. Finally, extensive computer simulations were conducted to validate the analytical derivations.

Table of Contents

6 Conclusions and Future Work   106

APPENDICES   109

A Proofs of Lemmas in Chapter 4   126

B Proofs of Lemmas in Chapter 5   130

List of Tables

List of Figures

Abbreviations

3G third-generation 1

4G fourth-generation 1

5G fifth-generation 1–3

64-QAM 64-quadrature amplitude modulation 16

6G sixth-generation 2

ADC analog-to-digital converter 13, 14, 21, 22, 24, 25, 43

AF amplify-and-forward 23

AP access point 4, 22, 27–32, 108

AWGN additive white Gaussian noise 14, 15, 48, 50

BS base station 2–4, 11, 18–23, 25, 43, 44, 46–49, 51–54, 57, 59, 66, 69–76, 80–85, 88, 89, 101, 102, 106–108

CSI channel state information 4, 5, 7, 20–22, 24, 90, 91, 93, 94, 96–99, 101–104, 106–108, 133, 136

DAC digital-to-analog converter 13, 21, 22, 24, 25, 43

dB decibel 2, 20

DF decode-and-forward 23

PHY physical layer 2

PN phase noise 24

Q quadrature-phase 13

QN quantization noise 22

QoS quality of service 3, 5–7, 27, 28, 32, 44, 53, 56, 70, 72, 74, 75, 79, 106, 107, 129

QPSK quadrature phase-shift keying 16

RF radio frequency 10, 12, 14, 20, 24, 80

RIS reconfigurable intelligent surfaces 20, 27, 108

RIS-SSK reconfigurable intelligent surface space-shift keying 24

SDMA space-division multiple access 2, 80

SE spectral efficiency 2–7, 10, 20–24, 26–32, 35–37, 39, 40, 43, 44, 47, 49–51, 53, 56, 57, 59, 63, 66–69, 72, 77–81, 88, 91–93, 102, 103, 106–108, 132, 134, 135

SI self-interference 2, 3, 11, 20–22, 25, 27–29, 31, 32, 39, 41, 43, 46, 53, 59, 68, 75, 77–79, 81

SINR signal-to-interference-plus-noise ratio 50, 52, 53, 90–94, 132–134

SISO single-input single-output 3–6, 29, 106

SNR signal-to-noise ratio 15, 23, 43, 80, 103

TDD time-division duplex 2, 19

THz terahertz 2

UAV unmanned aerial vehicle 108

UDN ultra-dense network 2

List of Symbols

x	scalar x
$\mathbf{x}$	vector $\mathbf{x}$
$\mathbf{X}$	matrix $\mathbf{X}$
$\mathbf{I}$	identity matrix
$\mathbf{0}$	all-zero vector
$(\cdot)^{-1}$	matrix inverse
$(\cdot)^{\mathrm{T}}$	matrix transpose
$(\cdot)^{*}$	complex conjugate
$(\cdot)^{\mathrm{H}}$	hermitian transposition
$\lvert \cdot \rvert$	magnitude of the complex number
$\lVert \cdot \rVert$	the Euclidean norm of the vector
$\mathbb{E}\{\cdot\}$	the statistical expectation
$\hat{x}$	the estimated value of x
$\mathrm{diag}(\mathbf{x})$	diagonal matrix whose diagonal elements are in vector $\mathbf{x}$
$\mathcal{CN}(\mu, \sigma^2)$	complex Gaussian random variable with μ mean and σ^2 variance
$\mathcal{CN}(\boldsymbol{\mu}, \boldsymbol{\Gamma})$	complex Gaussian random variable where $\boldsymbol{\mu}$ is the mean vector and $\boldsymbol{\Gamma}$ is the covariance matrix

Chapter 1

Introduction

1.1 Background and Motivation

THERE has been a significant growth of wireless services that require higher data rates, lower latency, and more reliable communications. Cisco Systems, Inc., predicted a significant increase in mobile (third-generation (3G), fourth-generation (4G), fifth-generation (5G)) networking demand in the near future. Wherein March 2020 report, quantitative projections are provided on the growth of Internet users, devices and connections as well as network performance and new application requirements. For example, it was reported that wireless fidelity (Wi-Fi) speeds from mobile devices will triple, mobile (cellular) speeds will more than triple and over 70 percent of the global population will have mobile connectivity in 2023 [2]. The most recent Ericsson mobility report that has been published in November 2022, the outlook for 2028 is that 5G subscriptions will pass 5 billion, and wireless connections will reach 300 million. Moreover, it is projected that all mobile subscriptions will be increased to around 9.2 from 8.4 billion by the end of 2028 [3]. Such growth will obviously accompany ubiquitous demands of ever-increasing data rates with low latency and high spectral and energy efficiency, which present themselves as the major challenges for the upcoming generations of wireless communications.

There are considerable challenges because the amount of available spectrum is limited. In order to meet these requirements, immense research has been carried out to develop new

wireless technologies. As such, many techniques have been recently proposed, including massive multiple-input multiple-output (MIMO) [4,5], millimeter wave (mmWave) communications [6], ultra-dense network (UDN), index modulation (IM), non-orthogonal multiple access (NOMA) and terahertz (THz) communications, alternative/advanced waveforms, and new antenna technologies [7, 8]. Moreover, combining both space-division multiple access (SDMA) and MIMO techniques is a substantial method to efficiently utilize the limited available wireless spectrum and enhance the spectral efficiency (SE), where it is proven that the sum SE increases proportionally to the number of users in SDMA transmission. This is achieved by serving K users simultaneously and increasing the number of base station (BS) antennas to obtain an array gain that counteracts the increased interference [1]. However, network energy consumption and hardware cost remain critical issues in practical systems [9], and being able to find spectrum and energy efficient techniques with low hardware costs remains a relevant issue [10]. Indeed, the initial 5G standard has provided increasing flexibility in the physical layer (PHY). Nonetheless, researchers keep working on alternative technologies for later releases of 5G. New applications/use-cases and networking trends of sixth-generation (6G) and beyond systems may bring more intractable problems, consequently creating the need for such novel communication paradigms [11].

On the parallel orientation, the concept of full duplex (FD) with optimal power allocation has emerged as an out-of-the-box novel technology that aims to enhance both SE and energy efficiency (EE) of wireless communication systems in a cost-effective manner [12–19]. As such, using FD technique is a vital key to improve the SE for the next communication systems where the SE can be theoretically doubled, since the signals can be transmitted and received at the same time-frequency resource. On the other hand, the half-duplex (HD) communication uses different frequency bands to transmit and receive the signals in frequency-division duplex (FDD) technique or different time slots in time-division duplex (TDD) technique [20, 21]. However, the main challenge in FD technology is the self-interference (SI) that comes from the downlink (DL) transmitted signals which cause substantial interference to the uplink (UL) received signals at the BS where it may be observed that the SI signal strength is stronger than the desired received signal about 100 decibel (dB) [20], on the consequence, it can be concluded that the game-player in im-

plementing the FD communication is the SI suppression and cancellation. An exhaustive overview of the potential FD techniques including their main applications in wireless communications, advantages over contemporary technologies, challenges, solutions, and future research directions was provided in [20, 21].

Modern digital communication systems require considerable digital signal processing (DSP) and advanced analog circuitry. However, the signal is subject to many sources of impairments at the transceivers because the hardware impairment (HWI)s are inherited in the electronic devices. Practically, the physical transceivers suffer from inevitable HWIs such as analog imperfectness, phase noise, in-phase/quadrature-phase (I/Q) imbalance, power amplifier non-linearities, time and frequency synchronization errors, etc. Hence, HWIs may dramatically degrade the communication system's performance [22–24]. Even though these impairments are commonly encountered in current communication systems, they might become readily more severe in the case of FD systems. One reason makes the effects of HWIs critical issue for the next-generation communication systems is that the requirements of 5G networks to support massive number of wireless devices in the Internet of things (IoT). IoT will interconnect billions of devices under machine-to-machine (M2M) communication links. For example, smart homes will be equipped with Wi-Fi-connected lighting, air-conditioning, heating and security devices. Also, wearable technology such as virtual glasses, smartwatches, and fitness bands to monitor heartbeats and temperature, etc. and GPS tracking tools. This can be achieved by manufacturing low-cost transceivers which are expected to come with poor quality [25, 26]. Hence, this massive connectivity with imperfect hardware will degrade the performance of the networks. Considering these challenging aspects in the research adds more complexity to the analysis and design.

The serious effects of HWIs and the shortcomings in the current literature engorged us to pursue the following objectives

- To study the performance of FD single-input single-output (SISO) and MIMO communication systems under the effects of HWIs at the BS and the UL/DL users.

- To maximize the FD SE and EE performance in SISO and MIMO communication systems subjects to fulfill minimum quality of service (QoS) and power budget con-

straints, and study the effects of HWIs on the SE and EE under optimal power allocation.

- To study the performance of FD multi-user multiple-input multiple-output (MU-MIMO) systems under HWIs considering perfect and imperfect channel state information (CSI) when using maximum ratio combining (MRC)/maximum ratio transmission (MRT) and zero-forcing reception (ZFR)/zero-forcing transmission (ZFT) linear detectors/precoders.

- To study the impact of the channel estimation error and HWIs on the system performance and to investigate the effects of the HWIs on the channel estimation accuracy in MU-MIMO communication systems when using the linear minimum mean square error (LMMSE) and least square (LS) estimations.

- To study different models of fading channels as Nakagami-m distribution which represents a more general model where some other channel models (such as Rayleigh, Weibull and Chi-squared distributions) can be considered as special cases. Moreover, Nakagami-m fits better than the other distributions for fading channels [27]. In addition, the Rayleigh fading channel model is studied.

- Finally, to conduct computer simulations under different scenarios to validate the obtained analytical results and the feasibility of the proposed algorithms.

1.2 Thesis Contributions

Compared to the existing literature and motivated by the importance of the thesis topic, the contributions of this work can be summarized as follows:

1. The performance of the FD SISO and MIMO systems in terms of SE and EE is studied by assuming imperfect hardware at all end terminals of the systems (i.e., at the access point (AP), BS, the UL user and DL user), perfect CSI and modeling all fading channels as Nakagami-m distribution. Moreover, closed-form expressions for the lower bounds of the average FD UL and DL achievable rates are derived by exploiting the

relationship between various distributions (e.g., Gamma, inverse of Gamma and Beta distribution). In addition, the average SE of UL/DL HD expressions are derived for comparative purposes.

2. Power allocation optimization problems to maximize the average SE, max-min SE, EE and max-min EE with QoS and power budget constraints are formulated for the FD SISO and MIMO systems. Algorithms to solve these problems using different optimization techniques are proposed. The Karush–Kuhn–Tucker (KKT) conditions technique solves the optimization problem that maximizes the SE. Moreover, two optimization techniques to solve the max-min SE optimization problem by introducing a slack variable and an appropriate transformation are combined. Furthermore, to maximize the EE and the max-min EE, the Dinkelbach approach to transform the fractional non-concave optimization problem into an equivalent parametric optimization is utilized. Interestingly, the FD SE algorithm is refined and a simpler solution is presented. Furthermore, the channels' statistical information rather than the instantaneous states of the channels are utilized, which increases the overall SE and EE without the cost of greater complexity.

3. The performance of the FD MU-MIMO systems under imperfect transceivers, assuming imperfect CSI when using MRC/MRT and ZFR/ZFT linear detectors/precoders, and modeling all fading channels as Rayleigh distribution is analyzed. Mathematical frameworks for the lower bounds of the average FD UL/DL SE under imperfect CSI in the presence of HWIs at all system terminals are derived. Moreover, comprehensive analyses have been conducted and many special cases are obtained.

4. The impact of the HWIs and channel estimation error when using LMMSE and LS estimations on the system performance is investigated. The effects of the number of training pilot symbols and the transmitted power on the mean squared error (MSE) is studied. The MRC/MRT and ZFR/ZFT linear detectors/precoders are used at the BS for receiving and transmitting. Using the zero-forcing (ZF) technique, the inter-user interference (IUI) can be eliminated and considerable improvements in the performance of the FD MU-MIMO compared to the MRC one can be achieved.

5. Tow estimators of LMMSE and LS for the impaired FD MU-MIMO systems are designed. It is shown that at high transmission power, there is an error floor in the channel estimation, which depends on the hardware quality. On the other hand, this estimation error tends to zero in the case of ideal hardware. Increasing the number of pilots can eliminate the estimation error for both ideal and impaired systems.

1.3   Thesis Organization

The rest of the thesis is organized as follows:

In Chapter 2, some related background to the promising technology of FD communication system fundamentals and principles are introduced. Moreover, a brief introduction about the different sources that cause HWIs in wireless communication systems such as imperfect I/Q balance, imperfect local oscillator (LO) and non-linearities of the power amplifier (PAMP) is discussed. In addition, the used HWIs model and Nakagami-m fading channel distribution are explained. Furthermore, the LMMSE and the LS estimations are discussed. Finally, a literature review of the existing work is provided.

In Chapter 3, the effects of HWIs at all system end terminals on FD SISO wireless communication systems is studied. First, the proposed work is introduced, where the FD system and channel models are explained. Next, the transceiver HWI model is discussed. Moreover, the performance analyses of FD UL/DL SEs are discussed in detail, where the lower bounds of the average FD UL and DL SEs are obtained. In addition, an optimal power allocation optimization problem that maximizes the average FD SE and EE considering QoS and power budget constraints is formulated. Then, a novel algorithm to solve the problem by using the fractional programming and KKT conditions technique is proposed. Furthermore, the simulation results and discussion that validate the analytical frameworks are provided. Finally, the study is summed up.

In Chapter 4, the impact of HWIs on FD MIMO wireless communication systems is studied. First, some preliminaries and concepts are introduced. Next, the MIMO system model is explained and the signal model under the HWIs model at the transmitter and

receiver is discussed. Moreover, the system performance in the UL and DL scenarios are presented, where the average FD SE in the presence of HWIs is derived. Additionally, different power allocation optimization problems are formulated, such as maximizing (SE, EE, max-min SE and max-min EE to fulfill the QoS and power budget constraints. Then, these optimization problems are solved by utilizing advanced optimizing techniques which result in proposing novel algorithms and developing a simplified version of the proposed algorithm. Next, the analytical findings and the feasibility of the proposed algorithms are verified by the simulation and the results are discussed. Finally, the chapter concludes with the important findings.

In Chapter 5, the impact of the channel estimation error and HWIs on the performance of MU-MIMO systems is studied. First, the system and channel models considering the non-ideal transceivers are explained. Next, the channel estimation model when using LMMSE and LS estimations is discussed. Then, the average FD UL and DL achievable sum rates under HWIs and imperfect CSI are derived when using MRC/MRT and ZFR/ZFT linear detectors/precoders. Moreover, many special cases are obtained. In addition, LMMSE and LS estimators for the impaired FD MU-MIMO systems are designed. Next, the effects of increasing the number of training pilot symbols and the transmitted power on the channel estimation error are discussed. Then, a computer simulation validates the analytical derivations and the results are explained. Finally, a summary of the important results is provided.

In Chapter 6, the essential results of our analyses and refer to some opportunities for future research on this topic are summed up.

1.4   List of Publications

- **Related to the thesis**

  1. E. Saleh, M. M. Alsmadi, and S. Ikki, *"Towards a Practical FD MU-MIMO System: Performance Analysis Considering Imperfect CSI and Non-ideal Transceivers," Submitted, IEEE Transactions on Communication, 2023.*

I am the main contributor of this work, and I played a leading role in the theoretical modeling and planning of the publication.

2. E. Saleh, M. M. Alsmadi, and S. Ikki, *"Spectral-energy efficiency and power allocation in full-duplex networks: the effects of hardware impairment and Nakagami-m fading channels,"* IEEE Transactions on Vehicular Technology, pp. 1–16, 2022.

   I am the main contributor of this work, and I played a leading role in the theoretical modeling and planning of the publication.

3. E. Saleh, M. M. Alsmadi, and S. Ikki, *"Spectral efficiency of full-duplex MIMO systems under the effects of hardware impairments,"* in 2022 IEEE 95th Vehicular Technology Conference: (VTC2022-Spring), 2022, pp. 1–7.

   I am the main contributor of this work, and I played a leading role in the theoretical modeling and planning of the publication.

4. E. Saleh, M. M. Alsmadi, and S. Ikki, *" Energy Efficiency and Power Allocation Optimization in Hardware-Impaired Full-Duplex Access Point, in 2022 IEEE Global Communications Conference: Selected Areas in Communications: Full-Duplex Communications, Rio de Janeiro, Brazil, Dec. 2022.*

   I am the main contributor of this work, and I played a leading role in the theoretical modeling and planning of the publication.

- **Unrelated to the thesis**

  1. E. Saleh, M. M. Alsmadi, A. Bouhlel, A. E. Canbilen, N. A. Ali, and S. Ikki, "Impact of channel correlation and hardware impairments on large intelligent surfaces-aided communication systems," *in 2021 IEEE 32nd Annual International Symposium on Personal, Indoor and Mobile Radio Communications (PIMRC),* 2021, pp. 805–810.

     I am the main contributor of this work, and I played a leading role in the theoretical modeling and planning of the publication.

  2. F. Ghaseminajm, E. Saleh, M. Alsmadi, and S. S. Ikki, "Localization error bounds for 5G mmWave systems under hardware impairments," *in 2021 IEEE*

32nd Annual International Symposium on Personal, Indoor and Mobile Radio Communications (PIMRC), 2021, pp.1228–1233.

I helped in the performance analysis, simulation, writing and revision the paper.

3. A. Bouhlel, M. Alsmadi, E. Saleh, and S. Ikki, "Performance analysis of RIS-SSK in the presence of hardware impairments," *in 2021 IEEE 32nd Annual International Symposium on Personal, Indoor and Mobile Radio Communications (PIMRC), 2021, pp. 537-542.*

I helped in the performance analysis, simulation and revision of the paper.

4. Hamzih Alsmadi, Emad Saleh, Malek Alsmadi, and Salama Ikki, "Capacity Analysis of UAV Communications Under the Non-ideal Transceiver Effects" *Accepted with minor revision, IEEE Communications Letters, 2023.*

I helped in the performance analysis, simulation and revision of the paper.

Chapter 2

Preliminaries and Literature Review

THIS chapter gives a general idea about the fundamentals and principles of FD systems, imperfect radio frequency (RF) components that cause HWIs, the used HWIs model, Nakagami-m fading channel distribution and reviews the recent related works. Based on this review, this chapter highlights the motivations and the contributions of our research to fill in the gap by developing novel algorithms, providing mathematical frameworks and new ideas related to FD systems.

2.1   Preliminaries

2.1.1   Full Duplex Communication System

FD is an emerging transmission technology of wireless communication systems. It is proposed as a promising technology for future communication systems in terms of its capability to double the SE and enhance the EE, but this is accompanied by a number of challenges at all layers, starting from the antenna and circuit design to the development of theoretical frameworks for wireless networks [28]. A cooperative FD MIMO scenario can achieve large gains in SE and link reliability, thanks to the ability of the MIMO system in exploiting spatial diversity with multiple antennas at the BS. Because the SE increases with the number of antennas without the cost of increasing bandwidth or the transmit power [29–31].
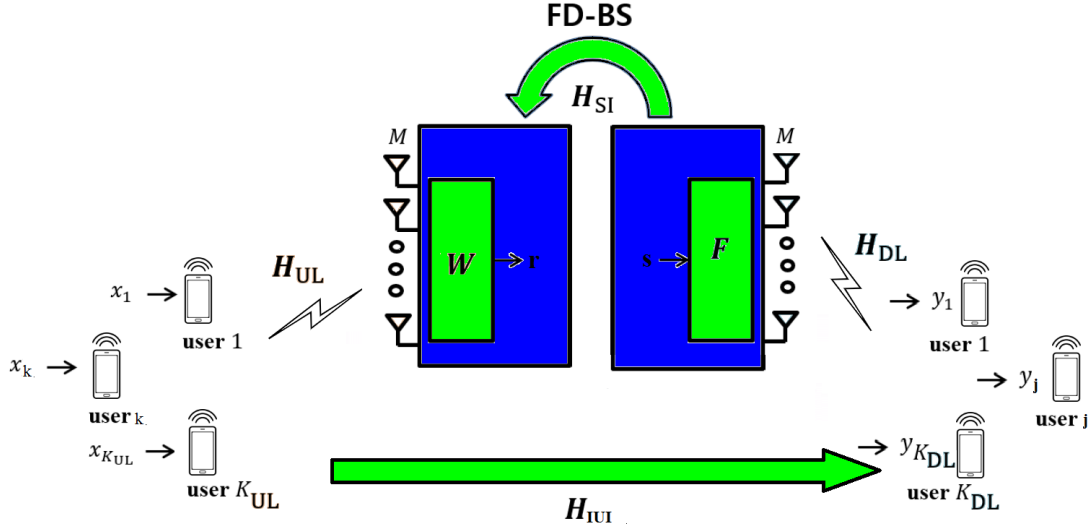
Figure 2.1: Full-duplex MU-MIMO communication system structure.

A general FD MU-MIMO communication system is illustrated in Fig. 2.1, that has M transmit and M receive antennas at the BS that serves K_{UL} and K_{DL} users equipped with one antenna for each. Due to the FD mode, in which the BS can transmit and receive simultaneously over the entire time and bandwidth, SI exists at the BS which is the interference from the transmit antenna array to the receive antenna array, where the effects of the SI can be mitigated by employing interference cancellation. Herein, $\mathbf{H}_{\mathrm{SI}} \in C^{M \times M}$ is used to represent the residual SI channel matrix, whose entries can be modeled as independent identical distributed (i.i.d) with each element following $\sim \mathcal{CN}(0, \sigma_{\mathrm{SI}}^2)$ [14–19], where $z \sim \mathcal{CN}(0, \sigma^2)$ is a complex Gaussian random variable with zero mean and σ^2 variance. Moreover, σ_{SI}^2 represents the residual SI power. Similarly, the UL users cause interference to the DL users called IUI, where $\mathbf{H}_{\mathrm{IUI}} \in C^{K \times K}$ represents the channel between the set of UL and the DL users. Furthermore, the UL channel matrix from the K UL users to the BS is denoted as $\mathbf{H}_{\mathrm{UL}} \in C^{M \times K}$ and the DL channel matrix from the BS to the K DL users is denoted as $\mathbf{H}_{\mathrm{DL}} \in C^{M \times K}$.

2.1.2 Spectral/Energy Efficiency and Power Allocation Methods

One of the main contributions of this thesis is to maximize the SE and EE, where the SE can be defined as the average number of bits of information per complex-valued sample that

can reliably transmit over the channel under consideration and it has a unit bit/s/Hz [1], while the EE refers to the benefit-cost ratio, it is defined as the ratio of the transmitted information bits to the total consumed energy and it has a unit bits/Joule. The dominant key in this issue is how to appropriately allocate the UL and DL transmit powers to minimize interference because the transmit power in wireless networks plays a vital role in the management of interference, energy, and connectivity. This becomes more serious in FD communications due to the existence of SI where the UL transmit power affects the DL SE and the DL transmit power affects the UL SE. As such, in this work, power allocation algorithms to find optimal values of the transmit power are proposed. However, there are many methods were used in the literature for power allocation in wireless networks. For example, authors in [32–34] studied power control with fixed signal-to-interference ratio (SIR) where transmit power is the only variable, constrained by fixed target SIR, and optimized to minimize the total power. The fixed SIR method to power control is appropriate for low-traffic networks such as voice. However, for high-traffic networks, it is difficult to set the target SIR to be attainable. So, the authors in [35–37] studied power control with variable SIR. Another power control method is to spend more power and increase rate as channel quality improves which is known as opportunistic power control [38–40]. Finally, a comprehensive discussion about the power control algorithms in wireless networks can be found in [41].

2.1.3 Hardware Impairments

The HWIs are present in practical wireless communication systems. Since the physical transceiver implementations have many electrical devices and circuits and hence distort the signals in different manners. Therefore, the transmitted signal will be distorted and a mismatch between the intended signal and the actual transmitted signal has occurred. For more illustration the imperfect RF components that cause HWIs are demonstrated in Fig. 2.2. Where the real and imaginary parts of the original baseband complex signal x are separated as I/Q signals then after some signal processing are up-converted to the desired RF, in such way, $\tilde{x}$ is transmitted over the channel instead of x. During the transmission,

$$\tilde{x}(t) = \cos\left(2\pi f_c t\right) + jg\sin\left(2\pi f_c t + \phi\right)$$
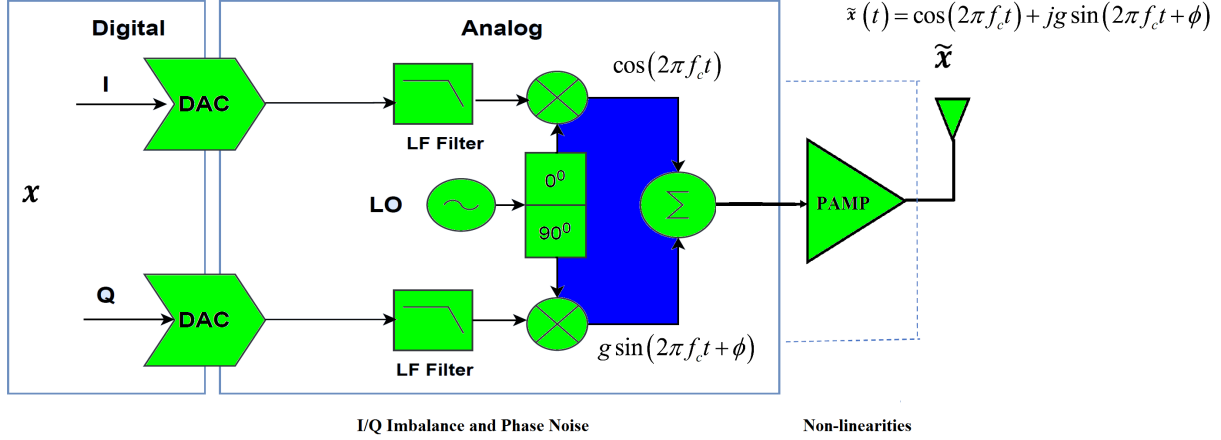
Figure 2.2: The RF transmitter block diagram in the communication systems.

the signal is distorted in many stages due to imperfect hardware. Firstly, the intended signal x is processed by digital-to-analog converter (DAC)s at the transmitter because a digital signal needs to be converted to an analog one, or analog-to-digital converter (ADC)s at the receiver, as such the signal is distorted due to sampling frequency offset and quantization error because of adopting low-resolution ADCs, where the use of high-resolution ADCs can cause excessive overhead and power consumption. After that, I/Q signals are filtered and mixed with respective I/Q versions (90 degrees out of phase) of a LO. The LO frequency is the carrier frequency f_c of the RF signal.

Secondly, the signal is distorted by the imperfect I/Q mixer, LO and phase shifter that is referred to as I/Q imbalance and phase noise. For example, a perfect LO is intended to provide an exact 90 degrees phase shift between the I/Q branches along with equal gain. However, due to the non-idealities of the LO, a phase imbalance between the I/Q branches of the transmitter and/or receiver signals might be observed, because the provided phase shift is not exactly 90 degrees. This also causes gain mismatch which is called amplitude imbalance due to small variations between the amplitude of the I/Q branches of the signal at the transmitter and/or receiver. This is illustrated in Fig. 2.2, where ϕ and g are the phase difference and the gain mismatch between the I/Q branches, respectively. As it can be seen in Fig. 2.2, the in-phase (I) signal is presented by $\cos\left(2\pi f_c t\right)$, and the quadrature-phase (Q) signal is presented by $g\sin\left(2\pi f_c t + \phi\right)$. Consequently, the combined effect of the gain and phase imbalances is referred to as I/Q imbalance since they are not identical

13

and have different gains. As a result, I/Q imbalance can dramatically degrade the system's performance by altering the transmitted signal at the transmitter or distorting the received signal at the receiver.

Finally, the PAMP at the transmitter and the low noise amplifier (LNA) at the receiver are essential components in the RF chain. In practice, they are designed to provide maximum efficiency in the saturation region. However, they are the main sources of non-linear distortion in the communication systems. Practically, when the PAMP operates in its nonlinear region, amplitude and phase distortions occur on the transmitted signal. A non-linear distortion of the PAMP is generally characterized by amplitude-to-amplitude and amplitude-to-phase distortion functions [22, 42, 43]. As such, $\tilde{x}$ becomes the final RF signal to be transmitted.

Hardware Impairment Model

Wireless communication channels are commonly modeled as linear filters that take an analog input signal from the transmitter and generate an output signal with distortion, which is measured at the receiver in the presence of additive white Gaussian noise (AWGN). For example, when the power amplifier in the transmitter works in the saturation region, it provides less amplification gain to stronger input signals which means it does not have a linear amplification. On the other hand, at the receiver side, the finite-resolution quantization in ADC causes another non-linear operation, which is additionally destructive and cannot be undone. These imperfect operations represent the HWIs. Fig. 2.3 illustrates an analog channel without and with HWIs [1]. At the transmitter side, the output of the non-ideal hardware which represents the HWIs is modeled as additive distortion noise as follows [1, 44]

$$\tilde{x} = \sqrt{P\kappa_t}\, x + \eta_t, \tag{2.1}$$

where the actual transmitted signal is $\tilde{x}$ rather than the designated signal x which satisfies $\mathbb{E}\{|x|^2\} = 1$, the transmitted power is P, the transmitter's HWI factor is $\kappa_t \in (0,1]$ and the complex transmitter additive distortion noise is $\eta_t \sim \mathcal{CN}(0, (1 - \kappa_t)P)$ which is independent of x. The distortion power is therefore proportional to the input power P, with
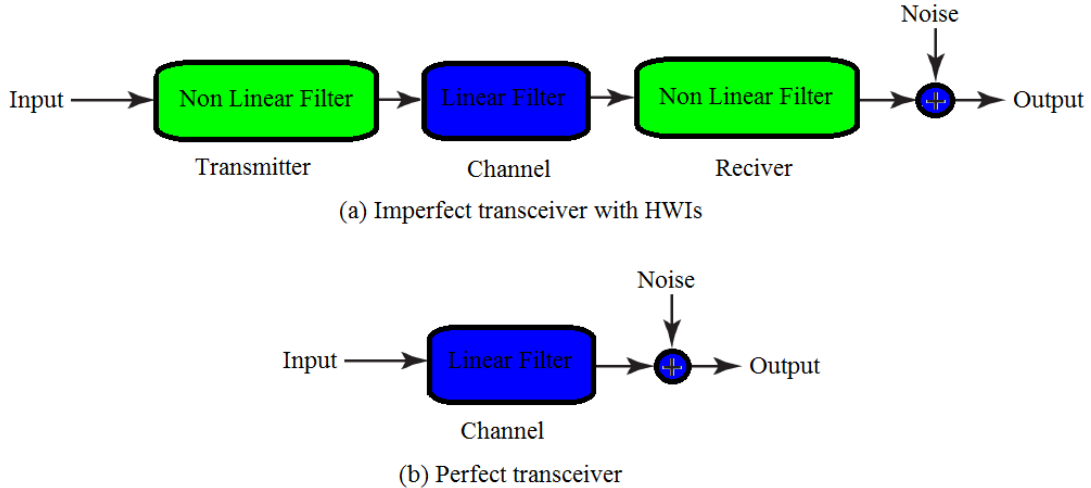
Figure 2.3: A communication system model (a) with HWIs and (b) without considering HWIs [1].

the proportionality constant $(1-\kappa_t)$. This makes the additive distortion term different from the conventional AWGN noise at the receiver, which is independent of the input power. When operating at high signal-to-noise ratio (SNR) regime, where the noise is negligible, the distortion becomes a main limiting factor for the performance. Similarly, the impaired signal at the receiver can be given as

$$y = \underbrace{\sqrt{P\kappa_r\kappa_t}\ h\ x}_{\text{Desired signal}} + \underbrace{\sqrt{\kappa_r}\ h\ \eta_t + \eta_r}_{\text{Distortion noise}} + \underbrace{w}_{\text{AWGN}}, \tag{2.2}$$

where h is the complex channel gain between the transmitter and the receiver, the receiver's HWI factor is $\kappa_r \in (0, 1]$, the complex receiver additive distortion noise is $\eta_r \sim \mathcal{CN}\left(0, (1 - \kappa_r)P\,|h|^2\right)$, and the AWGN is $w \sim \mathcal{CN}(0, \sigma_w^2)$. Hence, the distortion power is proportional to the input power P. In the case of perfect hardware, $\kappa_r = \kappa_t = 1$, $\eta_r = \eta_t = 0$ and $\tilde{x} = x$.

It is notable that the HWI factor κ_t is the proportionality coefficient that defines the level of HWIs and it is associated with the error vector magnitude (EVM). The EVM is a common metric for measuring the distortion level in practical transceiver hardware. It is defined as the square root of the ratio of the average distortion power to the average signal power [45]. Additionally, the transmitted signal (modulation) quality is connected with EVM, which means, to ensure sufficiently high quality of the transmitted signal, specific

15

Table 2.1: EVM requirements

Modulation scheme	Required EVM	HWI factor κ_t
QPSK	17.5 %	0.970
16QAM	12.5 %	0.984
64QAM	8 %	0.994
256QAM	3.5 %	0.999

EVM requirements should be met [46]. For the transmitted signal x in model (2.1), EVM can be expressed as [1]

$$\text{EVM} = \sqrt{\frac{\mathbb{E}\{\eta_t\}}{P\mathbb{E}\{|x|^2\}}} = \sqrt{\frac{(1 - \kappa_t)P}{P}} = \sqrt{1 - \kappa_t}. \tag{2.3}$$

Table 2.1 [45–47] alongside the relationship in (2.3) show that the quality of the transmitted signal directly relies on the hardware quality. For example, the long-term evolution (LTE) standard requires EVM ≤ 0.08 in the transmitter hardware if 64-quadrature amplitude modulation (64-QAM) should be supported. This corresponds to $\kappa_t = 1 - \text{EVM}^2 \geq 0.994$. If the transmitter should only support quadrature phase-shift keying (QPSK), then LTE only requires EVM ≤ 0.175 and this corresponds to $\kappa_t \geq 0.97$ [45, 46]. While practical LTE transceivers typically support 64-QAM, EVMs larger than 0.08 are of interest to FD MIMO since they can relax the hardware design constraints. The EVM is one of the key metrics that are specified on the data sheets of RF transceivers.

2.2 Channel Models

Wireless communication systems are built on randomness because the transmitted signal propagates in all directions and travels in different paths before it arrives at the destination. As a result, there are many challenges facing the wireless channel as a medium for reliable communication. For example, the fading phenomenon occurs because multi copies of the transmitted signal arrive at the receiver side at different times and face different attenuation levels. Moreover, path loss and shadowing are other characteristics that degrade

the transmitted signal because of the distance and the obstacles between the source and the destination. Since the emergence of wireless communication systems, the statistical modeling of fading channels has gained a remarkable interest [27, 48–57].

2.2.1   Nakagami-m Fading Channel Distribution

The Nakagami-m distribution, also called Nakagami distribution, first appeared in 1960 [49]. It is one of the most common probability distributions for modeling real-world applications including modeling wireless signal and radio wave propagation. Extensive empirical measurements showed that this distribution is appropriate for modeling the radio signals and it fits the empirical multipath fading measurements better than the other fading models [27, 48]. It has a probability density function formula as

$$f(x; m, \Omega) = \frac{2m^m}{\Gamma(m)\Omega^m} x^{2m-1} \exp\left(-\frac{m}{\Omega} x^2\right) \qquad x \geq 0, \tag{2.4}$$

where $\Gamma(\cdot)$ is the Gamma function. $m \geq 1/2$ is shape parameter and $\Omega > 0$ is spread parameter are given as $m = \dfrac{\left(\mathbb{E}\left[X^2\right]\right)^2}{\text{Var}\left[X^2\right]}$, and $\Omega = \mathbb{E}\left[X^2\right]$.

It is worth mentioning that, the Nakagami-m distribution is flexible and includes several distributions as special cases. For example, it contains the Rayleigh distribution when $m = 1$ and the scaled Chi distribution when $2m = k$. Also, the half-Normal distribution can be obtained when $m = 0.5$. Moreover, the Nakagami-m distribution very well approximates the Ricean distribution [58].

2.2.2   Rayleigh Fading Channel Distribution

The Rayleigh distribution is a common used model to represent multipath fading channels with no direct line-of-sight (LOS) path and it is referred to as fast fading [58]. As it is mentioned earlier, the Rayleigh distribution can be obtained from the Nakagami-m distribution by setting m=1. It has a probability density function formula as

$$f(x) = \frac{x}{\sigma^2} \exp\left(-\frac{x^2}{2\sigma^2}\right) \qquad x \geq 0, \tag{2.5}$$

where σ is the scale parameter of the distribution.

2.2.3 Ricean Fading Channel Distribution

In the Ricean distribution, the fast fading channel realizations can be modeled as a sum of two components: The deterministic component corresponds to the LOS signal and the Rayleigh distribution of the scattered signal. The Rician parameter K_{ric} represents the ratio of the LOS component power to the Rayleigh-distributed component power. The fading channel is given as in [13, 59, 60]

$$\mathbf{h} = \sqrt{\frac{K_{ric}}{K_{ric}+1}} \bar{\mathbf{h}} + \sqrt{\frac{1}{K_{ric}+1}} \mathbf{h}_{ray}, \qquad (2.6)$$

where $\bar{\mathbf{h}} = [1, e^{-j\frac{2\pi d}{\lambda}\sin(\theta)}, \cdots, e^{-j(M-1)\frac{2\pi d}{\lambda}\sin(\theta)}]$, is the LOS channel component, and $\mathbf{h}_{ray} \sim \mathcal{CN}(\mathbf{0}, \mathbf{I}_M)$ is the diffused channel component. Here d is the antenna spacing, λ is the wavelength, and θ is the arrival angle. Note that when $K_{ric} = 0$, the Ricean channel has only the Rayleigh distribution of the scattered signal. When $K_{ric} \to \inf$, the Ricean channel has only LOS component channel. It has a probability density function formula as [61]

$$f(x) = \frac{1}{2\sigma^2} \exp\left(-\frac{x^2+v^2}{2\sigma^2}\right) I_0\left\{\frac{xv}{\sigma^2}\right\} \qquad x \geq 0, \qquad (2.7)$$

where v^2 is the average power of the LOS component, σ^2 is the power in the scattered component, $I_0(v)$ is the modified Bessel function of the first kind.

2.3 Channel Estimation

In general, the estimation aims to obtain an approximate value of an unknown variable based on some observations. In practical MU-MIMO wireless communication systems, the receiver side does not know the channel matrix $\mathbf{H}$, and channel estimation techniques are used to obtain the estimated channel matrix $\hat{\mathbf{H}}$. In the presence of an estimation error, the following fact [62–68] can be used

$$\mathbf{H} = \hat{\mathbf{H}} + \mathbf{H}_e , \qquad (2.8)$$

where $\mathbf{H}_e$ is the channel estimation error matrix. In each coherence block, there are samples reserved for UL training pilot symbols. Each user uses a certain pilot sequence. The BS has

knowledge about these samples and knows which pilot sequence each user transmits. As such, the BS can estimate the channels of the users. So the pilots should be deterministic sequences and the pilot assignment is normally made when the user connects to the BS. Channel estimates from interfering users in other cells can also be exploited to conduct interference cancellation during data transmission.

Pilot contamination: For the most reasonable estimate, different UEs in the entire network would transmit mutually orthogonal training pilot symbols. However, practically it is not possible because of the limited size channel coherence interval and it is necessary to reuse pilot sequences across cells. A good solution is to maintain intra-cell orthogonality among training pilots of different users in the same cell, but not inter-cell orthogonality among the training pilots of users in other cells. As a result, inter-cell non-orthogonality leads to a phenomenon known as pilot contamination, thereby increasing the MSE and reducing the accuracy of the channel estimation. To overcome the pilot contamination issue, many algorithms have been proposed. For example, it was shown that optimizing and scheduling pilot transmission can mitigate the impact of pilot contamination [69–72].

The most common efficient estimator known as LMMSE which estimates the channel based on the observations and utilizes the channel statistics. It depends on the first-order moments and the second-order moments of the unknown variable and the observation. It is relatively easy to estimate these moments, resulting in making the LMMSE estimator particularly appropriate for practical implementations. On the other hand, it is difficult to estimate the full probability density function (PDF) of the unknown variable and the observation because it might follow an unknown distribution. A simpler estimator known as LS does not require prior statistical information and can be used when these statistics are unknown [73, 74]. Further details and explanations about the estimation of unknown variables can be found in [75]. In FDD-based massive MIMO systems, channel estimation is challenging because the number of antennas at the BS is much higher than the number of users that requires a large number of training pilots and causes feedback overhead. More details about the channel estimation in TDD and FDD-based massive MIMO systems can be found in [76]. The key factors that determine the accuracy of the estimated channel are the transmit power, the number of training pilots and the hardware quality [77]. Section

5.3 discusses how the BS carries out the channel estimation by utilizing the UL pilot transmission.

2.4 Literature Review

FD communication has a lot of attention as a potential key to enhance the SE and EE [13, 14, 17–19, 78–92]. The main challenge in implementing FD systems is the SI. As such, the received signal at the BS is extremely affected by the DL transmit power of the BS. To overcome the SI, considerable work has been conducted to tackle the SI suppression and cancellation. For example, the authors in [93] showed that the SI can be mitigated using passive suppression. Furthermore, analog and digital SI cancellation are studied in [94], where the study concluded that a combination of antenna cancellation, RF interference cancellation and digital interference cancellation can reduce the SI to within a few dB of the noise floor. In addition, the authors in [21] investigated the potential FD techniques including passive suppression, active analog cancellation, and active digital cancellation.

In [79, 90], the authors have studied FD relaying system scenarios, where in [79] the achievable data rate and EE of FD relaying system are discussed. In such a system, the transmission between the source and the destination takes place through an intermediary device that can either be a FD relay or reconfigurable intelligent surfaces (RIS). The results showed that the FD relaying system outperforms the RIS system. However, the study has been done under perfect CSI and ideal transceivers. In [80, 81], the authors recently have studied the EE maximization problem for FD RIS assisted systems, and proposed a new simultaneous transmission and reflection reconfigurable intelligent surface (STAR-RIS) to maximize EE by jointly optimizing the transmit power of the BS and the UL user and the passive beamforming at the STAR-RIS aided FD communication systems. In [83], the effect of HWIs on RIS-assisted FD MIMO communication systems has been studied by considering them in terms of additive errors and a channel estimation method is proposed to estimate all CSI. In [84], the impact of imperfect CSI and discrete phase-shift design on the performance of FD two-way RIS-assisted communication systems have been discussed. It was shown that at high transit power regions, imperfect CSI leads to the performance

floor and better CSI estimation improves the system performance as well as increasing the number of RIS's elements.

In [82], a unified framework for FD cellular networks with low-resolution ADCs/DACs was provided and analytical expressions for the signal-to-quantization-plus-interference-plus-noise ratio (SQINR) and SE were obtained. It was shown that there are rate losses due to the quantization error, SI, and IUI. However, using high-resolution ADCs/DACs and a large number of BS antennas can compensate for the rate loss. Furthermore, the authors in [95] studied the SE of FD cell-free massive MIMO system with low-resolution ADCs at the BSs and DL users. The results of this work showed that increasing the number of receiving antennas at the BSs can compensate for the UL SE loss due to the quantization noise. On the other hand, the DL SE loss could not be compensated by increasing the number of transmit antennas because the desired signal and the quantization noise are both quadratic and grow at the same rate as the number of transmit antennas. The authors of [78] also have studied the SE/EE of the FD cell-free massive MIMO with low-resolution ADCs. Their results showed that the UL SE is degraded by the increase in DL power, whereas the growth in UL power deteriorates the DL SE. The impact of the residual SI and the interference are worsened by the low-resolution ADCs.

In [13], the achievable rate and BS EE of FD massive MIMO systems with low-resolution ADCs/DACs over Rician fading channels have been studied using the linear maximum ratio combining/maximum ratio transmission (MRC/MRT) processing at the BS. It was shown that adding more BS antennas can compensate the achievable rate loss due to the low-resolution ADCs/DACs, SI and IUI. Furthermore, the trade-off between the achievable rate and the EE of the BS leads to a significant improvement in the EE of BS by small sacrificing the achievable rate of the FD system. In [14], the achievable rate of a multi-pair massive MIMO relaying system with a mixed-ADCs/DACs architecture was investigated. Furthermore, EE was obtained to study the trade-off between the achievable rate and power consumption for different numbers of low-resolution ADCs/DACs. The results revealed that the transmit power can be scaled down inversely proportional to the number of antennas at the relay when using a power scaling law, beside that a significant reduction in the power consumption and hardware cost for massive MIMO systems can be achieved by deploying

a large antenna array to enable the mixed ADCs/DACs architecture.

In [17], it was shown that the sum-rate of a heterogeneous network is degraded due to the quantization noise (QN) when using low resolution ADCs/DACs and this system performance loss due to QN and SI is effectively compensated by increasing the number of receive antennas at the BS. In [18], the achievable rates for UL and DL with perfect CSI of FD massive MIMO system have been investigated in which low-resolution ADCs/DACs are considered and MRC/MRT processing are used, their results agree with the finding in [17], in which the quantization error of the low-resolution ADCs/DACs and SI cause a loss of system performance. However, deploying more antennas and using a proper power scaling law can eliminate the interference and noise, and compensate the performance degradation, so it is reasonable to employ low-resolution ADCs/DACs in FD massive MIMO systems.

In [19, 89] power allocation methods in the FD multi-user MIMO systems have been studied, where in [19] power allocation (PA) scenarios are proposed to maximize the EE and the sum SE with the constraint of maximum powers at the BS and users. It was shown that the multi-user FD massive MIMO system outperforms the HD by using the PA scheme. Additionally, the effect of the SI and multi user interference can be cancelled by deploying a large number of antennas at the BS and applying the law of power scaling. In [85], the achievable rate of FD massive MIMO relay system over Rician fading channels was investigated. It was shown that the SI can be effectively cancelled by ZF processing at the decode-and-forward relay when the number of antennas increased to infinity. In [96] the UL and DL achievable rate of FD MIMO systems over Rician fading channels based on MRC/MRT and zero-forcing reception/zero-forcing transmission (ZFR/ZFT) processing under perfect CSI, the finding showed that for a large number of BS antennas, the power scaling law can be used and eliminate the multi-user interference and SI.

In [97] the ergodic achievable rates for the case of linear precoders and receivers of a multi-cell MU-MIMO FD system was studied and it was shown that the SI can be significantly removed by increasing the number of BS antennas and achieve spectral efficiency gain. In [98] joint communication of FD and sensing/radar systems is discussed and the challenges are investigated. FD hybrid AP is studied in [99], where the AP transmits to a

set of cellular users in the DL channel while receiving signals from a set of communication devices such as user equipment in the UL channel. This study calculated the approximate and asymptotic achievable rates, maximizing the DL sum-rate of cellular users while ensuring that the UL sum-rate of the other users is above a fixed threshold.

To emphasize the potential of FD communication systems, many researchers combined different communication techniques with FD systems [100–107]. Recently, the authors in [100] investigated the effect of multiple intelligent reflecting surfaces (IRS)s on the performance of multi-user FD communication. The study concluded that, in FD communication, using multiple distributed IRSs is more efficient than using a single centralized IRS. However, this study provided a sub-optimal algorithm based on an iterative optimization approach considering only constraints on the BS power budget and UL users. The study also obtained the instantaneous achievable transmission rate, not the average one, making it challenging, especially when using a large number of reflectors in the IRSs. The works in [86, 101, 106, 107] studied a cooperative FD NOMA scenario. Where the work in [101] obtained approximate expressions for the outage probability (OP) and the ergodic rate of the FD cooperative NOMA, which outperforms the HD one. The authors in [102] studied the effect of HWIs on the OPs and ergodic capacities of both one-way and two-way amplify-and-forward (AF) FD relaying systems. The authors concluded that, due to the HWIs and SI, the OP and ergodic capacity saturated in the high SNR region. Similarly, the work in [103] investigated the performance of the FD decode-and-forward (DF) two-way relay, confirming the non-negligible effect of HWIs on the system performance. The authors in [104] obtained the SE of impaired multi-pair two-way FD massive MIMO relay.

The authors in [105] provided a comprehensive study about massive MIMO DF and AF FD relaying systems. The work obtained the lower bounds of the system SEs with MRC/MRT and ZF, all while considering imperfect channel-state information and HWIs. This work concluded that to implement low-cost massive MIMO FD relaying systems, high-quality hardware at the sources and destinations is preferable over the relay, in case of small loop interference. On the other hand, the hardware qualities at the sources, destinations, and relay have the same effects on the system performance in the case of high loop interference. However, the works in [101–105] focused on the performance analyses and

did not study the EE nor did they pursue any power allocation optimization to maximize the SE.

Moreover, It is well-known that the presence of HWIs limits the system performance. For example, it has been shown that I/Q imbalance affects the system performance, and this effect is maximized in the case of imperfect CSI [23]. The authors in [108,109] discussed the impacts of the phase noise (PN) and I/Q imbalance on multi-carrier communication systems. They concluded that these physical impairments extremely degrade the performance of the system and proposed an algorithm to compensate for these two impairments.

The authors in [24] studied the effect of HWIs on large intelligent surfaces (LIS)-Aided systems, and it was proven that the HWIs limit the spectrum and energy efficiencies of the system even when the number of transmit antennas and LIS reflectors grow infinitely large. This study was done under the assumption of a deterministic channel. In [110], the authors studied the performance of reconfigurable intelligent surface space-shift keying (RIS-SSK) communication system in the presence of HWIs. The study concluded that negative effects of modeling the HWIs are observed for robust RIS-SSK system implementation. The work in [111] showed that the HWIs can significantly decrease the capacity of LIS-Aided communication systems. The authors in [22] studied the impact of the nonlinearity of high-power amplifier (HPA)s on MIMO communication systems and they proposed a compensation method for HPAs nonlinearity in the cases with and without knowledge of the HPAs parameters at the transmitter and receiver.

The existing literature generally studies cases of FD massive MIMO relay systems and plentiful papers focused on investigating FD massive MIMO systems with low-resolution ADCs/DACs. Power allocation optimization algorithms were proposed. Moreover, most of the work used the law of large number in the analysis which simplifies the mathematical manipulations. Based on this review, our research objectives aimed to fill the gap in the literature as illustrated in Section 1.1. For example, each RF component has its own model and can be considered when studying this certain RF component. As such the non-ideal behaviour of each component can be modeled in detail for the purpose of designing compensation algorithms, but even after compensation, there remain residual transceiver impair-

ments due to insufficient modeling accuracy, imperfect estimation of model parameters, and time-varying characteristics induced by noise. However, this work considers a general model of the residual impairments which are the aggregate noise that is left after properly compensating rather than considering a specific model such as ADCs/DACs [5, 13–18, 78, 95]. In addition, different from the literature, this work studies the FD MU-MIMO system considering practical conditions such as non-ideal transceivers at all system terminals (i.e., DL users, UL users, transmit and receive antenna array at the BS), channel estimation errors, SI, the interference between the UL and DL users, the interference among the UL users as well as the interference among the DL users themselves. As a result, comprehensive mathematical manipulations and calculations are conducted during the analysis, where mathematical frameworks for the lower bounds of the average FD DL/UL SE under the joint effects of these conditions are derived. Moreover, this work designs LMMSE and LS estimators for the impaired FD MU-MIMO system. It shows that due to HWIs, there is an error floor in the channel estimation, the hardware quality affects the error level and increasing the transmit power will not eliminate the estimation error. On the other hand, in the case of ideal hardware, this estimation error can be completely eliminated by increasing the transmit power. Interestingly, increasing the number of pilots can eliminate the estimation error for both ideal and impaired systems. Finally, this work proposes novel algorithms to optimize the UL and DL transmit power to maximize the SE and EE with less complexity.

Chapter 3

Energy Efficiency and Power Allocation Optimization in Hardware-Impaired Full-Duplex Access Point

3.1 Introduction and Related Works

IT is obvious that technology, and especially connectivity, increasingly supports many aspects of our everyday lives. As a result, there has been considerable growth in wireless services that require higher data rates, lower latency, and more reliable communications. Such growth will obviously accompany ubiquitous demands of high SE and EE, which present themselves as the main challenges for the upcoming generations of wireless communications and networks. These are considerable challenges because the amount of available spectrum is limited. In order to meet these requirements, immense research has been carried out to develop new wireless technologies. However, network energy consumption and hardware cost remain critical issues in practical systems and being able to find spectrum and energy-efficient techniques with low hardware costs remains an attended challenge [112, 113].

FD communication has emerged as a promising technique that aims to enhance both SE and EE in wireless communication networks in a cost-effective manner [12–14,18,19]. In FD

communication, SE can be theoretically doubled compared with conventional HD systems, since the FD devices have the ability to transmit and receive all the time throughout the entire bandwidth. However, the major challenges here are the SI which can have an extreme impact on the UL received signal at the AP, and the IUI which can affect the DL received signal at the user [20,114]. It was also pointed out that one of the most important open issues related to FD technology is to propose cost-efficient solutions with low energy consumption [114]. This can be achieved by using the proper power allocation algorithm to reduce the effects of SI and IUI. At the same time, the estimation accuracy of the SI channel is a game player in the SI cancellation. In theory, perfect channel estimation can successfully mitigate the SI. However, the presence of HWIs affects the estimation accuracy which implies imperfect SI mitigation. This is a good reason to study the HWIs in the FD systems [114,115]. Modern digital communication systems require considerable digital signal processing and advanced analog circuitry. At the same time, the signal is subject to many sources of impairments at the transceivers such as analog imperfectness, phase noise, in-phase/quadrature-phase imbalance, power amplifier non-linearities, etc. Hence, HWIs can dramatically degrade the communication system's performance [14,18,95,111,116].

A power allocation algorithm that maximizes the achievable SE was proposed in [12]. In this work, the channel between the UL and DL users was estimated, and then used to cancel the IUI. It also concluded that a remarkable SE gain was obtained and FD always outperforms the HD and the FD systems without using the channel estimation protocol. However, this study did not consider different levels of SI which is the main challenge of FD systems. Moreover, the EE of the RIS assisted FD system was optimized in [117], where the transmit power and the RIS phase shifts matrix were optimized iteratively. It was shown that the FD system achieved double EE and SE performance compared to the HD system. However, this study did not consider any QoS constraints or different levels of SI. Although the works in [12,19,117] have shown interesting results, they have been done assuming ideal hardware conditions. Different from the current works, and motivated by the importance of this topic, the contribution of this chapter can be summarized as

- Derives lower bounds of the average FD DL and UL SE when all system end terminals

27

are under the effect of HWIs.

- Formulates a power allocation optimization problem that maximizes the average FD SE and EE considering QoS and power budget constraints. Then, a sub-optimal solution is obtained by utilizing both the fractional programming theory and the Karush–Kuhn–Tucker (KKT) conditions.

- Studies the effect of HWIs at all system end terminals (i.e., at the AP, the UL user, and the DL user).

- Models all fading channels as Nakagami-m distribution which represents a more general model where some other channel models (such as Rayleigh, Weibull and Chi-squared distributions) can be considered as special cases. Moreover, Nakagami-m fits better than the other distributions for fading channels [27]. Furthermore, the channels' statistics are utilized rather than the instantaneous channels' states which reduce the system's complexity.

The rest of the chapter is structured as follows: The signal and system models are illustrated in Section 3.2. Performance analyses are provided and explained in Section 3.3. Next, power allocation optimization is presented in Section 3.4. After that, simulation results are discussed in Section 3.5. Finally, the work is concluded in Section 3.6.

3.2   System and Signal Models

This work considers the FD system model as in [12]. The AP is equipped with a single transmit and single receive antenna, and serves a single DL and single UL user, with each having a single HD antenna. h_u and h_d represent the UL channel between the UL user and AP, and the DL channel between the AP and DL user, respectively. Also, h_I represents the IUI channel between the UL and DL users, and h_s represents the residual SI channel between the AP's transmit and receive antennas. All channels are assumed to be independent and identically distributed (i.i.d) Nakagami-m fading channels with m_i shape parameter and Ω_i scale parameter, where $i \in \{u, d, s, I\}$. In literature, the residual

28

SI channel is modeled by Rayleigh distribution [12–14, 18]. Moreover, [118] modeled the SI as Rician distribution with a large K-factor because it has a strong LOS component before the active cancellation. Then, the experiments showed that the analog cancellation attenuated the strong LOS component of the SI channel and the residual SI channel follows a Rician distribution with a small K-factor or a Rayleigh distribution [12, 118]. It was also shown in [119] that a Rician distribution is well approximated by Nakagami-m. In addition, Nakagami-m fits better than Rayleigh distribution for fading channel [27] which makes it more tractable in the analysis.

3.3 System Performance Analysis

This section discusses the DL/UL SE performance of the FD SISO systems under the effects of HWIs and assuming Nakagami-m fading channels. It also studies the HD SISO system for a better understanding of the FD system and gets more insightful analyses. The residual impairments that are left after properly compensating the impaired signals at the transmitter and receiver, can be modeled as independent additive complex Gaussian noise with a zero mean and variance proportionate to the average signal power [1]. Considering the transceiver HWI model in (2.1) and (2.2), the actual transmitted signal over the channel becomes the impaired signal rather than the designated one, and the received signal of the impaired transceiver will be distorted by the non-idealities.

3.3.1 Full Duplex Downlink Spectral Efficiency under HWIs

Considering the FD DL scenario. The AP is supposed to transmit the intended signal $x_d \sim \mathcal{CN}(0,1)$ to the DL user. However, this signal is distorted by the HWIs at the AP, and then the received signal can be presented as

$$r_d = \underbrace{\sqrt{P_d \kappa^d \kappa_t^{\text{AP}}} h_d x_d}_{\text{Desired signal}} + \underbrace{\sqrt{P_u \kappa^d \kappa^u} h_I x_u}_{\text{IUI signal}} + \underbrace{\sqrt{\kappa^d} h_d \eta_{\text{AP}}^t + \sqrt{\kappa^d} h_I \eta_u + \eta_{\text{d}}}_{\text{Distortion noise}} + \underbrace{n_d}_{\text{AWGN}}, \qquad (3.1)$$

where P_d and P_u are the transmitted powers at the AP and UL user. $x_u \sim \mathcal{CN}(0,1)$ is the transmitted signal of the UL user and $n_d \sim \mathcal{CN}(0, \sigma_d^2)$ is AWGN at the DL user.

κ^u, κ^d and κ_t^{AP} are the HWI factors at the UL, DL users' antenna and AP's transmit antenna, and $\eta_u \sim \mathcal{CN}(0, (1 - \kappa^u)P_u)$, $\eta_d \sim \mathcal{CN}\left(0, (1 - \kappa^d)(P_u |h_I|^2 + P_d |h_d|^2)\right)$ and $\eta_{\mathrm{AP}}^t \sim \mathcal{CN}\left(0, (1 - \kappa_t^{\mathrm{AP}})P_d\right)$ are the hardware additive distortion noises at the UL, DL users and the AP's transmit antenna, respectively. Consequently, the received signal-to-interference-plus-noise ratio (SINR) γ_d can be expressed as

$$\gamma_d = \frac{P_d \kappa^d \kappa_t^{\mathrm{AP}} |h_d|^2}{P_u |h_I|^2 + (1 - \kappa^d \kappa_t^{\mathrm{AP}})P_d |h_d|^2 + \sigma_d^2}. \tag{3.2}$$

Now, using Jensen's inequality, the average DL SE can be lower bounded as [1,4]

$$\bar{\mathcal{R}}_d = \mathbb{E}\left\{\log_2\left(1 + \gamma_d\right)\right\} \geq \log_2\left(1 + \left(\mathbb{E}\left\{\frac{1}{\gamma_d}\right\}\right)^{-1}\right), \tag{3.3}$$

where $\mathbb{E}\{\cdot\}$ is the statistical expectation. Considering that h_d and h_I are independent, the term $\mathbb{E}\left\{\frac{1}{\gamma_d}\right\}$ can be calculated as

$$\mathbb{E}\left\{\frac{1}{\gamma_d}\right\} = \mathbb{E}\left\{\frac{P_u |h_I|^2}{P_d \kappa^d \kappa_t^{\mathrm{AP}}} + \frac{\sigma_d^2}{P_d \kappa^d \kappa_t^{\mathrm{AP}}}\right\} \mathbb{E}\left\{\frac{1}{|h_d|^2}\right\} + \frac{1 - \kappa^d \kappa_t^{\mathrm{AP}}}{\kappa^d \kappa_t^{\mathrm{AP}}}. \tag{3.4}$$

Assuming Nakagami-m fading, and using the fact that $\mathbb{E}\left\{\frac{1}{|h_d|^2}\right\} = \frac{m_d}{(m_d - 1)\Omega_d}$ and $\mathbb{E}\{|h_I|^2\} = \Omega_I$, where $m_d > 1$ is the shape parameter and Ω_d, Ω_I are the scale parameters of the Nakagami-m distribution [120, eq. 5], hence $\mathbb{E}\left\{\frac{1}{\gamma_d}\right\}$ can be given as

$$\mathbb{E}\left\{\frac{1}{\gamma_d}\right\} = \frac{m_d}{m_d - 1} \frac{P_u \Omega_I + \sigma_d^2}{P_d \kappa^d \kappa_t^{\mathrm{AP}} \Omega_d} + \frac{(1 - \kappa^d \kappa_t^{\mathrm{AP}})}{\kappa^d \kappa_t^{\mathrm{AP}}}. \tag{3.5}$$

By substituting (3.5) in (3.3), the lower bound of the average FD DL SE can be given as

$$\bar{\mathcal{R}}_d \geq \log_2\left(1 + \frac{P_d \Omega_d}{\frac{m_d}{m_d - 1} \frac{P_u \Omega_I + \sigma_d^2}{\kappa^d \kappa_t^{\mathrm{AP}}} + \frac{P_d(1 - \kappa^d \kappa_t^{\mathrm{AP}})\Omega_d}{\kappa^d \kappa_t^{\mathrm{AP}}}}\right). \tag{3.6}$$

It is worth mentioning that for a fixed UL power P_u, with P_d growing boundlessly, (3.6) can be bounded as

$$\lim_{P_d \to \infty} \bar{\mathcal{R}}_d \geq \log_2\left(\frac{1}{1 - \kappa^d \kappa_t^{\mathrm{AP}}}\right). \tag{3.7}$$

3.3.2 Full Duplex Uplink Spectral Efficiency under HWIs

Considering the FD UL scenario, the intended transmitted signal of the user $x_u \sim \mathcal{CN}(0, 1)$ is distorted by the HWIs. Then, following the same steps in the DL case, the average UL

SE can be lower bounded as

$$\bar{\mathcal{R}}_u \geq \log_2 \left(1 + \frac{P_u \Omega_u}{\frac{m_u}{m_u - 1} \frac{P_d \Omega_s + \sigma_u^2}{\kappa^u \kappa_r^{\text{AP}}} + \frac{P_u (1 - \kappa^u \kappa_r^{\text{AP}}) \Omega_u}{\kappa^u \kappa_r^{\text{AP}}}} \right), \tag{3.8}$$

where κ_r^{AP} is the HWI factor at the AP's receive antenna, σ_u^2 is the variance of AWGN at the AP's receive antenna, and Ω_s is the scale parameter of the Nakagami-m distribution of the SI channel. It is worth mentioning that for a fixed DL power P_d, with P_u growing boundlessly, (3.8) can be bounded as

$$\lim_{P_u \to \infty} \bar{\mathcal{R}}_u \geq \log_2 \left(\frac{1}{1 - \kappa^u \kappa_r^{\text{AP}}} \right). \tag{3.9}$$

Remark: as P_d and P_u grow without bound, $\bar{\mathcal{R}}^d$ and $\bar{\mathcal{R}}^u$ are upper bounded as

$$\bar{\mathcal{R}}_d \geq \left\{ \lim_{P_d, P_u \to \infty} \bar{\mathcal{R}}_d = \log_2 \left(\frac{\frac{m_d}{m_d - 1} \Omega_I + \Omega_d}{\frac{m_d}{m_d - 1} \Omega_I + \Omega_d (1 - \kappa^d \kappa_t^{\text{AP}})} \right) \right\}. \tag{3.10}$$

$$\bar{\mathcal{R}}_u \geq \left\{ \lim_{P_d, P_u \to \infty} \bar{\mathcal{R}}_u = \log_2 \left(\frac{\frac{m_u}{m_u - 1} \Omega_s + \Omega_u}{\frac{m_u}{m_u - 1} \Omega_s + \Omega_u (1 - \kappa^u \kappa_r^{\text{AP}})} \right) \right\}. \tag{3.11}$$

As demonstrated by this remark, the performance degradation in the FD system is accumulated by the SI, IUI, and HWIs. However, when fixing the transmit power of the AP and increasing the UL user power to approach a very large value, the system performance is only upper bounded by the HWI levels as shown in (3.7). The same is valid when fixing the UL user transmit power and increasing the transmit power of the AP to approach a very large value, as shown in (3.9). This happens because the HWIs force the system into an interference-limited regime, where no more SE performance gain can be obtained. This regime appears when cellular networks regularly operate these days. So, it emphasizes that studying the HWIs in the FD system is crucial.

To have a complete view of the effect of the HWIs on the FD system, the HD system is studied which can be used as a benchmark to compare and demonstrate the feasibility of the FD systems. Considering the DL scenario and assuming the absence of the IUI. From, (3.6) and neglecting the IUI, by setting $\Omega_I = 0$, the average lower bound HD DL SE can be obtained. Similar to the HD DL scenario, when neglecting the SI by setting $\Omega_s = 0$, the average lower bound HD UL SE can be obtained from (3.8).

3.4 Power Allocation Optimization

As explained before, the major challenges in FD systems are the SI, IUI and HWIs. To tackle these challenges, a power allocation optimization problem to maximize the average SE and EE by optimizing the UL and DL transmit power is formulated. This optimization considers the HWIs, power budget and QoS constraints. A novel algorithm to solve the problem by using the fractional programming and KKT conditions technique is proposed. As the EE refers to the benefit-cost ratio, it is defined as the ratio of the transmitted information bits to the total consumed energy. Hence, the EE optimization problem can be formulated as

$$\mathcal{OP}1: \quad \max_{P_d, P_u} \mathcal{E} = \frac{\bar{\mathcal{R}}_d \left(P_d, P_u\right) + \bar{\mathcal{R}}_u \left(P_d, P_u\right)}{P_d + P_u + P_c} \tag{3.12a}$$

$$\text{Subject to:} \quad \mathcal{C}1: \bar{\mathcal{R}}_d \left(P_d, P_u\right) \geq \mathcal{R}_{\text{th}}^d \tag{3.12b}$$

$$\mathcal{C}2: \bar{\mathcal{R}}_u \left(P_d, P_u\right) \geq \mathcal{R}_{\text{th}}^u \tag{3.12c}$$

$$\mathcal{C}3: 0 \leq P_d \leq P_d^{\max} \tag{3.12d}$$

$$\mathcal{C}4: 0 \leq P_u \leq P_u^{\max}, \tag{3.12e}$$

where P_c is the total power consumption in all circuit blocks, including the process to achieve a certain level of SI cancellation, $P_d^{\max}$ and $P_u^{\max}$ are the maximum power of the AP and UL user, $\bar{\mathcal{R}}_d \left(P_d, P_u\right)$ and $\bar{\mathcal{R}}_u \left(P_d, P_u\right)$ are defined in (3.6) and (3.8), and $\mathcal{R}_{\text{th}}^d$, $\mathcal{R}_{\text{th}}^u$ are the minimum SE requirements. The constraints $\mathcal{C}1$ and $\mathcal{C}2$ guarantee that the achievable SEs must satisfy $\mathcal{R}_{\text{th}}^d$ and $\mathcal{R}_{\text{th}}^u$, and the constraints $\mathcal{C}3$ and $\mathcal{C}4$ limit the power allocation to the defined budget. The optimization problem in (3.12) is a non-concave problem due to non-concavity of the objective function. As a result, obtaining an optimal solution is quite difficult. Fortunately, the fractional non-concave optimization problem in (3.12) can be transformed to an equivalent parametric optimization problem using the Dinkelbach approach [121].

Using this transformation, the new optimization problem can be reformulated in a form with its numerator and denominator decoupled as

$$\mathcal{OP}2: \quad \max_{P_d, P_u} \mathcal{F} = \bar{\mathcal{R}}_d\left(P_d, P_u\right) + \bar{\mathcal{R}}_u\left(P_d, P_u\right) - q(P_d + P_u + P_c) \tag{3.13a}$$

$$\text{Subject to:} \quad \mathcal{C}1 - \mathcal{C}4, \tag{3.13b}$$

where q is a non-negative constant. It was proved in [121] that P_d^* and P_u^* are optimal for (3.12) if and only if they are optimal for (3.13) for any $q = q^*$. Note that these results are correct without placing any convexity condition on (3.12). The parameter q is iteratively updated by

$$q^{(k+1)} = \frac{\bar{\mathcal{R}}_d\left(P_d^{(k)}, P_u^{(k)}\right) + \bar{\mathcal{R}}_u\left(P_d^{(k)}, P_u^{(k)}\right)}{P_d^{(k)} + P_u^{(k)} + P_c}, \tag{3.14}$$

where k is the iteration index, $q^{(1)}$ is the initial value (e.g. $q^{(1)} = 0$), and $(P_d^{(k)}, P_u^{(k)})$ are the power values obtained from the first iteration. It was proved in [121] that the convergence is guaranteed by alternatively updating q using (3.14) and solving for P_d and P_u in (3.13). The sub-optimal solution can be obtained, by solving (3.13) using the KKT conditions technique. Consequently, the related Lagrangian function can be given as

$$\mathcal{L}\left(P_d, P_u\right) = -\left(\bar{\mathcal{R}}_d\left(P_d, P_u\right) + \bar{\mathcal{R}}_u\left(P_d, P_u\right) - q(P_d + P_u + P_c)\right) - \lambda_1\left(\bar{\mathcal{R}}_d\left(P_d, P_u\right) - \mathcal{R}_{\text{th}}^d\right)$$
$$- \lambda_2\left(P_d^{\max} - P_d\right) - \lambda_3\left(\bar{\mathcal{R}}_u\left(P_d, P_u\right) - \mathcal{R}_{\text{th}}^u\right) - \lambda_4\left(P_u^{\max} - P_u\right), \tag{3.15}$$

where each Lagrange multiplier is given by $\lambda_i \geq 0, \forall i \in \{1, 2, 3, 4\}$.

Now, the KKT conditions can be written as [122].

$$\frac{\partial \mathcal{L}\left(P_d^*, P_u^*\right)}{\partial P_d} = 0, \tag{3.16a}$$

$$\frac{\partial \mathcal{L}\left(P_d^*, P_u^*\right)}{\partial P_u} = 0, \tag{3.16b}$$

$$\lambda_1^* \left(\bar{\mathcal{R}}_d\left(P_d^*, P_u^*\right) - \mathcal{R}_{\text{th}}^d\right) = 0, \tag{3.16c}$$

$$\lambda_2^* \left(P_d^{\max} - P_d^*\right) = 0, \tag{3.16d}$$

$$\lambda_3^* \left(\bar{\mathcal{R}}_u\left(P_d^*, P_u^*\right) - \mathcal{R}_{\text{th}}^u\right) = 0, \tag{3.16e}$$

$$\lambda_4^* \left(P_u^{\max} - P_u^*\right) = 0, \tag{3.16f}$$

$$\bar{\mathcal{R}}_d\left(P_d^*, P_u^*\right) - \mathcal{R}_{\text{th}}^d \geq 0, \tag{3.16g}$$

$$\left(P_d^{\max} - P_d^*\right) \geq 0, \tag{3.16h}$$

$$\bar{\mathcal{R}}_u\left(P_d^*, P_u^*\right) - \mathcal{R}_{\text{th}}^u \geq 0, \tag{3.16i}$$

$$\left(P_u^{\max} - P_u^*\right) \geq 0, \tag{3.16j}$$

$$\lambda_i^* \geq 0 \quad \forall i \in \{1, 2, 3, 4\}, \tag{3.16k}$$

where (3.16a) and (3.16b) can be given as

$$(1 + \lambda_1^*)\frac{\frac{m_d}{m_d - 1}(P_u^* \Omega_I + \sigma_d^2)\Omega_d \kappa^d \kappa_t^{\text{AP}}}{\ln(2)\left(\frac{m_d}{m_d - 1}\left(P_u^* \Omega_I + \sigma_d^2\right) + P_d^* \Omega_d\right)\left(\frac{m_d}{m_d - 1}\left(P_u^* \Omega_I + \sigma_d^2\right) + P_d^*(1 - \kappa^d \kappa_t^{\text{AP}})\Omega_d\right)} -$$

$$(1 + \lambda_3^*)\frac{\frac{m_u}{m_u - 1}(P_u^* \Omega_u \Omega_s \kappa^u \kappa_r^{\text{AP}})}{\ln(2)\left(\frac{m_u}{m_u - 1}\left(P_d^* \Omega_s + \sigma_u^2\right) + P_u^* \Omega_u\right)\left(\frac{m_u}{m_u - 1}\left(P_d^* \Omega_s + \sigma_u^2\right) + P_u^*(1 - \kappa^u \kappa_r^{\text{AP}})\Omega_u\right)} -$$

$$\lambda_2^* - q = 0, \tag{3.16a}$$

$$(1 + \lambda_1^*)\frac{\frac{-m_d}{m_d - 1}(P_d^* \Omega_d \Omega_I \kappa^d \kappa_t^{\text{AP}})}{\ln(2)\left(\frac{m_d}{m_d - 1}\left(P_u^* \Omega_I + \sigma_d^2\right) + P_d^* \Omega_d\right)\left(\frac{m_d}{m_d - 1}\left(P_u^* \Omega_I + \sigma_d^2\right) + P_d^*(1 - \kappa^d \kappa_t^{\text{AP}})\Omega_d\right)} +$$

$$(1 + \lambda_3^*)\frac{\frac{m_u}{m_u - 1}(P_d^* \Omega_s + \sigma_u^2)\Omega_u \kappa^u \kappa_r^{\text{AP}}}{\ln(2)\left(\frac{m_u}{m_u - 1}\left(P_d^* \Omega_s + \sigma_u^2\right) + P_u^* \Omega_u\right)\left(\frac{m_u}{m_u - 1}\left(P_d^* \Omega_s + \sigma_u^2\right) + P_u^*(1 - \kappa^u \kappa_r^{\text{AP}})\Omega_u\right)} -$$

$$\lambda_4^* - q = 0. \tag{3.16b}$$

Algorithm 1 Energy Efficiency KKT Conditions Solution

Inputs: $\left(\mathcal{R}_{\text{th}}^d, \mathcal{R}_{\text{th}}^u, P_d^{\max}, P_u^{\max}, P_c, \kappa_r^{\text{AP}}, \kappa_t^{\text{AP}}, \kappa^u, \kappa^d, \Omega_d, \Omega_u, \Omega_s, \Omega_I, m_d, m_u, \sigma_d^2, \sigma_u^2, \delta, q^{\text{init}} = 0\right)$

Solution: The solution can be obtained as follow, set $k = 1$ and $q^{(k)} = q^{\text{init}}$.

- **Step 1:** Solve (3.13) using the KKT conditions technique and calculate the sub-optimal solution P_d^* and P_u^* by setting $q = q^{(k)}$. Store $P_d^{(k)} = P_d^*$, $P_u^{(k)} = P_u^*$ and $q^* = q^{(k)}$.

- **Step 2:** Calculate $q^{(k+1)}$ from (3.14).

if $q^{(k+1)} - q^* > \delta$ **then**

  Update $q^* = q^{(k+1)}$, $k = k + 1$ and return to **Step 1**

else

  Update $q^* = q^{(k+1)}$ and stop.

end if

Outputs: P_d^*, P_u^* and q^*, where q^* is the maximum EE.

The sub-optimal solution can be obtained by solving (3.16a)-(3.16f) simultaneously, either analytically or numerically using any mathematical software (e.g., MATLAB). The obtained solution, though, must satisfy all the above KKT conditions. Since there are four constraints $\mathcal{C}1 - \mathcal{C}4$, there are four Lagrangian multipliers $\lambda_1 - \lambda_4$, and as such, 16 cases are possible corresponding for the binding or non-binding constraints. $\lambda_i \neq 0$ for the binding constraint and $\lambda_i = 0$ for the non-binding one $\forall i \in \{1, \cdots, 4\}$. Among these cases, the solution that gives the maximum value will be chosen. After that, this solution is used to update q in (3.14) until it converges to q^* when $q^{(k+1)} - q^{(k)} \leq \delta$ (the acceptable convergence tolerance). **Algorithm** 1 summarizes the proposed solution.

Fortunately, the maximum average FD SE can be obtained from (3.13) by setting $q = 0$ and only considering the solution of the first iteration in **Algorithm** 1. After that, the values of P_d^* and P_u^* are used to calculate the maximum FD SE from (3.6) and (3.8). In practice, P_c is known and can be obtained from the data sheet of the devices. Regarding P_d
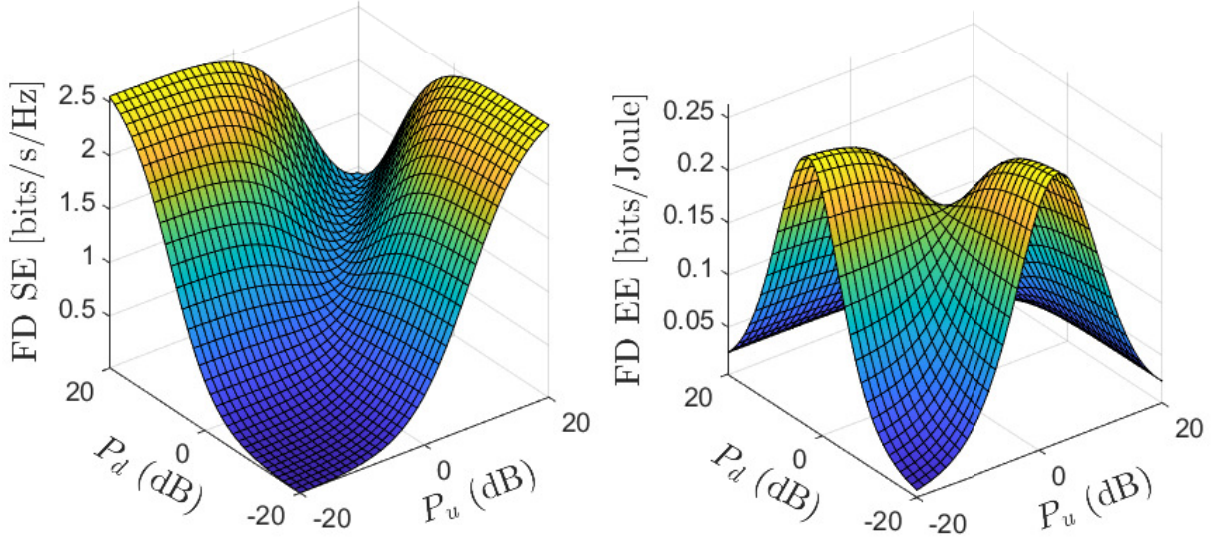
Figure 3.1: Average FD SE and EE with different transmit powers at $\kappa = 0.92$.

and P_u, these are the variables to be optimized and after the optimal values are obtained at the BS, the BS uses P_d in the DL transmission. Regarding the UL transmission, the BS feeds P_u back to the UL user to use it in the UL transmission.

3.5   Simulation Results and Discussion

Unless otherwise indicated, all fading channels are assumed to be Nakagami-m distribution with $m_x = 10$ shape parameter and $\Omega_x = 1$ scale parameter, where $x \in \{u, d, s, I\}$, $P_c = 0$ dBW (1 watt), $\sigma_d^2 = \sigma_u^2 = 1$, $\gamma_{0,d}^{\max} = P_d^{\max}/\sigma_d^2$, $\gamma_{0,u}^{\max} = P_u^{\max}/\sigma_u^2$, which is directly associated with the power budget, and without loss of generality, $\gamma_0 = \gamma_{0,d}^{\max} = \gamma_{0,u}^{\max}$, and $\kappa = \kappa_t^{\mathrm{AP}} = \kappa_r^{\mathrm{AP}} = \kappa^u = \kappa^d$. Extensive computer simulations were conducted to validate the theoretical derivations and the performance of the proposed algorithm.   Also, this work is compared with an exhaustive search scheme because it is the first work in this style and it can be a valuable resource for future works comparison.

Fig. 3.1 shows that both the average FD SE and EE are non-concave. It also shows the effect of increasing the UL/DL transmit powers on the average efficiencies in the case

36
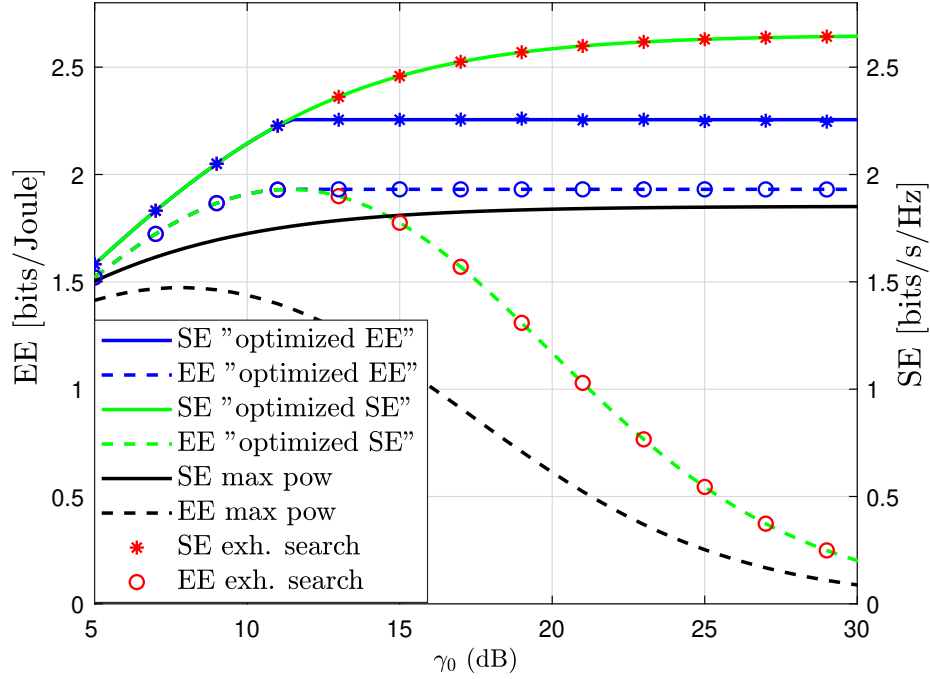
Figure 3.2: Average FD EE and SE with different scenarios at $\kappa = 1$, $\sigma_d^2 = \sigma_u^2 = 0.01$. Here, $\mathcal{R}_{\text{th}}^d = 0.5$ and $\mathcal{R}_{\text{th}}^u = 0.25$ bits/s/Hz.

where both UL/DL users have the same operating conditions. It is clear that transmitting maximum powers are not optimal in FD communication networks, where increasing the UL transmit power improves the UL performance. On the other hand, it has a detrimental impact on the DL performance. The same is valid when increasing the DL transmit power. So that, optimal power allocation is crucial in such networks.

Fig. 3.2 illustrates the average FD EE and SE at different scenarios when optimizing power allocation. The first scenario represents the efficiencies when maximizing the SE and it is illustrated by the green curves. The second scenario represents the efficiencies when maximizing the EE and it is illustrated by the blue curves. The third scenario represents the efficiencies when transmitting with the maximum power and it is illustrated by the black curves. This figure shows that a significant improvement is achieved, for both efficiencies, when using the proposed power allocation algorithm. It also illustrates that, in a low-power regime, the proposed SE and EE algorithms achieve the same performance. On the other hand, in the high power regime, sacrificing some SE can save a considerable
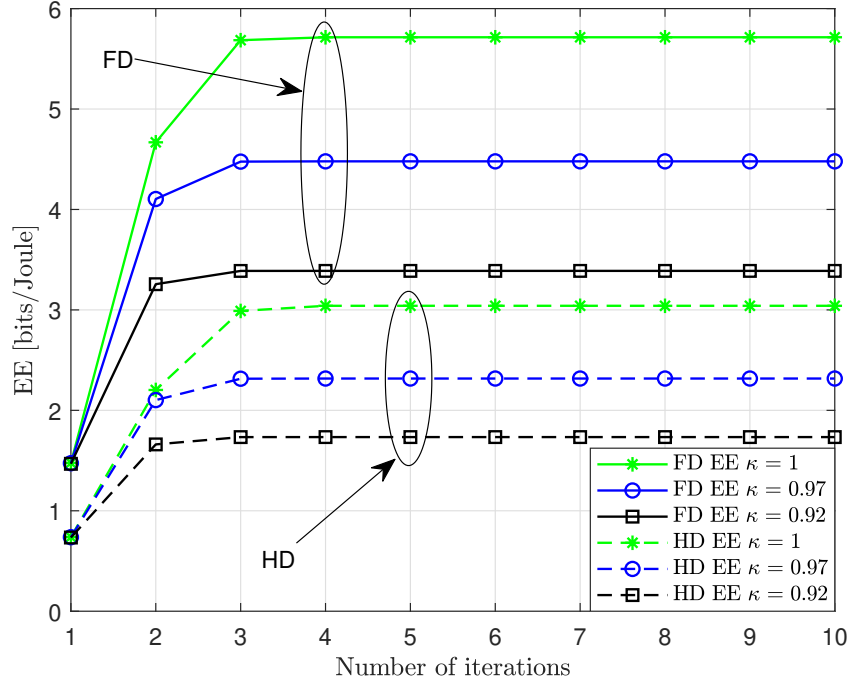
Figure 3.3: Convergence of the proposed algorithm when the transmit power budgets $P_d^{\max} = P_u^{\max} = 10$ dB, $\Omega_I = \Omega_s = \sigma_d^2 = \sigma_u^2 = 0.01$. Here, $\mathcal{R}_{\text{th}}^d = 1$ and $\mathcal{R}_{\text{th}}^u = 0.5$ bits/s/Hz.

Table 3.1: Optimal powers to maximize SE and EE.

	γ_0 (dB)	5	9	11	15	19	21	25	29
SE	$\gamma_{0,u}^*$ (dB)	-0.58	2.74	4.56	8.4	12.3	14.3	18.2	22.2
	$\gamma_{0,d}^*$ (dB)	5	9	11	15	19	21	25	29
EE	$\gamma_{0,u}^*$ (dB)	-0.58	2.74	4.56	4.9	4.9	4.9	4.9	4.9
	$\gamma_{0,d}^*$ (dB)	5	9	11	11.4	11.4	11.4	11.4	11.4

amount of energy when maximizing the EE because we stick with the optimal values even if an unlimited power budget is available as it can be seen in Table 3.1. This is very important as we are going toward green communications. Finally and most importantly, the performance of the proposed algorithm is compared with the exhaustive search scheme. It is clear that they achieve the same performance which implies the proposed solution reaches the optimal one. This emphasizes the effectiveness of the proposed algorithm in

reducing the system's complexity.

Fig. 3.3 shows the convergence of the proposed algorithm of the FD and HD systems, for a certain set of parameters, at different levels of HWIs. It is remarked that the proposed algorithm presents monotonic convergence within a few iterations for both systems. Also, it was verified by simulation that the convergence behaviour is the same when using different parameters. Moreover, this figure illustrates the negative impact of the HWIs on EE performance of the systems. This degradation is worsened when increasing HWIs level. In addition, it shows that the EE performance of FD is about double of the HD system under the same HWIs level.

Fig. 3.4 discusses the performance of the proposed algorithm. It illustrates the effect of increasing the transmit power budget on SE and EE performance of both the FD and HD considering different levels of HWIs. Here, the FD SE and EE outperform the HD performance when there is a good SI cancellation. Also, in the case of ideal hardware, the SEs of the FD and HD grow when increasing the transmit power. On the other hand, they saturate due to the HWIs, at high power regions where no more benefit can be obtained by increasing the transmit power. Also, increasing the transmit power improves the EEs of both the FD and HD until a certain value where a maximum EE is achieved, and after this peak, no further improvements can be obtained. Interestingly, this is true for both the ideal and the impaired systems.

Fig. 3.5 demonstrates the SE and EE performance of the proposed algorithm for both the FD and HD considering various values of SI under different levels of HWIs. Here, when the SI has small values, the FD outperform the HD in terms of both the SE and EE. However, as the SI increases, the performance of the FD decreases where it reaches a point when it underperforms the HD. This point depends on the HWIs factor. The interesting observation here is that the impaired FD systems outperform the ideal HD at a range of SI values which relaxes some design restrictions.
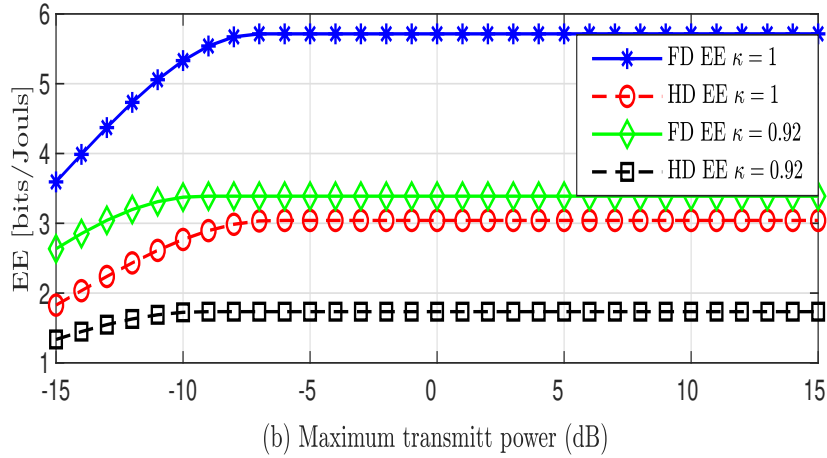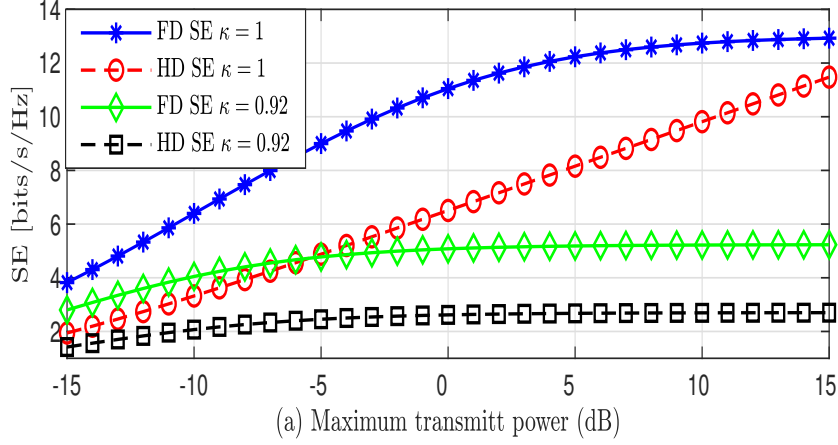
Figure 3.4: Average FD/HD SE and EE at $\Omega_I = \Omega_s = \sigma_d^2 = \sigma_u^2 = 0.01$. Here, $\mathcal{R}_{\text{th}}^d = 1$ and $\mathcal{R}_{\text{th}}^u = 0.5$ bits/s/Hz.

3.6 Conclusion

The potential of FD wireless communication networks under the effect of HWIs has been investigated in this chapter. Power allocation optimization problem is formulated. Then, a novel algorithm has been proposed to solve them by utilizing the fractional programming theory and KKT conditions technique.

The results show that the average FD SE is upper bounded due to the HWIs even if the powers grow boundlessly. The interesting remark of this study is that by employing
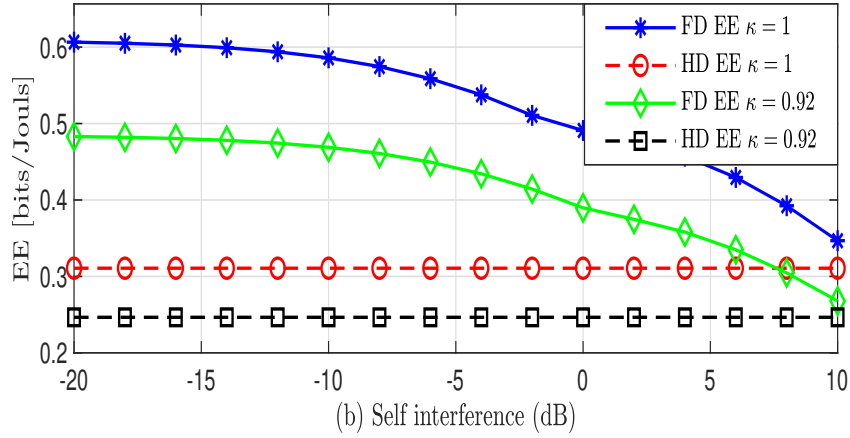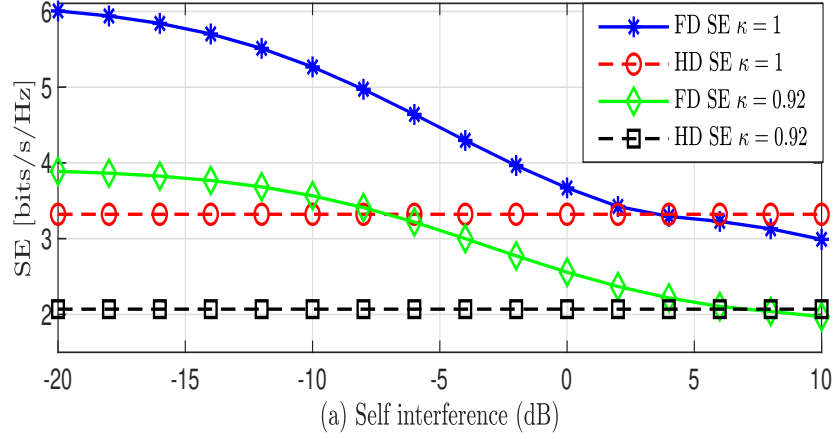
Figure 3.5: Average FD/HD SE and EE with different levels of SI at $\Omega_I = 0.05$, $P_d = P_u =$ 10 dB. Here, $\mathcal{R}_{\text{th}}^d = 1$ and $\mathcal{R}_{\text{th}}^u = 0.1$ bits/s/Hz.

a good SI cancellation, the impaired FD communications beat the HD communications with ideal hardware; that implies FD is more robust against HWIs than HD. This, in turn, relaxes the design constraints of FD systems. Finally, the results reveal that proper power allocation is critical in FD communication networks and the FD systems are spectrum and energy-efficient.

Chapter 4

Spectral-Energy Efficiency and Power Allocation in Full-Duplex Networks: the Effects of Hardware Impairment and Nakagami-m Fading Channels

4.1   Introduction and Related Works

T<small>HE</small> ubiquitous nature of wireless systems has made them an essential part of everyday life. According to the International Telecommunication Union forecast, global mobile data traffic is expected to increase by approximately 55 percent annually from 2020 to 2030, reaching 607 exabytes (EB) in 2025 and 5,016 EB in 2030 [123]. This growth is driven by a number of factors, including the increasing adoption of smartphones and other mobile devices, the rollout of 5G networks, and the growing popularity of mobile applications and streaming services. In a report done by Cisco Systems, Inc., it was predicted that the number of networked devices will approach 29.3 billion in 2023 [2]. Such growth will naturally be accompanied by demands for higher data rates, lower latency, and greater spectral efficiency. All of the above present themselves as major challenges for the upcoming generations of wireless communication systems. FD communication has

emerged as a promising technique to enhance SE in wireless systems [12–14, 17–19]. In FD communication, SE can be theoretically doubled since the signals can be transmitted and received using the same time-frequency resources. As such, FD devices have the ability to transmit and receive all the time using the entire bandwidth. On the other hand, HD communication uses either different frequency bands or different time slots to transmit and receive signals. The implication here is that FD communication is more spectrum-efficient than HD communication [20, 21].

However, the main challenge regarding FD is that interference can severely affect the UL and DL signals. In particular, SI affects the UL received signals at the BS, where it may be observed that the received signal strength is much weaker than that of the SI signal [20]. On the other hand, the IUI affects the DL received signal at the user. To this end, substantial work has been done to tackle SI suppression and cancellation. For example, the authors in [21] investigated potential FD techniques, including passive suppression, active analog cancellation, and active digital cancellation. Furthermore, analog and digital SI cancellation were studied in [94], where it was concluded that a combination of antenna cancellation, analog interference cancellation and digital interference cancellation can greatly reduce the SI. The authors in [93] showed that SI can also be mitigated using passive suppression.

In a practical sense, physical transceivers inevitably suffer from HWIs, such as analog imperfectness, phase noise, in-phase quadrature-phase imbalance (IQI), power amplifier nonlinearities, as well as time and frequency synchronization errors. In [111], it was shown that the system performance saturates at a high SNR due to the HWIs, at which point no further improvement can be achieved. Moreover, the authors in [116] illustrated that HWIs can dramatically degrade the localization performance. Furthermore, the study in [23] demonstrated the harmful effects of IQI on the system performance, illustrating that this effect is maximized in the case of imperfect channel state information. Besides, the work in [17, 18] showed that the sum rate of the FD system is degraded because of the quantization noise that occurs when low-resolution ADCs/DACs are used.

However, the analysis in [12, 19, 99] was done assuming ideal hardware. Additionally, all the mentioned works assumed Rayleigh or Rician fading models. Based on this, and moti-

vated by the importance of this topic, the contributions of this chapter can be summarized as follows

- Studies the average SE of FD MIMO systems by assuming imperfect hardware at all the end terminals of the system (i.e., at the BS, the UL user and the DL user). Closed-form expressions for the lower bounds of the UL and DL achievable rates are derived by exploiting the relationship between various distributions (e.g., Gamma, inverse of Gamma and Beta distribution). In addition, the average SE of UL/DL HD expressions are derived for comparative purposes.

- Formulates power allocation optimization problems to maximize the average FD SE, max-min SE, EE and max-min EE with QoS and power budget constraints. Algorithms to solve these problems using different optimization techniques are proposed. The KKT conditions technique solves the optimization problem that maximizes the SE. Moreover, two optimization techniques to solve the max-min SE optimization problem by introducing a slack variable and an appropriate transformation are combined. Furthermore, to maximize the EE and the max-min EE, the Dinkelbach approach is utilized to transform the fractional non-concave optimization problem into an equivalent parametric optimization. Interestingly, the FD SE algorithm is refined and presents a simpler solution.

- Compares the proposed solutions with the exhaustive search ones. Our results indicate a match in performance.

- Relies on the channels' statistical information rather than the instantaneous states of the channels, which increases the overall SE and EE without the cost of greater complexity. That said, our algorithms can be used to find the optimal power allocation when maximizing the instantaneous FD SE and EE.

- Models all fading channels as Nakagami-m distributions, where it was shown in [27,48] that the Nakagami-m distribution provides a better fitting model for general and special fading channels (e.g., Rayleigh distribution, where the shape parameter $m = 1$).
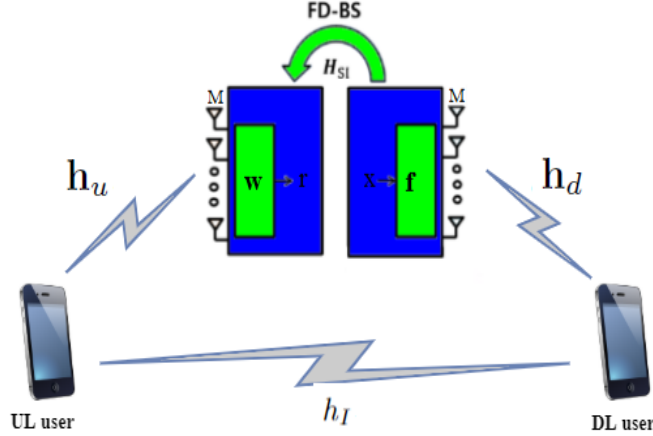
Figure 4.1: Full-duplex MIMO system model.

The rest of the chapter is structured as follows: The signal and system models are illustrated in Section 4.2. Performance analyses are provided and explained in Section 4.3. Next, the power allocation optimization is presented in Section 4.4. After that, simulation results are discussed in Section 4.5. Finally, the work is concluded in Section 4.6.

4.2   System and Signal Models

In this section, the considered system model is explained in detail and the signal model under HWIs is discussed. It also illustrates some useful preliminaries and principles about the Gamma distribution and random variables that will be used later in this chapter.

4.2.1   Gamma Distribution

A circularly symmetric complex Gaussian vector $\mathbf{v}$ is denoted as $\mathbf{v} \sim \mathcal{CN}(\mathbf{0}, \mathbf{\Sigma})$, where $\mathbf{0}$ is the mean vector and $\mathbf{\Sigma}$ is the covariance matrix. $X \sim \text{Gamma}(a, \theta)$ denotes a Gamma distribution with a shape and θ scale parameters, respectively. If $X \sim \text{Gamma}(a, \theta)$ and $Y \sim \text{Gamma}(b, \theta)$ are independent random variables, then $Z = \frac{X}{X+Y} \sim \text{Beta}(a, b)$, where a and b are the shape parameters of the Beta distribution. Next, a random variable $N \sim \text{Nakagami}(m, \Omega)$, with m shape and Ω scale parameters, can be obtained from a random variable $X \sim \text{Gamma}(a, \theta)$, by setting $a = m, \theta = \Omega/m$, and taking the square

root of $X \to N = \sqrt{X}$. If X_i has a Gamma(a_i, θ) distribution for $i = 1, 2, ..., M$ (i.e., all distributions have the same scale parameter θ), then $\sum_{i=1}^{M} X_i \sim$ Gamma $\left(\sum_{i=1}^{M} a_i, \theta \right)$. In addition, if $X \sim$ Gamma(a, θ) then $1/X \sim$ Inv-Gamma$(a, 1/\theta)$ is the inverse Gamma distribution. If $\mathbf{X} = \text{diag}(x_1, x_2)$ then $\mathbf{X}_{1,1} = x_1$, $\mathbf{X}_{2,2} = x_2$ and $\mathbf{X}_{1,2} = \mathbf{X}_{2,1} = 0$.

4.2.2 System Model

This work considers the single-cell FD MIMO system illustrated in Fig. 4.1. It consists of a BS that has M transmit antennas and M receive antennas serving one DL user and one UL user, each equipped with one HD antenna. Due to the FD mode, SI exists at the BS, which is the interference from the transmit antenna array to the receive antenna array. Interference cancellation is usually conducted to reduce the SI; $\mathbf{H}_{\text{SI}} \in \mathbb{C}^{M \times M}$ represents the residual SI channel matrix, whose entries' magnitude can be modeled as Nakagami-m independent and identically distributed (i.i.d.) fading channels, where each element has m_s shape parameter and Ω_s scale parameter. IUI from the UL to DL user is assumed. The UL channel vector, from the UL user to the BS, is denoted as $\mathbf{h}_u \in \mathbb{C}^{M \times 1}$. Similarly, the DL channel vector, from the BS to the DL user, is denoted as $\mathbf{h}_d \in \mathbb{C}^{M \times 1}$.

Moreover, it is assumed that the magnitude of $\mathbf{h}_u$ and $\mathbf{h}_d$ entries following Nakagami-m i.i.d fading, where each element of $\mathbf{h}_u$ and $\mathbf{h}_d$ has m_u, m_d shape parameters and Ω_u, Ω_d scale parameters, respectively. Furthermore, h_I represents the channel realization between the UL and the DL users. The magnitude of h_I is modeled as Nakagami-m fading with the m_I shape parameter and the Ω_I scale parameter. Finally, this work assumes that the BS knows the channels' state information and their statistics.

The literature has always modeled the residual SI channel by Rayleigh distributions [12–14, 17, 18]. Moreover, [118] modeled the SI as a Rician distribution with a large K-factor because it has a strong LOS component before the active cancellation. Then, the experiments showed that analog cancellation attenuated the strong LOS component of the SI channel. Hence, the residual SI channel follows a Rayleigh or a Rician distribution with a small K-factor [12, 118]. It was also shown in [119] that Nakagami-m accurately approximates the Rician distribution. In addition, Nakagami-m fits better than the Rayleigh

distribution for fading channel [27], which makes it more tractable in the analysis.

4.3   System Performance Analysis

This section discusses the SE performance in FD MIMO wireless communication systems under the effects of HWIs at the transceiver and assuming Nakagami-m fading channels. Furthermore, it is assumed that the BS consists of a homogeneous and identical set of antennas and that the hardware factors are the same for each antenna. HWIs are present in all practical wireless communication systems because the transceivers have many electronic circuits that can distort the signals in numerous ways. Therefore, a mismatch between the intended signal and the actual one can occur. The HWIs at the BS antennas and the end-users transmitter and receiver are considered. The transceiver HWIs model in (2.1) shows that the designated transmit signal will be affected by the HWIs at the transmitter. As a result, the actual transmitted signal over the channel will suffer from the distortion. Similarly, The transceiver HWIs model in (2.2) shows that the signal at the receiver suffers from the hardware imperfections.

Uplink scenario in FD MIMO systems: The transmitted data signal of the UL user is x_u. By applying the model in (2.1), $\tilde{x}_u = \sqrt{\kappa^u P_u} x_u + \eta_u$ will be sent instead of the original data x_u. Here, $\kappa^u \in (0, 1]$ determines the quality of the UL user's transmitter hardware, P_u is the transmitted power by the UL user, and $\eta_u \sim \mathcal{CN}(0, (1 - \kappa^u)P_u)$ is the hardware additive distortion noise of the UL user's transmitter.

Downlink scenario in FD MIMO systems: The BS is supposed to transmit the intended data signal x_d for the DL user. The BS applies the MRT precoding vector $\mathbf{f}_d = \frac{\mathbf{h}_d}{\|\mathbf{h}_d\|}$, which depends on the current channel realizations. As such, the transmitted vector over the channel becomes $\mathbf{s}_d = \sqrt{P_d}\frac{\mathbf{h}_d}{\|\mathbf{h}_d\|} x_d$ instead of x_d, where P_d is the total average transmit power by the BS. Since this signal suffers from the HWIs at the BS, the HWIs model from (2.1) can be applied to describe the impairments in the hardware attached to each transmit BS antenna. It is assumed that the transceiver hardware at different BS antennas is decoupled so that the respective distortion terms are independent. Finally, the transmitted data vector over the channel is $\tilde{\mathbf{s}}_d = \sqrt{\kappa_t^{\mathrm{BS}}}\mathbf{s}_d + \boldsymbol{\eta}_{\mathrm{BS}}^t$, where the factor $\kappa_t^{\mathrm{BS}} \in (0, 1]$ determines the quality of the BS transmitter hardware, and the hardware

additive distortion noise $\boldsymbol{\eta}^t_{\text{BS}} \in \mathbb{C}^{M \times 1}$ can be given as

$$\boldsymbol{\eta}^t_{\text{BS}} \sim \mathcal{CN}\left(\mathbf{0}_\text{M}, \mathbf{C}^t_{\boldsymbol{\eta}_{\text{BS}}}\right). \tag{4.1}$$

The covariance matrix $\mathbf{C}^t_{\boldsymbol{\eta}_{\text{BS}}} \in \mathbb{C}^{M \times M}$ is given as

$$\mathbf{C}^t_{\boldsymbol{\eta}_{\text{BS}}} = P_d(1 - \kappa^{\text{BS}}_t) \, \text{diag}\left(\frac{|h_d^{(1)}|^2}{\|\mathbf{h}_d\|^2}, \frac{|h_d^{(2)}|^2}{\|\mathbf{h}_d\|^2}, \cdots, \frac{|h_d^{(M)}|^2}{\|\mathbf{h}_d\|^2}\right), \tag{4.2}$$

where $h_d^{(m)}$ denotes the mth element of $\mathbf{h}_d$.

4.3.1 Full Duplex Uplink Spectral Efficiency with Hardware Impairments Analysis

This section discusses the impact of HWIs on the system performance in the UL scenario, where the received signal at the BS can be written as

$$\mathbf{r}_u = \sqrt{\kappa^{\text{BS}}_r}\mathbf{h}_u \tilde{x}_u + \sqrt{\kappa^{\text{BS}}_r}\mathbf{H}_{\text{SI}}\tilde{\mathbf{s}}_d + \boldsymbol{\eta}^r_{\text{BS}} + \mathbf{n}_u, \tag{4.3}$$

where $\mathbf{r}_u \in \mathbb{C}^{M \times 1}$, $\mathbf{n}_u \sim \mathcal{CN}\left(\mathbf{0}, \sigma^2_u\mathbf{I}_M\right)$ is the AWGN noise at the BS receive array, $\boldsymbol{\eta}^r_{\text{BS}} \sim \mathcal{CN}(\mathbf{0}_M, \mathbf{C}^r_{\boldsymbol{\eta}_{\text{BS}}})$ denotes the receiver distortion at the BS, and the covariance matrix $\mathbf{C}^r_{\boldsymbol{\eta}_{\text{BS}}} = (1 - \kappa^{\text{BS}}_r)[\mathbf{A} + \mathbf{B}]$, where the factor $\kappa^{\text{BS}}_r \in (0, 1]$ determines the quality of the BS receiver hardware, $\mathbf{A} \in \mathbb{C}^{M \times M}$ and $\mathbf{B} \in \mathbb{C}^{M \times M}$ are given as

$$\mathbf{A} = P_u \, \text{diag}\left(|h_u^{(1)}|^2, |h_u^{(2)}|^2, \cdots, |h_u^{(M)}|^2\right), \tag{4.4}$$

$$\mathbf{B} = P_d \, \text{diag}\left(\sum_{i=1}^{\text{M}}\left|\mathbf{H}^{1,i}_{\text{SI}}\frac{h_d^{(i)}}{\|\mathbf{h}_d\|}\right|^2, \sum_{i=1}^{\text{M}}\left|\mathbf{H}^{2,i}_{\text{SI}}\frac{h_d^{(i)}}{\|\mathbf{h}_d\|}\right|^2, \cdots, \sum_{i=1}^{M}\left|\mathbf{H}^{M,i}_{\text{SI}}\frac{h_d^{(i)}}{\|\mathbf{h}_d\|}\right|^2\right), \tag{4.5}$$

where $h_u^{(m)}$ denotes the mth element of $\mathbf{h}_u$ and $\mathbf{H}^{k,i}_{\text{SI}}$ is the ith element of the kth row of $\mathbf{H}_{\text{SI}}$. By substituting $\tilde{x}_u$ and $\tilde{\mathbf{s}}_d$ values in (4.3) the received signal can be given as

$$\mathbf{r}_u = \underbrace{\sqrt{P_u\kappa^{\text{BS}}_r\kappa^{\text{u}}}\,\mathbf{h}_u x_u}_{\text{Desired signal}} + \underbrace{\sqrt{P_d\kappa^{\text{BS}}_r\kappa^{\text{BS}}_t}\left(\frac{\mathbf{H}_{\text{SI}}\mathbf{h}_d}{\|\mathbf{h}_d\|}x_d\right)}_{\text{SI signal}} + \underbrace{\sqrt{\kappa^{\text{BS}}_r}\mathbf{h}_u\eta_{\text{u}} + \sqrt{\kappa^{\text{BS}}_r}\mathbf{H}_{\text{SI}}\boldsymbol{\eta}^t_{\text{BS}} + \boldsymbol{\eta}^r_{\text{BS}}}_{\text{Distortion noise}=\boldsymbol{\eta}^c_u} + \underbrace{\mathbf{n}_u}_{\text{AWGN}}.$$

$$\tag{4.6}$$

All additive distortions in (4.6) can be combined as $\boldsymbol{\eta}_u^c \sim \mathcal{CN}(\mathbf{0}_{\mathrm{M}}, \mathbf{C}_{\boldsymbol{\eta}_u^c})$, and the covariance matrix $\mathbf{C}_{\boldsymbol{\eta}_u^c} = (1 - \kappa_r^{\mathrm{BS}}\kappa^u)\mathbf{A} + (1 - \kappa_r^{\mathrm{BS}}\kappa_t^{\mathrm{BS}})\mathbf{B}$.

Now, MRC [1] linear detector can be applied at the BS to detect the UL transmitted signal. From (4.6), and considering the receive combining vector $\mathbf{w} = \mathbf{h}_u \in \mathbb{C}^{M \times 1}$, the received signal $r_u = \mathbf{w}^{\mathrm{H}}\mathbf{r}_u$ can be written as

$$r_u = \underbrace{\sqrt{\kappa_r^{\mathrm{BS}}\kappa^{\mathrm{u}} P_u}\mathbf{h}_u^{\mathrm{H}}\mathbf{h}_u x_u}_{\text{Desired signal}} + \underbrace{\sqrt{\kappa_r^{\mathrm{BS}}\kappa_t^{\mathrm{BS}} P_d}\frac{\mathbf{h}_u^{\mathrm{H}}\mathbf{H}_{\mathrm{SI}}\mathbf{h}_d}{\|\mathbf{h}_d\|}x_d}_{\text{SI signal}}$$
$$+ \underbrace{\sqrt{\kappa_r^{\mathrm{BS}}}\left(\mathbf{h}_u^{\mathrm{H}}\mathbf{h}_u\right)\eta_{\mathrm{u}} + \sqrt{\kappa_r^{\mathrm{BS}}}\mathbf{h}_u^{\mathrm{H}}\mathbf{H}_{\mathrm{SI}}\boldsymbol{\eta}_{\mathrm{BS}}^t + \mathbf{h}_u^{\mathrm{H}}\boldsymbol{\eta}_{\mathrm{BS}}^r}_{\text{Distortion noise}} + \underbrace{\mathbf{h}_u^{\mathrm{H}}\mathbf{n}_u}_{\text{AWGN}}. \quad (4.7)$$

Now, the received signal-to-interference-plus-noise ratio (SINR), γ_u, at the BS can be calculated from the received signal in (4.7) as

$$\gamma_u = \frac{\kappa_r^{\mathrm{BS}}\kappa^{\mathrm{u}} P_u \|\mathbf{h}_u\|^4}{\kappa_r^{\mathrm{BS}}\kappa_t^{\mathrm{BS}} P_d \left|\frac{\mathbf{h}_u^{\mathrm{H}}\mathbf{H}_{\mathrm{SI}}\mathbf{h}_d}{\|\mathbf{h}_d\|}\right|^2 + \mathbf{h}_u^{\mathrm{H}}\mathbf{C}_{\boldsymbol{\eta}_u^c}\mathbf{h}_u + \|\mathbf{h}_u\|^2\sigma_u^2}. \quad (4.8)$$

Consequently, the instantaneous UL SE can be calculated as $\mathcal{R}_u = \log_2\left(1 + \gamma_u\right)$, which is in bits/sec/Hz.

Lemma 4.3.1 *In full duplex MIMO communication systems under the presence of hardware impairments and Nakagami-m fading, the average UL achievable rate can be lower bounded as*

$$\bar{\mathcal{R}}_u \geq \log_2\left(1 + \bar{\gamma}_u\right), \quad (4.9)$$

where

$$\bar{\gamma}_u = \frac{P_u\kappa^{\mathrm{u}}\kappa_r^{\mathrm{BS}}(Mm_u - 1)\Omega_u}{P_d m_u\Omega_s + m_u\sigma_u^2 + \frac{P_u(Mm_u - 1)(m_u + 1)(1 - \kappa_r^{\mathrm{BS}}\kappa^u)\Omega_u}{(Mm_u + 1)}}. \quad (4.10)$$

Proof: See Appendix A.1.

Remark 1: For a fixed DL power P_d, with P_u growing boundlessly, then

$$\lim_{P_u \to \infty} \bar{\mathcal{R}}_u \geq \log_2\left(1 + \frac{\kappa_r^{\mathrm{BS}}\kappa^{\mathrm{u}}(Mm_u + 1)}{(m_u + 1)\left(1 - \kappa_r^{\mathrm{BS}}\kappa^u\right)}\right). \quad (4.11)$$

[1]There are other techniques, such as ZF and minimum mean-square-error (MMSE), that can be used. However, the linear MRC detector and MRT precoder are considered because they are the simplest ones.

4.3.2 Full Duplex Downlink Spectral Efficiency with Hardware Impairments Analysis

This section explains the impact of HWIs on the system performance in the DL scenario, where the received signal at the DL user can be calculated as

$$r_d = \sqrt{\kappa^d} \mathbf{h}_d^{\mathrm{H}} \tilde{\mathbf{s}}_d + \sqrt{\kappa^d} h_I \tilde{x}_u + \eta_d + n_d, \tag{4.12}$$

where, $n_d \sim \mathcal{CN}(0, \sigma_d^2)$ is the AWGN at the DL user, $\kappa^d \in (0, 1]$ determines the quality of the DL user's receiver hardware, and $\eta_d \sim \mathcal{CN}\left(0, (1 - \kappa^d)(a + b)\right)$ is the distortion noise at the DL user, in which a and b are given as $a = P_u |h_I|^2$ and $b = P_d \sum_{l=1}^{M} \frac{\left|h_d^{(l)}\right|^4}{\|\mathbf{h}_d\|^2}$. By substituting the values of $\tilde{\mathbf{s}}_d$ and $\tilde{x}_u$ in (4.12), the received signal at the user can be written as

$$r_d = \underbrace{\sqrt{\kappa^d \kappa_t^{\mathrm{BS}} P_d} \mathbf{h}_d^{\mathrm{H}} \frac{\mathbf{h}_d}{\|\mathbf{h}_d\|} x_d}_{\text{Desired signal}} + \underbrace{\sqrt{\kappa^d \kappa^u P_u} h_I x_u}_{\text{IUI signal}} + \underbrace{\sqrt{\kappa^d} h_I \eta_u + \sqrt{\kappa^d} \mathbf{h}_d^{\mathrm{H}} \boldsymbol{\eta}_{\mathrm{BS}}^t + \eta_{\mathrm{d}}}_{\text{Distortion noise}=\eta_d^c} + \underbrace{n_d}_{\text{AWGN}}. \tag{4.13}$$

The accumulative distortions in (4.13) can be combined as $\eta_d^c \sim \mathcal{CN}(0, \sigma_{\eta_d^c}^2)$, where $\sigma_{\eta_d^c}^2 = (1 - \kappa^d \kappa^u)a + (1 - \kappa^d \kappa_t^{\mathrm{BS}})b$. The received signal-to-interference-plus-noise ratio (SINR) γ_d at the DL user can consequently be calculated from the received signal in (4.13) as

$$\gamma_d = \frac{P_d \kappa^d \kappa_t^{\mathrm{BS}} \|\mathbf{h}_d\|^2}{P_u \kappa^d \kappa^u |h_I|^2 + \sigma_{\eta_d^c}^2 + \sigma_d^2}. \tag{4.14}$$

Consequently, the instantaneous DL SE can be calculated as

$$\mathcal{R}_d = \log_2 \left(1 + \frac{P_d \kappa^d \kappa_t^{\mathrm{BS}} \|\mathbf{h}_d\|^2}{P_u \kappa^d \kappa^u |h_I|^2 + \sigma_{\eta_d^c}^2 + \sigma_d^2} \right). \tag{4.15}$$

Lemma 4.3.2 *In full duplex MIMO communication systems under the presence of hardware impairments and Nakagami-m fading, the average download achievable rate can be lower bounded as*

$$\bar{\mathcal{R}}_d \geq \log_2 \left(1 + \bar{\gamma}_d \right), \tag{4.16}$$

where

$$\bar{\gamma}_d = \frac{P_d \kappa^d \kappa_t^{\mathrm{BS}} (M m_d - 1) \Omega_d}{P_u m_d \Omega_I + m_d \sigma_d^2 + \frac{P_d (M m_d - 1)(m_d + 1)(1 - \kappa^d \kappa_t^{\mathrm{BS}}) \Omega_d}{(M m_d + 1)}}. \tag{4.17}$$

Proof: See Appendix A.2.

Remark 2: For a fixed UL power P_u, with P_d growing boundlessly, then

$$\lim_{P_d \to \infty} \bar{\mathcal{R}}_d \geq \log_2 \left(1 + \frac{\kappa^d \kappa_t^{\text{BS}}(Mm_d + 1)}{(m_d + 1)(1 - \kappa^d \kappa_t^{\text{BS}})} \right). \tag{4.18}$$

Remark 3: As P_d and P_u grow without bound, $\bar{\mathcal{R}}^d$ and $\bar{\mathcal{R}}^u$ are upper bounded as

$$\bar{\mathcal{R}}_u \geq \left\{ \lim_{P_d,P_u \to \infty} \bar{\mathcal{R}}_u = \log_2 \left(1 + \frac{\kappa^u \kappa_r^{\text{BS}}(Mm_u + 1)}{\frac{m_u(Mm_u+1)\Omega_s}{(Mm_u-1)\Omega_u} + (m_u + 1)\left(1 - \kappa_r^{\text{BS}}\kappa^u\right)} \right) \right\}. \tag{4.19}$$

$$\bar{\mathcal{R}}_d \geq \left\{ \lim_{P_d,P_u \to \infty} \bar{\mathcal{R}}_d = \log_2 \left(1 + \frac{\kappa^d \kappa_t^{\text{BS}}(Mm_d + 1)}{\frac{m_d(Mm_d+1)\Omega_I}{(Mm_d-1)\Omega_d} + (m_d + 1)(1 - \kappa^d \kappa_t^{\text{BS}})} \right) \right\}. \tag{4.20}$$

Discussion of the effects of the HWIs and Interference

- It can be inferred from (4.9) and (4.16) that the HWIs degrade the system's performance because the factors κ^u, κ^d, κ_t^{BS} and κ_r^{BS} are less than one.

- From (4.9), the HWIs on the UL side do not affect the DL SE, as no UL HWI terms can be seen in this equation. The same is correct for the DL side and can be noticed in (4.16).

- As demonstrated by *Remark 3*, the performance degradation in the FD system is accumulated by the SI, IUI, and HWIs. However, when fixing the transmit power of the UL user and increasing the BS power to approach a very large value, the system performance is only upper bounded by the HWI levels as shown in (4.18). The same is valid when fixing the BS transmit power and increasing the transmit power of UL user to approach a very large value, as shown in (4.11). This happens because the HWIs force the system into an interference-limited regime, where no more SE performance gain can be obtained. This regime appears when cellular networks regularly operate these days, emphasizing the relevance of HWIs in FD systems.

4.3.3 Half Duplex Uplink Spectral Efficiency with Hardware Impairments

This section discusses the impact of HWIs on the HD system's performance in the UL scenario, which will be used for comparison and to demonstrate the feasibility of FD systems.

The received signal can be written as

$$\mathbf{y}_u = \sqrt{\kappa_r^{\mathrm{BS}}} \mathbf{h}_u \tilde{x}_u + \boldsymbol{\eta}_{\mathrm{BS}}^{r,\mathrm{hd}} + \mathbf{n}_u, \tag{4.21}$$

where $\boldsymbol{\eta}_{\mathrm{BS}}^{r,\mathrm{hd}} \sim \mathcal{CN}(\mathbf{0}_{\mathrm{M}}, \mathbf{C}_{\boldsymbol{\eta}_{\mathrm{BS}}}^{r,\mathrm{hd}})$ is the hardware additive distortion noise at the BS receive antenna array, and the covariance matrix $\mathbf{C}_{\boldsymbol{\eta}_{\mathrm{BS}}}^{r,\mathrm{hd}} = (1 - \kappa_r^{\mathrm{BS}}) \mathbf{A}$. This can be obtained by substituting the value of $\tilde{x}_u$ in (4.21), and applying the MRC combining vector.

The received signal can be rewritten as

$$y_u = \underbrace{\sqrt{\kappa_r^{\mathrm{BS}} \kappa^{\mathrm{u}} P_u} \mathbf{h}_u^{\mathrm{H}} \mathbf{h}_u x_u}_{\text{Desired signal}} + \underbrace{\sqrt{\kappa_r^{\mathrm{BS}}} \mathbf{h}_u^{\mathrm{H}} \mathbf{h}_u \eta_{\mathrm{u}} + \mathbf{h}_u^{\mathrm{H}} \boldsymbol{\eta}_{\mathrm{BS}}^{r,\mathrm{hd}}}_{\text{Distortion noise}} + \underbrace{\mathbf{h}_u^{\mathrm{H}} \mathbf{n}_u}_{\text{AWGN}}. \tag{4.22}$$

Hence, the SINR β_u can be calculated as

$$\beta_u = \frac{\kappa_r^{\mathrm{BS}} \kappa^{\mathrm{u}} P_u \|\mathbf{h}_u\|^4}{\mathbf{h}_u^{\mathrm{H}} \mathbf{C}_u^{c,\mathrm{hd}} \mathbf{h}_u + \|\mathbf{h}_u\|^2 \sigma_u^2}, \tag{4.23}$$

where $\mathbf{C}_u^{c,\mathrm{hd}}$ is the covariance matrix of the combined distortion noise at the BS.

Lemma 4.3.3 *In SIMO communication systems under the presence of HWIs and Nakagami-m fading, the average HD UL achievable rate can be lower bounded as*

$$\bar{\mathcal{R}}_u^{\mathrm{hd}} \geq \log_2 \left(1 + \frac{P_u \kappa^{\mathrm{u}} \kappa_r^{\mathrm{BS}} (M m_u - 1) \Omega_u}{m_u \sigma_u^2 + \frac{P_u (M m_u - 1)(m_u + 1)(1 - \kappa_r^{\mathrm{BS}} \kappa^{\mathrm{u}}) \Omega_u}{(M m_u + 1)}} \right). \tag{4.24}$$

It is obvious from (4.24) that, due to HWIs, the achievable rate is upper bounded when P_u approaches large values. This bound can be obtained as in *Remark 1*.

4.3.4 Half Duplex Downlink Spectral Efficiency with Hardware Impairments

Considering a DL situation, this section analyzes the impact of HWIs on the HD system's performance. Here, it is assumed that there is no IUI. Therefore, the received signal can be given as

$$y_d = \sqrt{\kappa^d} \mathbf{h}_d^{\mathrm{H}} \tilde{\mathbf{s}}_d + \eta_d^{\mathrm{hd}} + n_d, \tag{4.25}$$

where $\eta_d^{\mathrm{hd}} \sim \mathcal{CN}\left(0, (1 - \kappa^d) P_d \sum_{l=1}^{\mathrm{M}} \frac{\left| h_d^{(l)} \right|^4}{\|\mathbf{h}_d\|^2} \right)$ is the hardware additive distortion noise at the user receive antenna in the HD DL scenario.

By substituting the value of $\tilde{\mathbf{s}}_d$ in (4.25), the received signal can be rewritten as

$$y_d = \underbrace{\sqrt{\kappa^d \kappa_t^{\mathrm{BS}} P_d} \mathbf{h}_d^{\mathrm{H}} \frac{\mathbf{h}_d}{\|\mathbf{h}_d\|} x_d}_{\text{Desired signal}} + \underbrace{\sqrt{\kappa^d} \mathbf{h}_d^{\mathrm{H}} \boldsymbol{\eta}_{\mathrm{BS}}^t + \eta_{\mathrm{d}}^{\mathrm{hd}}}_{\text{Distortion noise}=\eta_d^{c,\mathrm{hd}}} + \underbrace{n_d}_{\text{AWGN}}. \tag{4.26}$$

Consequently, the received SINR β_d can be calculated as

$$\beta_d = \frac{P_d \kappa^d \kappa_t^{\mathrm{BS}} \|\mathbf{h}_d\|^2}{\sigma_{\eta_d^{c,\mathrm{hd}}}^2 + \sigma_d^2}, \tag{4.27}$$

where $\sigma_{\eta_d^{c,\mathrm{hd}}}^2$ is the power of combined distortion noise at the DL user.

Lemma 4.3.4 *In MISO communication systems under the presence of HWIs and Nakagami-m fading, the average HD DL achievable rate can be lower bounded as*

$$\bar{\mathcal{R}}_d^{\mathrm{hd}} \geq \log_2 \left(1 + \frac{P_d \kappa^d \kappa_t^{\mathrm{BS}} (M m_d - 1) \Omega_d}{m_d \sigma_d^2 + \frac{P_d (M m_d - 1)(m_d + 1)(1 - \kappa^d \kappa_t^{\mathrm{BS}}) \Omega_d}{(M m_d + 1)}} \right). \tag{4.28}$$

It is clear from (4.28) that HWI degrades the achievable rate. Moreover, it limits the system's performance as it saturates while P_d increases without bound. This limit can be also obtained as in *Remark 2*.

4.4   Power Allocation Optimization

As discussed before, the FD UL SE and EE are extremely affected by SI and the transmitted power of the BS. In most cases, the DL SE and EE are degraded by the transmitted power from the UL user, causing IUI. In this section, power allocation optimization problems to obtain the sub-optimal values of the transmitted powers for the UL user and the BS are formulated, thereby maximizing the average FD SE and EE while considering power budget and QoS constraints. Additionally, the max-min SE and max-min EE to maintain fairness between the users are optimized. First, the FD scenario is studied, then the HD for comparison.

4.4.1 Power Allocation Optimization for Maximizing the FD Spectral Efficiency

The joint optimization problem can be formulated as

$$\mathcal{OP}1: \quad \max_{P_d, P_u} \bar{\mathcal{R}}_d\left(P_d, P_u\right) + \bar{\mathcal{R}}_u\left(P_d, P_u\right) \tag{4.29a}$$

$$\text{Subject to:} \quad \mathcal{C}1: \bar{\mathcal{R}}_d\left(P_d, P_u\right) \geq \mathcal{R}_{\text{th}}^d \tag{4.29b}$$

$$\mathcal{C}2: \bar{\mathcal{R}}_u\left(P_d, P_u\right) \geq \mathcal{R}_{\text{th}}^u \tag{4.29c}$$

$$\mathcal{C}3: 0 \leq P_d \leq P_d^{\text{max}} \tag{4.29d}$$

$$\mathcal{C}4: 0 \leq P_u \leq P_u^{\text{max}}, \tag{4.29e}$$

where $\bar{\mathcal{R}}_u\left(P_d, P_u\right)$ and $\bar{\mathcal{R}}_d\left(P_d, P_u\right)$ are defined in (4.9) and (4.16), and $\mathcal{R}_{\text{th}}^d$, $\mathcal{R}_{\text{th}}^u$, P_d^{max} and P_u^{max} are the minimum SE requirements and the maximum power of the BS and UL user, respectively. The constraints $\mathcal{C}1$ and $\mathcal{C}2$ guarantee that the achievable SEs must satisfy $\mathcal{R}_{\text{th}}^d$ and $\mathcal{R}_{\text{th}}^u$, and the constraints $\mathcal{C}3$ and $\mathcal{C}4$ limit the power allocation to the defined budget. The optimization problem in (4.29) is a non-concave problem due to non-concavity of the objective function. As a result, obtaining an optimal solution is quite difficult. However, this problem can be solved by using the KKT conditions to obtain a sub-optimal solution with reduced complexity. In consequence, the Lagrangian function connected to the optimization problem in (4.29) can be given as

$$\mathcal{L}\left(P_d, P_u\right) = -\left(\bar{\mathcal{R}}_d\left(P_d, P_u\right) + \bar{\mathcal{R}}_u\left(P_d, P_u\right)\right) - \lambda_1\left(\bar{\mathcal{R}}_d\left(P_d, P_u\right) - \mathcal{R}_{\text{th}}^d\right) - \lambda_2\left(P_d^{\text{max}} - P_d\right)$$
$$- \lambda_3\left(\bar{\mathcal{R}}_u\left(P_d, P_u\right) - \mathcal{R}_{\text{th}}^u\right) - \lambda_4\left(P_u^{\text{max}} - P_u\right), \tag{4.30}$$

where $\lambda_i \geq 0 \ \ \forall i \in \{1, 2, 3, 4\}$ are the Lagrange multipliers. Before solving the problem, it is important to check the solution existence, as shown in Lemma (4.4.1).

KKT Conditions Solution

To find a sub-optimal solution for a non-convex problem with a differentiable objective and constraint functions, the solution must satisfy the KKT conditions [122]. These conditions can be summarized as follows: Let P_d^*, P_u^* and $\boldsymbol{\lambda}^*$ be any optimal values. Since P_d^* and P_u^*

minimize $\mathcal{L}(P_d, P_u, \boldsymbol{\lambda}^*)$ over P_d and P_u, its gradient must vanish at P_d^* and P_u^*, therefore implying that

$$\nabla\left(\bar{\mathcal{R}}_d\left(P_d^*, P_u^*\right) + \bar{\mathcal{R}}_u\left(P_d^*, P_u^*\right)\right) + \lambda_1^*\nabla\left(\bar{\mathcal{R}}_d\left(P_d^*, P_u^*\right) - \mathcal{R}_{\text{th}}^d\right) + \lambda_2^*\nabla\left(P_d^{\text{max}} - P_d^*\right)$$
$$+ \lambda_3^*\nabla\left(\bar{\mathcal{R}}_u\left(P_d^*, P_u^*\right) - \mathcal{R}_{\text{th}}^u\right) + \lambda_4^*\nabla\left(P_u^{\text{max}} - P_u^*\right) = 0.$$
$$(4.31)$$

The KKT conditions can therefore be written as [122]

$$\frac{\partial\mathcal{L}\left(P_d^*, P_u^*\right)}{\partial P_d} = 0, \tag{4.32a}$$

$$\frac{\partial\mathcal{L}\left(P_d^*, P_u^*\right)}{\partial P_u} = 0, \tag{4.32b}$$

$$\lambda_1^*\left(\bar{\mathcal{R}}_d\left(P_d^*, P_u^*\right) - \mathcal{R}_{\text{th}}^d\right) = 0, \tag{4.32c}$$

$$\lambda_2^*\left(P_d^{\text{max}} - P_d^*\right) = 0, \tag{4.32d}$$

$$\lambda_3^*\left(\bar{\mathcal{R}}_u\left(P_d^*, P_u^*\right) - \mathcal{R}_{\text{th}}^u\right) = 0, \tag{4.32e}$$

$$\lambda_4^*\left(P_u^{\text{max}} - P_u^*\right) = 0, \tag{4.32f}$$

$$\bar{\mathcal{R}}_d\left(P_d^*, P_u^*\right) - \mathcal{R}_{\text{th}}^d \geq 0, \tag{4.32g}$$

$$\left(P_d^{\text{max}} - P_d^*\right) \geq 0, \tag{4.32h}$$

$$\bar{\mathcal{R}}_u\left(P_d^*, P_u^*\right) - \mathcal{R}_{\text{th}}^u \geq 0, \tag{4.32i}$$

$$\left(P_u^{\text{max}} - P_u^*\right) \geq 0, \tag{4.32j}$$

$$\lambda_i^* \geq 0 \quad \forall i \in \{1, 2, 3, 4\}. \tag{4.32k}$$

The sub-optimal solution can be obtained by solving (4.32a)-(4.32f) simultaneously, either analytically or numerically using any mathematical software (e.g., MATLAB). The obtained solution, though, must satisfy all the above KKT conditions. Since there are four constraints $\mathcal{C}1 - \mathcal{C}4$, there are four Lagrangian multipliers $\lambda_1 - \lambda_4$, and as such, 16 cases are possible corresponding to the binding or non-binding constraints. $\lambda_i \neq 0$ for the binding constraint and $\lambda_i = 0$ for the non-binding one.

Simplified Solution

In this section, a simple novel algorithm that reaches the same solution as the one obtained by the KKT conditions in the previous section is proposed. Both solutions under different

---
Algorithm 2 The Simplified Solution

Inputs: $\left(\mathcal{R}_{\text{th}}^d, \mathcal{R}_{\text{th}}^u, P_d^{\max}, P_u^{\max}, \kappa_r^{\text{BS}}, \kappa_t^{\text{BS}}, \kappa^u, \kappa^d, \Omega_d, \Omega_u, \Omega_s, \Omega_I, M, m_d, m_u, \sigma_d^2, \sigma_u^2\right)$

Existence: Check the solution existence as in Lemma 4.4.1

if the solution is exist **then**

    Solution: The solution can be obtained from (4.16) and (4.9) considering three steps as follow

- **Step 1:** Calculate $\bar{\mathcal{R}}_d$ and $\bar{\mathcal{R}}_u$ from (4.16) and (4.9) using $P_d^{\max}$ and $P_u^{\max}$, store $P_d^* = P_d^{\max}$ and $P_u^* = P_u^{\max}$

- **Step 2:** Set $\bar{\mathcal{R}}_d = \mathcal{R}_{\text{th}}^d$ and $P_u^* = P_u^{\max}$, calculate P_d^* from (4.16), then calculate $\bar{\mathcal{R}}_u$ from (4.9)

- **Step 3:** Set $\bar{\mathcal{R}}_u = \mathcal{R}_{\text{th}}^u$ and $P_d^* = P_d^{\max}$, calculate P_u^* from (4.9), then calculate $\bar{\mathcal{R}}_d$ from (4.16)

    Output: P_d^* and P_u^* associates with the solution that gives the maximum average FD SE in **steps 1-3**.

end if
---

operating conditions, including various degrees of channel fading, SI, IUI, HWIs factors, power budgets and QoS constraints are compared. **Algorithm** 2 summarizes our proposed solution.

Lemma 4.4.1 *From, (4.9), (4.16), (4.29b) and (4.29c), the sufficient conditions that guarantee the solution existence can be summarized by the following inequalities*

$$\mathcal{R}_{\text{th}}^d \leq \tilde{\mathcal{R}}_{\text{th}}^d, \tag{4.33a}$$

$$\mathcal{R}_{\text{th}}^u \leq \tilde{\mathcal{R}}_{\text{th}}^u, \tag{4.33b}$$

$$P_d^{\max} \geq \tilde{P}_d^{\text{th}}, \tag{4.33c}$$

$$P_u^{\max} \geq \tilde{P}_u^{\text{th}}, \tag{4.33d}$$

where $\tilde{\mathcal{R}}_{\text{th}}^d$, $\tilde{\mathcal{R}}_{\text{th}}^u$, $\tilde{P}_d^{\text{th}}$ and $\tilde{P}_u^{\text{th}}$ can be found in Appendix A.3.

4.4.2 Power Allocation Optimization for Maximizing the Minimum FD UL/DL Spectral Efficiency

In this section, the optimization problem aims to maximize the minimum UL and DL SE to guarantee fairness between the users. To that end, a max-min objective to achieve a rate balance among the DL and UL users is formulated. As such, the max-min SE optimization problem can be formulated as [2]

$$\mathcal{OP}2: \quad \max_{P_d, P_u} \min_{\bar{\mathcal{R}}_d, \bar{\mathcal{R}}_u} \quad \left\{ \bar{\mathcal{R}}_d\left(P_d, P_u\right), \bar{\mathcal{R}}_u\left(P_d, P_u\right) \right\} \tag{4.34a}$$

$$\text{Subject to:} \quad \mathcal{C}1 : 0 \leq P_d \leq P_d^{\max} \tag{4.34b}$$

$$\mathcal{C}2 : 0 \leq P_u \leq P_u^{\max}, \tag{4.34c}$$

where $P_d^{\max}$ and $P_u^{\max}$ are the maximum power of the BS and UL user, $\bar{\mathcal{R}}_d\left(P_d, P_u\right)$ and $\bar{\mathcal{R}}_u\left(P_d, P_u\right)$ are defined in (4.16) and (4.9). The constraints $\mathcal{C}1$ and $\mathcal{C}2$ limit the power allocation to the maximum power budget. The optimization problem in (4.34) is a non-concave problem due to the non-concavity of the objective function. As a result, obtaining an optimal solution is quite difficult. Fortunately, the problem in (4.34) can be transformed to an equivalent problem [124]. Using this transformation, the new optimization problem can be reformulated to solve the optimization problem as follows

$$\mathcal{OP}3: \quad \max_{P_d, P_u, \phi} \quad \phi \tag{4.35a}$$

$$\text{Subject to:} \quad \mathcal{C}1, \mathcal{C}2 \tag{4.35b}$$

$$\mathcal{C}3 : \bar{\mathcal{R}}_d\left(P_d, P_u\right) \geq \phi \tag{4.35c}$$

$$\mathcal{C}4 : \bar{\mathcal{R}}_u\left(P_d, P_u\right) \geq \phi, \tag{4.35d}$$

The sub-optimal solution can be obtained by solving (4.35) using the KKT conditions technique.

---

[2]The weighting max-min is a straightforward extension of this work.

Consequently, the related Lagrangian function is given as

$$\mathcal{L}\left(P_d, P_u, \phi\right) = -\phi - \lambda_1\left(\bar{\mathcal{R}}_d\left(P_d, P_u\right) - \phi\right) - \lambda_2\left(P_d^{\max} - P_d\right) - \lambda_3\left(\bar{\mathcal{R}}_u\left(P_d, P_u\right) - \phi\right)$$
$$- \lambda_4\left(P_u^{\max} - P_u\right), \tag{4.36}$$

where each Lagrange multiplier $\lambda_i \geq 0, \forall i \in \{1, 2, 3, 4\}$.

The KKT conditions can be written as

$$\frac{\partial \mathcal{L}\left(P_d^*, P_u^*, \phi^*\right)}{\partial P_d} = 0, \tag{4.37a}$$

$$\frac{\partial \mathcal{L}\left(P_d^*, P_u^*, \phi^*\right)}{\partial P_u} = 0, \tag{4.37b}$$

$$\frac{\partial \mathcal{L}\left(P_d^*, P_u^*, \phi^*\right)}{\partial \phi} = -1 + \lambda_1 + \lambda_3 = 0, \tag{4.37c}$$

$$\lambda_1^*\left(\bar{\mathcal{R}}_d\left(P_d^*, P_u^*\right) - \phi^*\right) = 0, \tag{4.37d}$$

$$\lambda_2^*\left(P_d^{\max} - P_d^*\right) = 0, \tag{4.37e}$$

$$\lambda_3^*\left(\bar{\mathcal{R}}_u\left(P_d^*, P_u^*\right) - \phi^*\right) = 0, \tag{4.37f}$$

$$\lambda_4^*\left(P_u^{\max} - P_u^*\right) = 0, \tag{4.37g}$$

$$\bar{\mathcal{R}}_d\left(P_d^*, P_u^*\right) - \phi^* \geq 0, \tag{4.37h}$$

$$\left(P_d^{\max} - P_d^*\right) \geq 0, \tag{4.37i}$$

$$\bar{\mathcal{R}}_u\left(P_d^*, P_u^*\right) - \phi^* \geq 0, \tag{4.37j}$$

$$\left(P_u^{\max} - P_u^*\right) \geq 0, \tag{4.37k}$$

$$\lambda_i^* \geq 0 \quad \forall i \in \{1, 2, 3, 4\}. \tag{4.37l}$$

The sub-optimal solution can be obtained by simultaneously solving (4.37a)-(4.37g), either analytically or numerically. The obtained solution, however, must satisfy all the above KKT conditions.

4.4.3 Power Allocation Optimization for Maximizing the FD Energy Efficiency

In this section, an optimization problem to maximize the EE is formulated. Hence, the EE optimization problem can be formulated as

$$\mathcal{OP}4: \quad \max_{P_d,P_u} \mathcal{E}^{\text{FD}} = \frac{\bar{\mathcal{R}}_d\left(P_d,P_u\right) + \bar{\mathcal{R}}_u\left(P_d,P_u\right)}{P_d + P_u + P_c} \tag{4.38a}$$

$$\text{Subject to:} \quad \mathcal{C}1 : \bar{\mathcal{R}}_d\left(P_d,P_u\right) \geq \mathcal{R}_{\text{th}}^d \tag{4.38b}$$

$$\mathcal{C}2 : \bar{\mathcal{R}}_u\left(P_d,P_u\right) \geq \mathcal{R}_{\text{th}}^u \tag{4.38c}$$

$$\mathcal{C}3 : 0 \leq P_d \leq P_d^{\max} \tag{4.38d}$$

$$\mathcal{C}4 : 0 \leq P_u \leq P_u^{\max}, \tag{4.38e}$$

where P_c is the total power consumption in all circuit blocks, including the process to achieve a certain level of SI cancellation. $P_d^{\max}$ and $P_u^{\max}$ are the maximum powers of the BS and UL user. $\bar{\mathcal{R}}_d\left(P_d,P_u\right)$ and $\bar{\mathcal{R}}_u\left(P_d,P_u\right)$ are defined in (4.16) and (4.9), and $\mathcal{R}_{\text{th}}^d$, $\mathcal{R}_{\text{th}}^u$ are the minimum SE requirements. The constraints $\mathcal{C}1$ and $\mathcal{C}2$ guarantee that the achievable SEs must satisfy $\mathcal{R}_{\text{th}}^d$ and $\mathcal{R}_{\text{th}}^u$, and the constraints $\mathcal{C}3$ and $\mathcal{C}4$ limit the power allocation to the predetermined budget.

The optimization problem in (4.38) is a non-concave problem due to the non-concavity of the objective function. As a result, obtaining an optimal solution is quite difficult. Fortunately, the fractional non-concave optimization problem in (4.38) can be transformed to an equivalent parametric optimization problem using the Dinkelbach approach [121, 125–127]. Using this transformation, the new optimization problem can be reformulated in such a way that its numerator and denominator are decoupled, which in turn simplifies its solution, as follows

$$\mathcal{OP}5: \quad \max_{P_d,P_u} \mathcal{F} = \bar{\mathcal{R}}_d\left(P_d,P_u\right) + \bar{\mathcal{R}}_u\left(P_d,P_u\right) - q(P_d + P_u + P_c) \tag{4.39a}$$

$$\text{Subject to:} \quad \mathcal{C}1 - \mathcal{C}4, \tag{4.39b}$$

where q is a non-negative constant. It was proven in [121] that P_d^* and P_u^* are optimal for (4.38) if and only if they are optimal for (4.39) for any $q = q^*$. Note that these results are

correct without placing any convexity condition on (4.38). The parameter q is iteratively updated by

$$q^{(k+1)} = \frac{\bar{\mathcal{R}}_d\left(P_d^{(k)}, P_u^{(k)}\right) + \bar{\mathcal{R}}_u\left(P_d^{(k)}, P_u^{(k)}\right)}{P_d^{(k)} + P_u^{(k)} + P_c}, \tag{4.40}$$

where k is the iteration index, $q^{(1)}$ is the initial value (e.g., $q^{(1)} = 0$), and $(P_d^{(k)}, P_u^{(k)})$ are the power values obtained from the first iteration. It was proven in [121] that convergence is guaranteed by alternatively updating q using (4.40) and solving for P_d and P_u in (4.39). The sub-optimal solution can be obtained by solving (4.39) using the KKT conditions technique. Consequently, the related Lagrangian function can be given as

$$\mathcal{L}\left(P_d, P_u\right) = -\left(\bar{\mathcal{R}}_d\left(P_d, P_u\right) + \bar{\mathcal{R}}_u\left(P_d, P_u\right)\right) + q(P_d + P_u + P_c) - \lambda_1\left(\bar{\mathcal{R}}_d\left(P_d, P_u\right) - \mathcal{R}_{\text{th}}^d\right)$$
$$- \lambda_2\left(P_d^{\max} - P_d\right) - \lambda_3\left(\bar{\mathcal{R}}_u\left(P_d, P_u\right) - \mathcal{R}_{\text{th}}^u\right) - \lambda_4\left(P_u^{\max} - P_u\right), \tag{4.41}$$

where each Lagrange multiplier is given by $\lambda_i \geq 0, \forall i \in \{1, 2, 3, 4\}$. Now, the KKT conditions can be written as

$$\frac{\partial \mathcal{L}\left(P_d^*, P_u^*\right)}{\partial P_d} = 0, \tag{4.42a}$$

$$\frac{\partial \mathcal{L}\left(P_d^*, P_u^*\right)}{\partial P_u} = 0, \tag{4.42b}$$

$$\lambda_1^*\left(\bar{\mathcal{R}}_d\left(P_d^*, P_u^*\right) - \mathcal{R}_{\text{th}}^d\right) = 0, \tag{4.42c}$$

$$\lambda_2^*\left(P_d^{\max} - P_d^*\right) = 0, \tag{4.42d}$$

$$\lambda_3^*\left(\bar{\mathcal{R}}_u\left(P_d^*, P_u^*\right) - \mathcal{R}_{\text{th}}^u\right) = 0, \tag{4.42e}$$

$$\lambda_4^*\left(P_u^{\max} - P_u^*\right) = 0, \tag{4.42f}$$

$$\bar{\mathcal{R}}_d\left(P_d^*, P_u^*\right) - \mathcal{R}_{\text{th}}^d \geq 0, \tag{4.42g}$$

$$\left(P_d^{\max} - P_d^*\right) \geq 0, \tag{4.42h}$$

$$\bar{\mathcal{R}}_u\left(P_d^*, P_u^*\right) - \mathcal{R}_{\text{th}}^u \geq 0, \tag{4.42i}$$

$$\left(P_u^{\max} - P_u^*\right) \geq 0, \tag{4.42j}$$

$$\lambda_i^* \geq 0 \quad \forall i \in \{1, 2, 3, 4\}. \tag{4.42k}$$

The sub-optimal solution can be obtained by simultaneously solving (4.42a)-(4.42f). The obtained solution, though, must satisfy all the above KKT conditions. After that, this

---

Algorithm 3 Energy Efficiency Solution

Inputs: $\left(\mathcal{R}_{\text{th}}^d, \mathcal{R}_{\text{th}}^u, P_d^{\max}, P_u^{\max}, P_c, \kappa_r^{\text{BS}}, \kappa_t^{\text{BS}}, \kappa^u, \kappa^d, \Omega_d, \Omega_u, \Omega_s, \Omega_I, M, m_d, m_u, \sigma_d^2, \sigma_u^2, \delta, q^{\text{init}} = 0\right)$

Solution: The solution can be obtained as follow, set $k = 1$ and $q^{(k)} = q^{\text{init}}$.

- **Step 1:** Solve (4.39) using the KKT conditions technique and calculate the sub-optimal solution P_d^* and P_u^* by setting $q = q^{(k)}$. Store $P_d^{(k)} = P_d^*$, $P_u^{(k)} = P_u^*$ and $q^* = q^{(k)}$.

- **Step 2:** Calculate $q^{(k+1)}$ from (4.40).

if $q^{(k+1)} - q^* > \delta$ **then**

  Update $q^* = q^{(k+1)}$, $k = k + 1$ and return to **Step 1**

else

  Update $q^* = q^{(k+1)}$ and stop.

end if

Outputs: P_d^*, P_u^* and q^*, where q^* is the maximum EE value.

---

solution can be used to update q in (4.40) until it converges to q^* when $q^{(k+1)} - q^{(k)} \leq \delta$ (the acceptable convergence tolerance). **Algorithm** 3 summarizes the proposed solution.

4.4.4 Power Allocation Optimization for Maximizing Minimum FD UL/DL Energy Efficiency

In this section, the optimization problem aims to maximize the minimum UL and DL EE to guarantee fairness between users. To that end, a max-min objective to achieve energy balance among the DL and UL powers is formulated. As such, the max-min EE optimization problem can be formulated as follows

$$\mathcal{OP}6: \quad \max_{P_d, P_u} \min_{j \in \{d, u\}} \frac{\bar{\mathcal{R}}_j(P_d, P_u)}{P_d + P_u + P_c} \tag{4.43a}$$

$$\text{Subject to:} \quad \mathcal{C}1 : 0 \leq P_d \leq P_d^{\max} \tag{4.43b}$$

$$\mathcal{C}2 : 0 \leq P_u \leq P_u^{\max}. \tag{4.43c}$$

The optimization problem in (4.43) is a non-concave problem due to the non-concavity of its objective function. As discussed in 4.4.3, a fractional non-concave optimization problem in (4.43) can be transformed to an equivalent parametric optimization problem. Then, the optimization problem in (4.43) can be written as

$$\mathcal{OP}7: \max_{P_d, P_u} \min_{j \in \{d,u\}} \bar{\mathcal{R}}_j (P_d, P_u) - \eta(P_d + P_u + P_c) \qquad (4.44a)$$

$$\text{Subject to:} \quad \mathcal{C}1, \mathcal{C}2, \qquad (4.44b)$$

where η is a non-negative constant. The parameter η is iteratively updated by

$$\eta^{(k+1)} = \min_{j \in \{d,u\}} \frac{\bar{\mathcal{R}}_j \left(P_d^{(k)}, P_u^{(k)} \right)}{P_d^{(k)} + P_u^{(k)} + P_c}, \qquad (4.45)$$

where k is the iteration index, $\eta^{(k)}$ is the initial value (e.g., $\eta^{(1)} = 0$) and $(P_d^{(k)}, P_u^{(k)})$ are the power values obtained from the first iteration. As explained previously, the convergence of (4.45) is guaranteed. Consequently, the optimization problem in (4.44) can be reformulated as

$$\mathcal{OP}8: \max_{P_d, P_u, \zeta} \zeta \qquad (4.46a)$$

$$\text{Subject to:} \quad \mathcal{C}1, \mathcal{C}2 \qquad (4.46b)$$

$$\mathcal{C}3: \bar{\mathcal{R}}_d (P_d, P_u) - \eta(P_d + P_u + P_c) \geq \zeta \qquad (4.46c)$$

$$\mathcal{C}4: \bar{\mathcal{R}}_u (P_d, P_u) - \eta(P_d + P_u + P_c) \geq \zeta. \qquad (4.46d)$$

The sub-optimal solution can be obtained by solving (4.46) using the KKT conditions technique. Hence, the Lagrangian function associated with (4.46) can be written as

$$\mathcal{G} (P_d, P_u, \zeta) = - \zeta - \lambda_1 \left(\bar{\mathcal{R}}_d (P_d, P_u) - \eta(P_d + P_u + P_c) \right) + \lambda_1 \zeta -$$
$$\lambda_3 \left(\bar{\mathcal{R}}_u (P_d, P_u) - \eta(P_d + P_u + P_c) \right) + \lambda_3 \zeta - \lambda_2 \left(P_d^{\max} - P_d \right) - \lambda_4 \left(P_u^{\max} - P_u \right),$$
$$(4.47)$$

where $\lambda_i \geq 0, \forall i \in \{1, 2, 3, 4\}$ are Lagrange multipliers. Consequently, the KKT conditions can be written as

$$\frac{\partial \mathcal{G}\left(P_d^*, P_u^*, \zeta^*\right)}{\partial P_d} = 0, \tag{4.48a}$$

$$\frac{\partial \mathcal{G}\left(P_d^*, P_u^*, \zeta^*\right)}{\partial P_u} = 0, \tag{4.48b}$$

$$\frac{\partial \mathcal{G}\left(P_d^*, P_u^*, \zeta^*\right)}{\partial \zeta} = -1 + \lambda_1 + \lambda_3 = 0, \tag{4.48c}$$

$$\lambda_1^* \left(\bar{\mathcal{R}}_d\left(P_d^*, P_u^*\right) - \eta(P_d^* + P_u^* + P_c) - \zeta^*\right) = 0, \tag{4.48d}$$

$$\lambda_2^* \left(P_d^{\max} - P_d^*\right) = 0, \tag{4.48e}$$

$$\lambda_3^* \left(\bar{\mathcal{R}}_u\left(P_d^*, P_u^*\right) - \eta(P_d^* + P_u^* + P_c) - \zeta^*\right) = 0, \tag{4.48f}$$

$$\lambda_4^* \left(P_u^{\max} - P_u^*\right) = 0, \tag{4.48g}$$

$$\bar{\mathcal{R}}_d\left(P_d^*, P_u^*\right) - \eta(P_d^* + P_u^* + P_c) - \zeta^* \geq 0, \tag{4.48h}$$

$$\left(P_d^{\max} - P_d^*\right) \geq 0, \tag{4.48i}$$

$$\bar{\mathcal{R}}_u\left(P_d^*, P_u^*\right) - \eta(P_d^* + P_u^* + P_c) - \zeta^* \geq 0, \tag{4.48j}$$

$$\left(P_u^{\max} - P_u^*\right) \geq 0, \tag{4.48k}$$

$$\lambda_i^* \geq 0 \quad \forall i \in \{1, 2, 3, 4\}. \tag{4.48l}$$

Then, the obtained solution is used to calculate β until it converges when $\beta^{(k)} \leq \delta$ (the acceptable convergence tolerance). It also used to update the value of η. **Algorithm** 4 summarizes the proposed solution.

4.4.5   Power Allocation Optimization for Maximizing HD SE

In this section, the average SE of the HD system is optimized to compare it with that of the FD system. Here, we take half the SE values of the HD UL and DL scenarios because HD systems use double the bandwidth/time slots that FD systems use. The optimization problem can consequently be formulated as

---

Algorithm 4 Max-min EE Solution

Inputs: $\left(P_d^{\max}, P_u^{\max}, P_c, \kappa_r^{\mathrm{BS}}, \kappa_t^{\mathrm{BS}}, \kappa^u, \kappa^d, \Omega_d, \Omega_u, \Omega_s, \Omega_I, M, m_d, m_u, \sigma_d^2, \sigma_u^2, \delta, \eta^{\mathrm{init}} = 0, \beta^{\mathrm{init}} = 1\right)$

Solution: The solution can be obtained as follow, set $k = 1$, $\eta^k = \eta^{\mathrm{init}}$ and $\beta^{(k)} = \beta^{\mathrm{init}}$.

while $\beta^{(k)} > \delta$ **do**

    Step 1: Solve (4.46) using the KKT conditions technique and calculate the sub-optimal solution P_d^* and P_u^* by setting $\eta = \eta^{(k)}$.

    Step 2: Set $k = k + 1$ and calculate $\beta^{(k)} = \min\limits_{j \in \{d,u\}} \bar{\mathcal{R}}_j \left(P_d^*, P_u^*\right) - \eta(P_d^* + P_u^* + P_c)$.

    Step 3: Calculate

$$\eta^{(k)} = \min_{j \in \{d,u\}} \frac{\bar{\mathcal{R}}_j \left(P_d^*, P_u^*\right)}{P_d^* + P_u^* + P_c}.$$

end while

Outputs: P_d^*, P_u^*.

$$\mathcal{OP}9: \quad \max_{P_d, P_u} \frac{1}{2} \left(\bar{\mathcal{R}}_d^{\mathrm{hd}} \left(P_d\right) + \bar{\mathcal{R}}_u^{\mathrm{hd}} \left(P_u\right) \right) \tag{4.49a}$$

$$\text{Subject to:} \quad \mathcal{C}1 : \bar{\mathcal{R}}_d^{\mathrm{hd}} \left(P_d\right) \geq \mathcal{R}_{\mathrm{th}}^d \tag{4.49b}$$

$$\mathcal{C}2 : \bar{\mathcal{R}}_u^{\mathrm{hd}} \left(P_u\right) \geq \mathcal{R}_{\mathrm{th}}^u \tag{4.49c}$$

$$\mathcal{C}3 : 0 \leq P_d \leq P_d^{\max} \tag{4.49d}$$

$$\mathcal{C}4 : 0 \leq P_u \leq P_u^{\max}, \tag{4.49e}$$

where $\bar{\mathcal{R}}_d^{\mathrm{hd}} \left(P_d\right)$ and $\bar{\mathcal{R}}_u^{\mathrm{hd}} \left(P_u\right)$ are defined in (4.28) and (4.24). $\mathcal{R}_{\mathrm{th}}^d$ and $\mathcal{R}_{\mathrm{th}}^u$ are the minimum SE requirements and cannot exceed the maximum values $\log_2 \left(1 + \frac{(Mm_d+1)\kappa^d\kappa_t^{\mathrm{BS}}}{(m_d+1)(1-\kappa^d\kappa_t^{\mathrm{BS}})}\right)$ and $\log_2 \left(1 + \frac{(Mm_u+1)\kappa_r^{\mathrm{BS}}\kappa^u}{(m_u+1)(1-\kappa_r^{\mathrm{BS}}\kappa^u)}\right)$, respectively. It is important to note that (4.28) and (4.24) are concave functions, meaning that (4.49) is also concave and that the optimal solution can be obtained. It is also worth mentioning that in the case of HD communication, $\bar{\mathcal{R}}_d^{\mathrm{hd}} \left(P_d\right)$ and $\bar{\mathcal{R}}_u^{\mathrm{hd}} \left(P_u\right)$ are independent. Therefore, the powers that maximize the sum are the ones that maximize each one individually. In that sense, transmitting at maximum power also leads to the maximum achievable rate.

4.4.6 Power Allocation Optimization for Maximizing HD EE

In this section, the average EE of the HD system is optimized to compare it with that of the FD system. Here, we take half the EE values of the HD UL and DL scenarios because HD systems use double the frequency bandwidth or time slots that FD systems use. The optimization problem can be formulated as

$$\mathcal{OP}10: \quad \max_{P_d, P_u} \mathcal{E}^{\text{hd}} = \frac{\bar{\mathcal{R}}_d^{\text{hd}}(P_d) + \bar{\mathcal{R}}_u^{\text{hd}}(P_u)}{2(P_d + P_u + P_c)} \tag{4.50a}$$

$$\text{Subject to:} \quad \mathcal{C}1 : \bar{\mathcal{R}}_d^{\text{hd}}(P_d) \geq \mathcal{R}_{\text{th}}^d \tag{4.50b}$$

$$\mathcal{C}2 : \bar{\mathcal{R}}_u^{\text{hd}}(P_u) \geq \mathcal{R}_{\text{th}}^u \tag{4.50c}$$

$$\mathcal{C}3 : 0 \leq P_d \leq P_d^{\max} \tag{4.50d}$$

$$\mathcal{C}4 : 0 \leq P_u \leq P_u^{\max}. \tag{4.50e}$$

The objective function of (4.50) is pseudo-concave, meaning that each stationary point of the objective is a global maximizer. Moreover, KKT conditions are necessary and sufficient for optimality [127, propositions 2.8 and 2.9]. Hence, the optimal solution can be obtained by using **Algorithm** 3.

4.4.7 Complexity Analysis

Using Big-$\mathcal{O}$ notation, the complexities of the proposed algorithms can be summarized as follows: First, **Algorithm** 2, the simplified solution, has $\mathcal{O}(1)$ complexity because it runs in for a constant time, and the statements are being used for basic operations. Second, the KKT-based Algorithm uses the interior point method and has a computational complexity of $\mathcal{O}(\sqrt{v}\log(v))$, where v represents the number of inequality constraints in $\mathcal{OP}1$, [122], [128]. Third, **Algorithm** 3 and **Algorithm** 4 use the interior point method to solve the problem in $\mathcal{OP}5$ and $\mathcal{OP}8$ at each iteration, and therefore have a computational complexity of $\mathcal{O}(\sqrt{v}\log(v))$, where v represents the number of inequality constraints in $\mathcal{OP}5$ and $\mathcal{OP}8$. Assuming that the number of iterations for these algorithms is $k^{\max}$, the computational complexity of **Algorithm** 3 and **Algorithm** 4 can be calculated as $k^{\max}\mathcal{O}(\sqrt{v}\log(v))$.
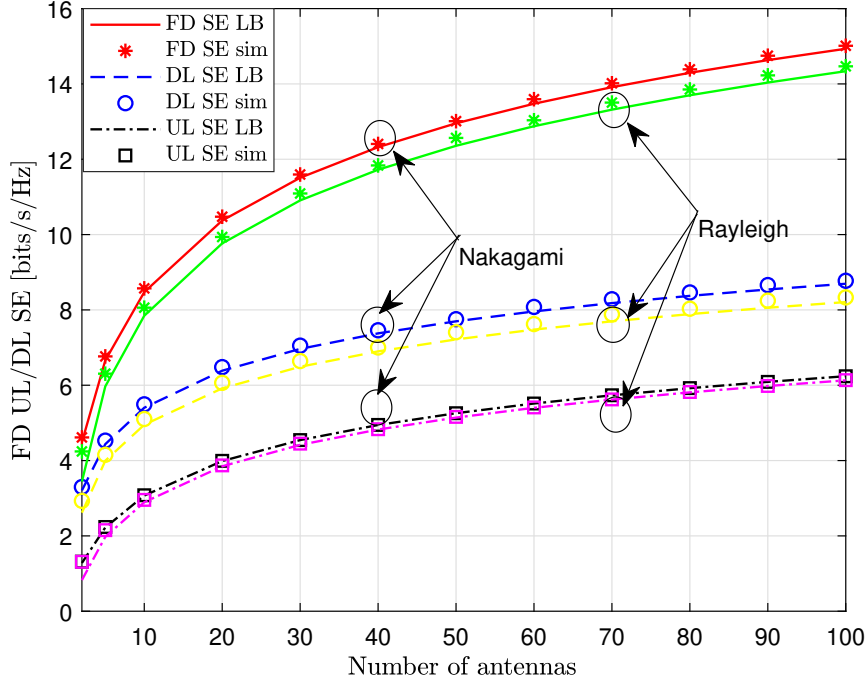
Figure 4.2: Average FD UL/DL SE with different number of BS antennas, where $P_d = P_u = 10$ dB, $\Omega_s = 1$, $\Omega_I = 0.1$, $\kappa^u = \kappa^d = 0.92$ and $\kappa_r^{\mathrm{BS}} = \kappa_t^{\mathrm{BS}} = 0.98$.

4.5 Simulation Results and Discussion

This section investigates the average FD SE of a wireless communication system under the effect of transceiver HWI. Unless otherwise specified, the shape and scale parameters of the Nakagami-m distribution are $m_x = 10$ and $\Omega_x = 1$, where $x \in \{u, d, s, I\}$. The noise variances are $\sigma_u^2 = \sigma_d^2 = 1$. Without loss of generality, it is assumed that $\kappa = \kappa_t^{\mathrm{BS}} = \kappa_r^{\mathrm{BS}} = \kappa^u = \kappa^d$. Extensive simulations were conducted to validate the theoretical derivations and the feasibility of the proposed algorithms. This work is also compared with an exhaustive search scheme, which serves as a benchmark to illustrate how the proposed solutions approach the optimal one.

In Fig. 4.2, a different number of BS antennas is considered, where $M = \{2, 5, 10, 20, \ldots, 100\}$ and $\kappa^u = \kappa^d = 0.92$ and $\kappa_r^{\mathrm{BS}} = \kappa_t^{\mathrm{BS}} = 0.98$. It is evident that the analytical results obtained in (4.9) and (4.16) are validated by this figure. It also shows that the system performance with Nakagami-m channels fading is better than the Rayleigh distribution.

66
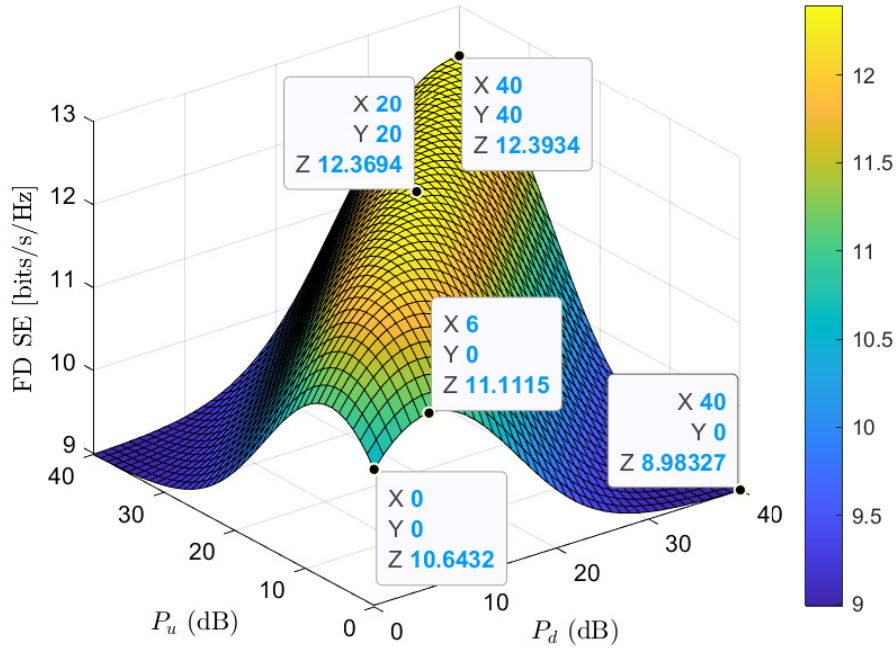
Figure 4.3: Average FD SE with different transmit power at $M = 100$ and $\kappa = 0.92$.

However, the gap between the Nakagami-m and Rayleigh performance depends on many parameters such as SI and IUI.

Fig. 4.3 demonstrates the impact of increasing the transmit UL/DL powers on the average FD SE, in the case where both UL/DL users experience the same conditions. Many important observations can be noted here. First, increasing the UL transmit power enhances the UL SE. On the other hand, it has a detrimental effect on the DL performance. The same is valid when increasing the DL transmit power. For example, when $P_u = 0$ dB and P_d increases from 0 to 40 dB, the FD SE increases from 10.64 bits/s/Hz until it reaches a peak of 11.11 bits/s/Hz when $P_d = 6$ dB. It then decreases to 8.98 bits/s/Hz when $P_d = 40$ dB. This implies that sending the maximum power is not the optimal solution in FD systems. Hence, there should be a balance between the UL and DL powers to maximize the total SE.

Second, it is obvious that the performance improves by increasing both the UL and DL transmit powers. For instance, when $P_u = P_d = 0$ dB, the average FD SE is 10.64 bits/s/Hz
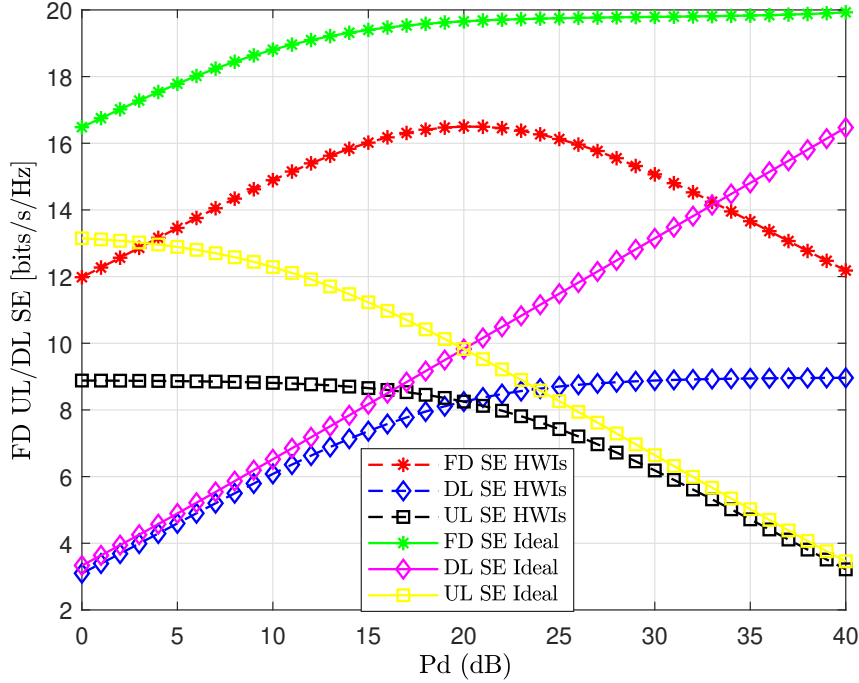
Figure 4.4: Average FD UL/DL SE at $P_u = 20$ dB, $M = 100$, $\Omega_I = \Omega_s = 0.1$ and $\kappa = 0.92$.

and it increases to 12.39 bits/s/Hz when $P_u = P_d = 40$ dB. Third, this figure confirms the result in (4.19) and (4.20) that HWIs can diminish the positive effect of increasing the P_u and P_d by pushing the network into an interference-limited regime where no extraordinary SE can be obtained. For instance, a negligible improvement (0.02 bits/s/Hz) is achieved by increasing the transmit power from 20 to 40 dB.

Fig. 4.4 illustrates the UL and DL SE behaviour for both the ideal and impaired systems when $P_u = 20$ dB and P_d increases from $0 - 40$ dB. For small values of P_d, the DL SE has a small value because P_u is much greater than P_d, and hence, the IUI has a profound impact on the DL SE. At the same time, a noticeable difference between the UL SE of the impaired and ideal systems can be noted. In the middle, for the system with HWIs, increasing P_d improves the average FD SE but degrades the UL SE because SI is increased. This positive change reaches its peak when $P_u = P_d$. Before this point, though, P_d in (4.16) increases the DL SE more than it decreases the UL SE in (4.9), which means that the overall FD SE increases. After this point, P_d becomes larger than P_u and as a result, the DL SE goes into the saturation region while the UL SE is still decreasing, which means that the overall

68
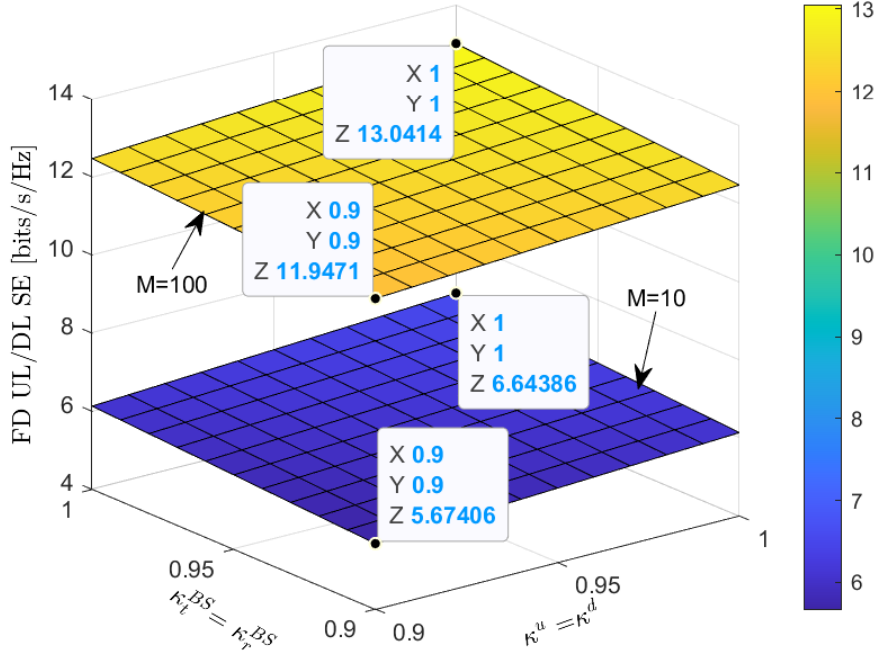
Figure 4.5: Average FD SE at different levels of HWIs at $P_u = P_d = 10$ dB and $M = [10, 100]$.

FD SE decreases. For the ideal system, as P_d increases, the DL SE increases without limit and the UL SE decreases.

Fig. 4.5 investigates the system performance under varying degrees of HWI and differing numbers of BS antennas. It is clear that the presence of HWIs has a negative impact on the overall system performance. In the case where $M = 100$, the maximum performance (SE $= 13.04$ bits/s/Hz) occurs at ideal hardware conditions when $\kappa = 1$ while it reaches (SE $= 11.95$ bits/s/Hz) when $\kappa = 0.90$. It is also worth mentioning that increasing the number of BS antennas decreases the negative impact of the HWIs, where a 14.60% performance degradation occurs when $M = 10$ while the degradation decreases to 8.36% when $M = 100$. This emphasizes that increasing the number of BS antennas can diminish the effect of the HWIs. Additionally, the HWIs of the BS have the same detrimental effects as the HWIs of the users under the same operating conditions.

Fig. 4.6 depicts the average FD SE when using the proposed power allocation algorithm
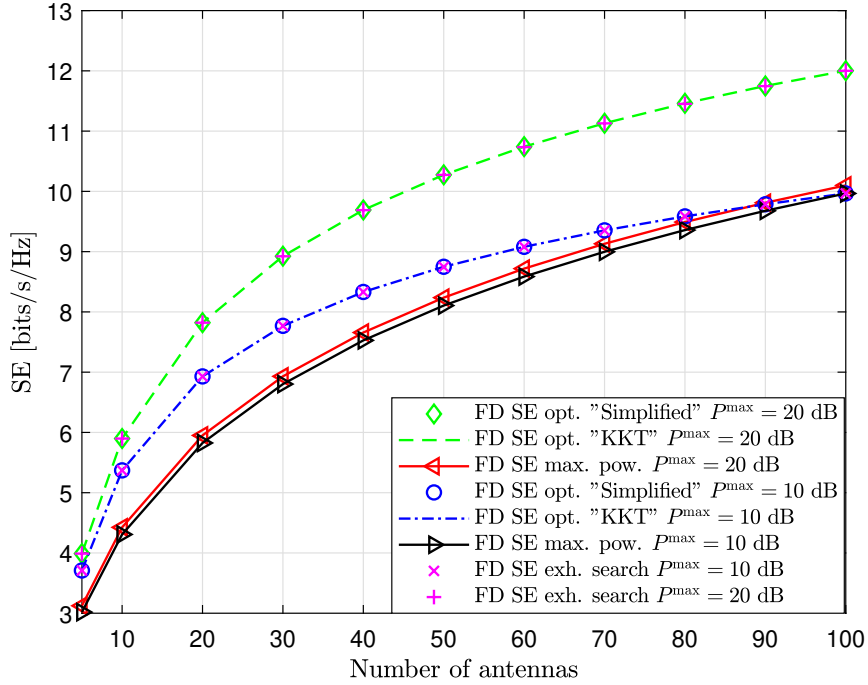
Figure 4.6: The performance of the proposed algorithm vs. the number of antenna. Here, $\Omega_s = 10$, $\kappa = 1$, $\mathcal{R}^d_{\text{th}} = 0.5$ bits/s/Hz and $\mathcal{R}^u_{\text{th}} = 0.25$ bits/s/Hz and $P^{\max}_u = P^{\max}_d = P^{\max}$.

Table 4.1: Optimal values of transmit powers in dB that maximize the SE when $\Omega_s = 10$, $\Omega_I = 1$, $\mathcal{R}^d_{\text{th}} = 0.50$ bits/s/Hz, $\mathcal{R}^u_{\text{th}} = 0.25$ bits/s/Hz and $P^{\max} = 20$ dB.

M	5	10	20	30	40	50	60	70	80	90	100
P^*_u	15.87	12.82	9.76	8.02	6.76	5.79	5	4.33	3.75	3.24	2.78
P^*_d	20	20	20	20	20	20	20	20	20	20	20
$\bar{\mathcal{R}}_u$	0.25	0.25	0.25	0.25	0.25	0.25	0.25	0.25	0.25	0.25	0.25
$\bar{\mathcal{R}}_d$	3.74	5.65	7.57	8.65	9.44	10.03	10.49	10.88	11.21	11.50	11.75

and when increasing the number of BS antennas. Here, both power and QoS constraints are considered. The maximum power transmission is used as a baseline scheme to assess the performance of the proposed algorithm. Many remarks can be made by looking at this figure. First, the simplified algorithm has the same solution as the one obtained using the KKT conditions, and both of them match the exhaustive search results. Second, it
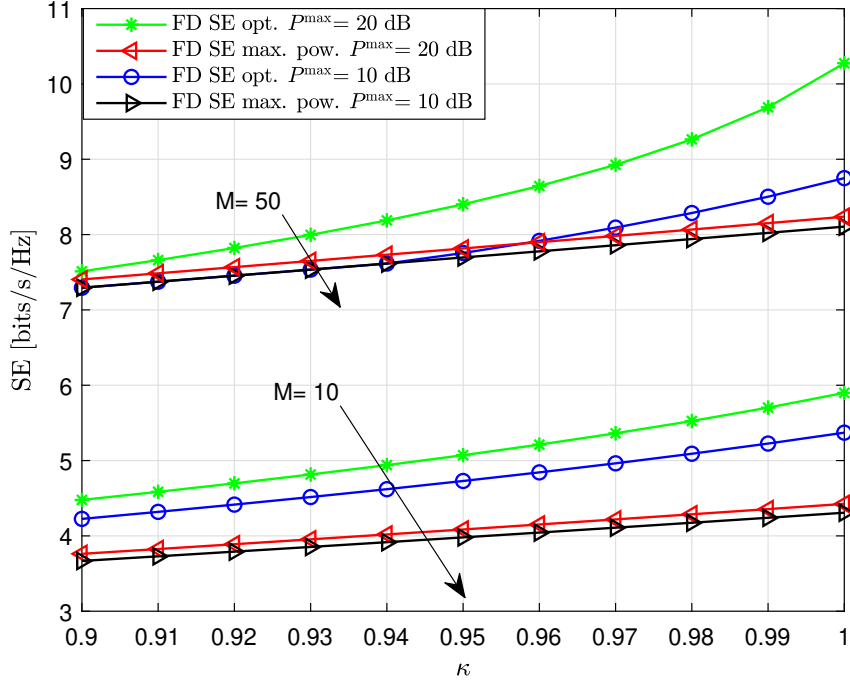
Figure 4.7: The performance of the proposed algorithm vs. different levels of HWIs. Here, $\Omega_s = 10$, $\mathcal{R}_{\text{th}}^d = 0.50$ bits/s/Hz and $\mathcal{R}_{\text{th}}^u = 0.25$ bits/s/Hz.

Table 4.2: Optimal values of transmit powers in dB that maximize the SE when $\Omega_s = 1$, $\Omega_I = 10$, $\mathcal{R}_{\text{th}}^d = 0.25$ bits/s/Hz, $\mathcal{R}_{\text{th}}^u = 0.50$ bits/s/Hz and $P^{\max} = 20$ dB.

M	5	10	20	30	40	50	60	70	80	90	100
P_u^*	20	20	20	20	20	20	20	20	20	20	20
P_d^*	15.87	12.82	9.76	8.02	6.76	5.79	5	4.33	3.75	3.24	2.78
$\bar{\mathcal{R}}_u$	3.74	5.65	7.57	8.65	9.44	10.03	10.49	10.88	11.21	11.50	11.75
$\bar{\mathcal{R}}_d$	0.25	0.25	0.25	0.25	0.25	0.25	0.25	0.25	0.25	0.25	0.25

shows that the gain of the proposed algorithms, compared with the maximum transmitting power, increases when the number of BS antennas M increases until a certain number of antennas. After that, it decreases until both have the same performance because M becomes dominant.

Figure 4.8: The performance of the Max-min SE proposed algorithm vs. different transmit power. Here, $P_u^{\max} = P_d^{\max}$, $\Omega_s = 1$, $\Omega_I = 0.1$, $M = 10$, $\kappa^u = \kappa^d = 0.92$ and $\kappa_r^{\mathrm{BS}} = \kappa_t^{\mathrm{BS}} = 0.98$.

Table 4.1 shows the optimal P_u^* and P_d^* values of the SE in Fig.6. Here, the BS transmits at maximum power while the algorithm allocates the UL user power to meet the required QoS. This occurs because the DL has better conditions (i.e. $\Omega_s = 10$ and $\Omega_I = 1$). These foundations agree with the result in Table 4.2 when the UL user has better conditions (i.e. $\Omega_s = 1$ and $\Omega_I = 10$). Table 4.1, and Table 4.2, show that the proposed algorithms highly reduce the power budget when deploying a large antenna array.

Fig. 4.7 shows the impact of the HWIs and the number of antennas on the average FD SE with different power budgets. More HWIs degrade the system's performance, and the gain obtained when using the proposed algorithm. Increasing the number of BS antennas can actually compensate for the HWIs degradation. Moreover, the proposed algorithm can achieve more gain when there is more power budget.

Fig. 4.8 shows the performance of the max-min SE algorithm, where the fairness be-
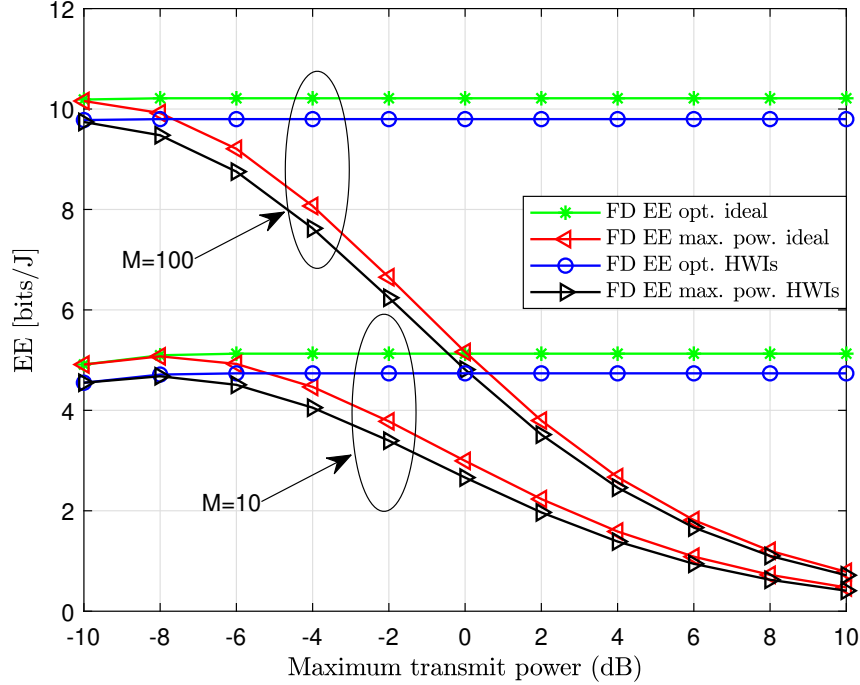
Figure 4.9: Average FD EE at $\Omega_I = \sigma_d^2 = \sigma_u^2 = 0.1$, $\Omega_s = 1$, $\kappa^u = \kappa^d = 0.92$ and $\kappa_r^{\mathrm{BS}} = \kappa_t^{\mathrm{BS}} = 0.98$. Here, $\mathcal{R}_{\mathrm{th}}^d = 0.5$ and $\mathcal{R}_{\mathrm{th}}^u = 0.25$ bits/s/Hz.

tween the UL and DL users can be compared with the maximum power transmission. The algorithm allocates the maximum power to the user with bad conditions (i.e. UL user) while optimizing the transmitted power of the BS that has good conditions (i.e. BS DL) to guarantee fairness. The optimal power values here can be found in Table 4.3.

Fig. 4.9 illustrates the performance of the proposed EE algorithm considering a different number of BS antennas under HWIs. The proposed algorithm achieves remarkable improvements, especially in the high power regime. Additionally, the higher the number of BS antennas, the higher the gain. This result is valid for both ideal and imperfect hardware. Interestingly, increasing the power budgets does not improve the EE because once the optimal powers are obtained we stick with them. It can be explained from (4.38) where increasing P_d and P_u results in a logarithmic increase in the numerator besides, it may decrease it due to HWIs when it reaches the saturation region. On the other hand, increasing P_d and P_u results in a linear increase in the denominator which is much greater than the logarithmic increase. Eventually, the EE will be decreased. The proposed algorithm

73
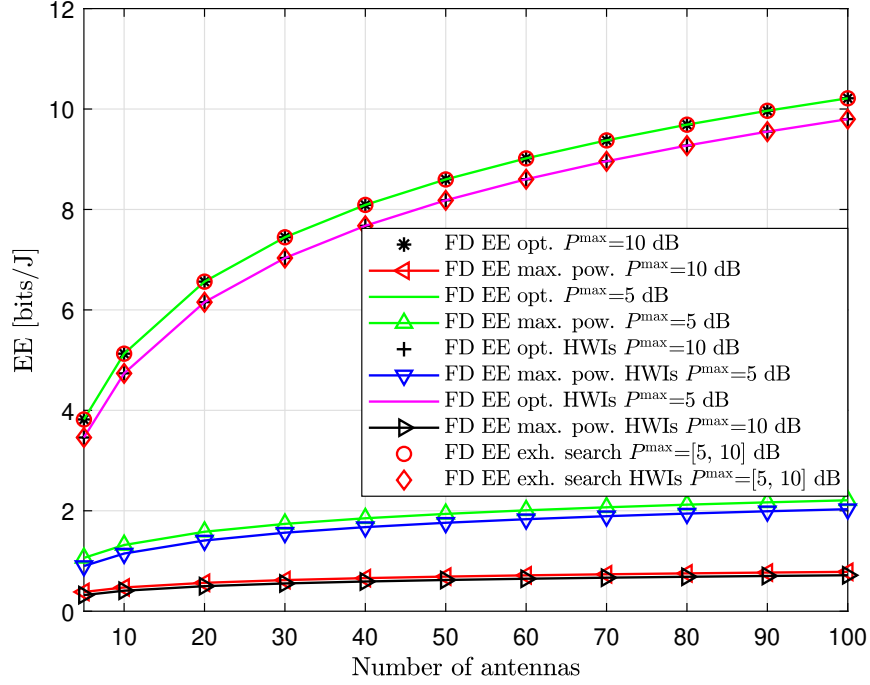
Figure 4.10: Average FD EE at $\Omega_I = \sigma_d^2 = \sigma_u^2 = 0.1$, $\Omega_s = 1$, $\kappa^u = \kappa^d = 0.92$ and $\kappa_r^{\mathrm{BS}} = \kappa_t^{\mathrm{BS}} = 0.98$. Here, $\mathcal{R}_{\mathrm{th}}^d = 0.5$ and $\mathcal{R}_{\mathrm{th}}^u = 0.25$ bits/s/Hz.

Table 4.3: Optimal values of transmit powers in dB for SE Max-min.

$P^{\max}$	0	2	4	6	8	10	12	14	16	18	20
P_u^*	0	2	4	6	8	10	12	14	16	18	20
P_d^*	-1.8	-0.25	1.28	2.8	4.4	6	7.7	9.5	11.3	13.2	15.1

improves the EE by obtaining the best values of P_d and P_u that maximize the numerator and minimize the denominator at the same time.

Fig. 4.10 depicts the average FD EE considering the power and QoS constraints. The exhaustive search and maximum power transmission are used as baseline schemes to assess the performance of the proposed algorithm. First, the results show that the proposed algorithm matches the exhaustive search in performance. Second, the proposed algorithm achieves a significant gain, which increases with the number of BS antennas. However, this gain is slightly degraded due to the effects of HWIs. Third, regardless of the power budget
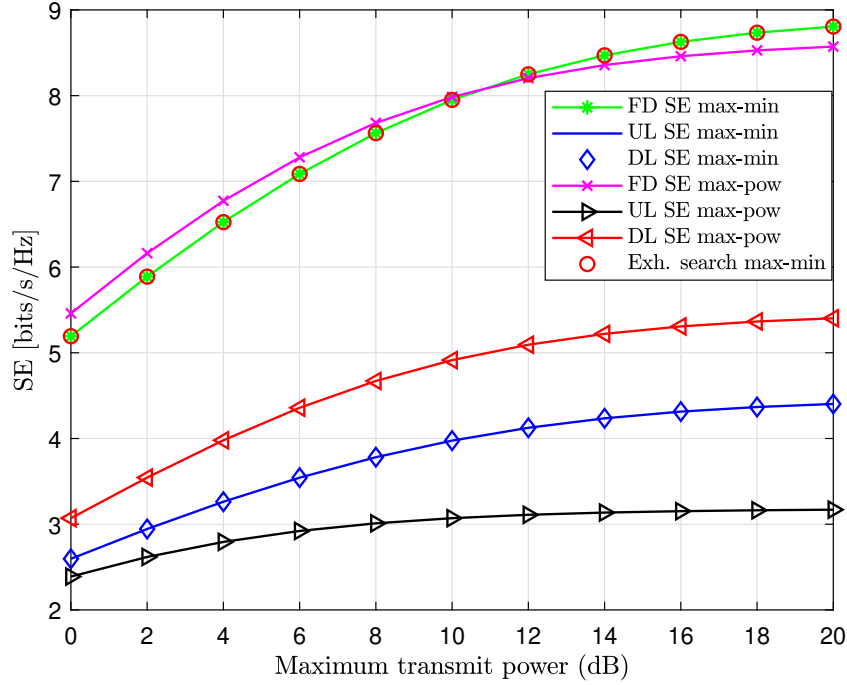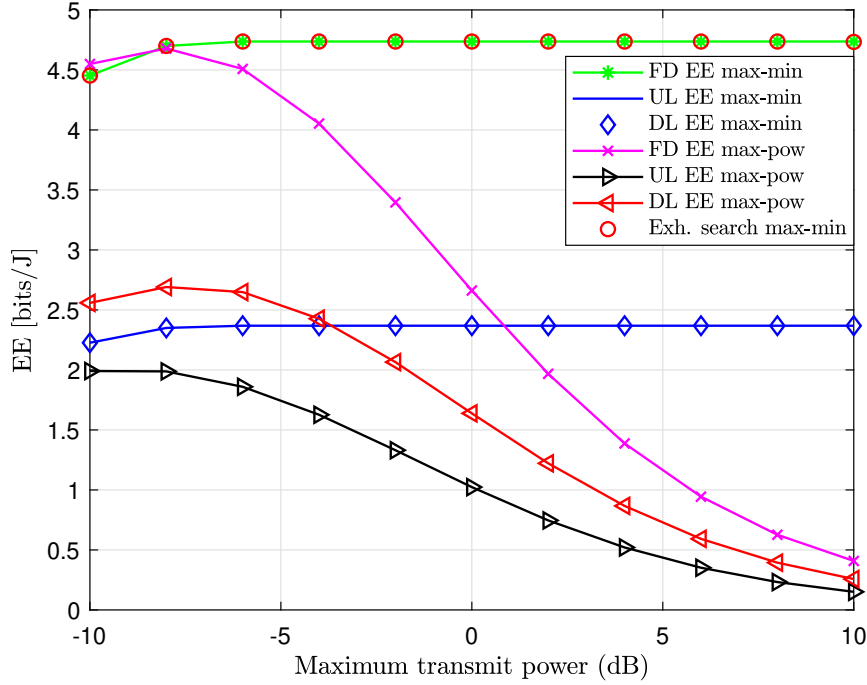
Figure 4.11: The performance of the Max-min EE proposed algorithm vs. different transmit power. Here, $P_u^{\max} = P_d^{\max}$, $\Omega_s = 1$, $\Omega_I = \sigma_d^2 = \sigma_u^2 = 0.1$, $M = 10$, $\kappa^u = \kappa^d = 0.92$ and $\kappa_r^{BS} = \kappa_t^{BS} = 0.98$.

Table 4.4: Optimal values of transmit powers in dB that maximize the EE when $P^{\max} = \{5, 10\}$ dB, $\kappa = 1$.

M	5	10	20	30	40	50	60	70	80	90	100
P_u^*	-5.96	-6.77	-7.53	-7.95	-8.235	-8.45	-8.62	-8.76	-8.88	-8.98	-9.07
P_d^*	-8.69	-9.31	-9.89	-10.21	-10.43	-10.59	-10.72	-10.83	-10.92	-11.00	-11.07

we have (e.g., $P^{\max}$= 5 or 10 dB), we do not stray from optimal values as Tables 4.4 and 4.5 indicate. Fourth, this figure emphasizes that transmitting with maximum power is not the optimal solution in FD systems subjected to power and QoS constraints. Finally, deploying more antennas at the BS mitigates the effect of both the SI and the HWIs. Tables 4.4 and 4.5 show the amount of power that can be saved.

Fig. 4.11 shows the performance of the max-min EE algorithm, where the fairness
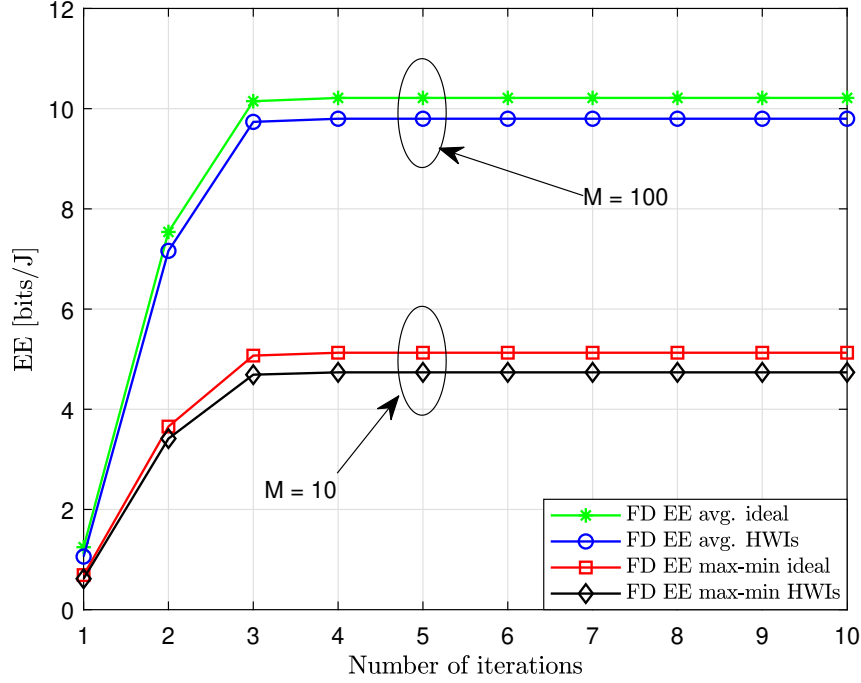
Figure 4.12: Convergence of the proposed algorithms when the power budgets $P_d^{\max} = P_u^{\max} = 10$ dB, $\Omega_s = 1$ $\Omega_I = \sigma_d^2 = \sigma_u^2 = 0.1$. Here, $\mathcal{R}_{\text{th}}^d = 0.5$, $\mathcal{R}_{\text{th}}^u = 0.25$ bits/s/Hz, $\kappa^u = \kappa^d = 0.92$ and $\kappa_r^{\text{BS}} = \kappa_t^{\text{BS}} = 0.98$.

Table 4.5: Optimal values of transmit powers in dB that maximize the EE when $P^{\max} = \{5, 10\}$ dB, $\kappa^u = \kappa^d = 0.92$ and $\kappa_r^{\text{BS}} = \kappa_t^{\text{BS}} = 0.98$.

M	5	10	20	30	40	50	60	70	80	90	100
P_u^*	-6.13	-6.92	-7.67	-8.08	-8.36	-8.58	-8.75	-8.88	-9.00	-9.11	-9.20
P_d^*	-8.82	-9.42	-9.99	-10.31	-10.53	-10.69	-10.82	-10.93	-11.02	-11.10	-11.17

between the UL and DL users can be compared with the maximum power transmission. The algorithm optimizes the transmit power of both the UL user and the BS to maximize the EE and achieve fairness simultaneously. Then we keep the obtained values. The optimal power values here can be found in Table 4.6. Fig. 4.11 also demonstrates that a remarkable EE can be obtained when using the proposed algorithm.

Fig. 4.12 shows the convergence of the proposed algorithms for a certain set of param-
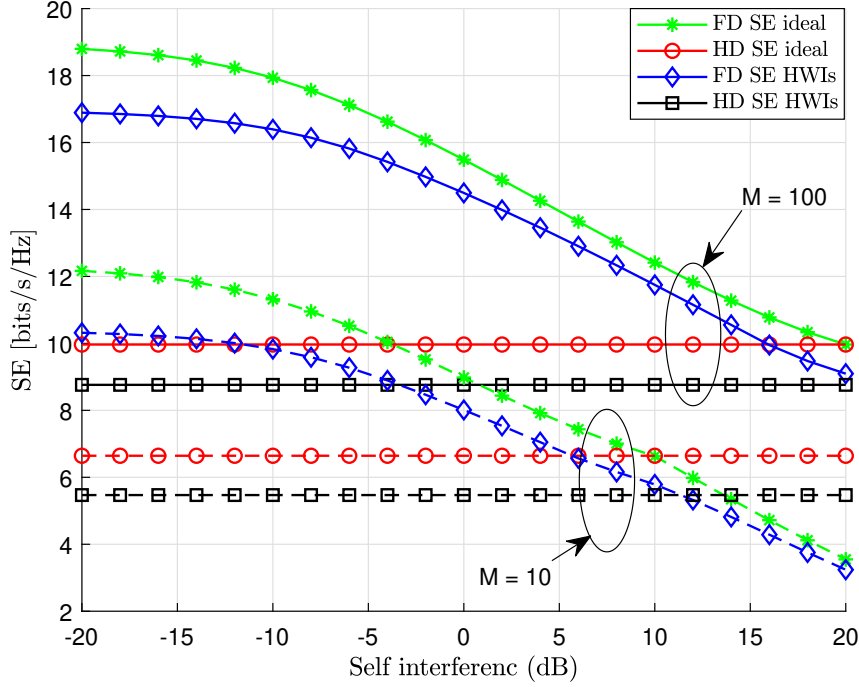
Figure 4.13: The performance of the proposed algorithm vs. the SI power. Here, $\mathcal{R}_{\text{th}}^d = 2$ bits/s/Hz and $\mathcal{R}_{\text{th}}^u = 1$ bits/s/Hz, $P_u^{\max} = P_d^{\max} = 10$ dB, $\Omega_s = 1$, $\Omega_I = 0.1$, $\kappa^u = \kappa^d = 0.92$ and $\kappa_r^{\text{BS}} = \kappa_t^{\text{BS}} = 0.98$.

Table 4.6: Optimal values of transmit powers in dB for EE Max-min.

$P^{\max}$	-10	-8	-6	-4	-2	0	2	4	$\cdots$	$\cdots$	20
P_u^*	-10.00	-8.00	-6.91	-6.91	-6.91	-6.91	-6.91	-6.91	$\cdots$	$\cdots$	-6.91
P_d^*	-11.79	-10.25	-9.42	-9.42	-9.42	-9.42	-9.42	-9.42	$\cdots$	$\cdots$	-9.42

eters. It can be noted that the proposed algorithms present monotonic convergence within a few iterations. It was also verified by simulation that the convergence behaviour is the same when using different parameters. Moreover, this figure illustrates the negative impact of HWIs on EE performance.

Figs. 4.13 and 4.14 compare the SE and EE performance of both the FD and HD systems considering various values of SI under HWIs when $M=10$ and 100. The FD SE and EE outperform those of HD systems at small values of SI. For example, when SI=-20
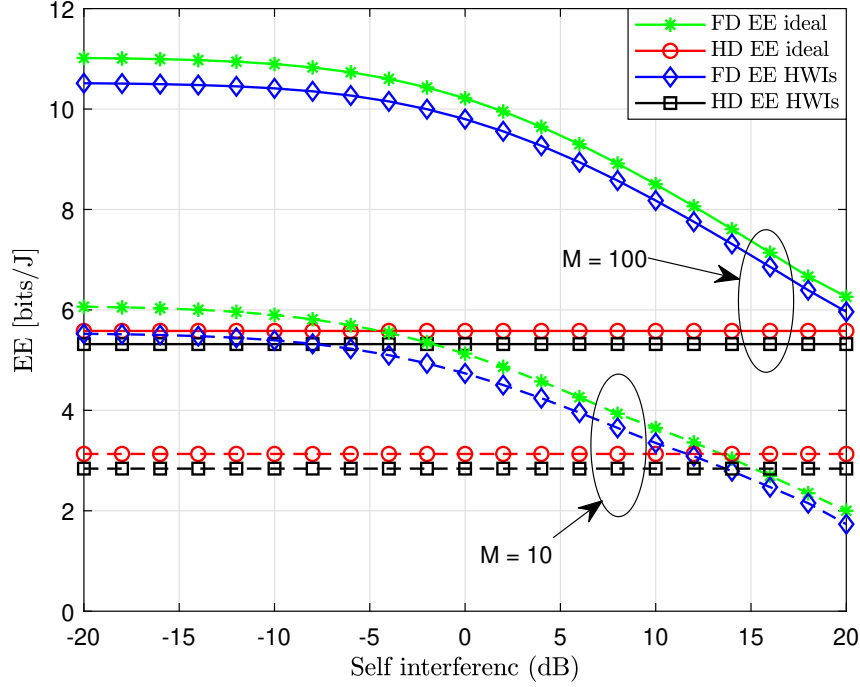
Figure 4.14: The performance of the proposed algorithm vs. the SI power. Here, $\mathcal{R}^d_{\text{th}} = 2$ bits/s/Hz and $\mathcal{R}^u_{\text{th}} = 1$ bits/s/Hz, $P^{\max}_u = P^{\max}_d = 10$ dB, $\Omega_s = 1$, $\Omega_I = \sigma^2_d = \sigma^2_u = 0.1$, $\kappa^u = \kappa^d = 0.92$ and $\kappa^{\text{BS}}_r = \kappa^{\text{BS}}_t = 0.98$.

dB, the FD SE and EE are near double the HD ones. The opposite occurs when the SI increases and the HD performance becomes better. For example, when SI= -20 dB and M=100, the FD SE gain of the proposed algorithm is 89% and 93% more than the HD for the ideal and impaired systems, respectively. This gain is 98% for the ideal and impaired systems considering the EE. In addition, Fig. 4.13 shows that HD SE systems outperform FD ones after the SI= 10 dB for the ideal hardware when M=10. This point (i.e., SI=10) shifts to the right in the presence of HWIs (i.e., SI=12 dB). Interestingly, at lower values of SI (e.g., SI < 6 dB), the impaired FD SE outperforms the ideal HD one when M=10. The same performance can be seen when SI< 16 dB if M=100.

4.6 Conclusion

This work examines the power allocation optimization of impaired FD systems. First, mathematical expressions for the average lower bound UL/DL SE and EE are derived to assess the system performance considering Nakagami-m fading channels. Second, different power allocation algorithms to find the optimal UL/DL powers aiming to maximize the SE and EE are proposed. The results indicate that the average FD SE saturates due to the HWIs and the interference. Moreover, transmitting the maximum power is not the optimal solution for FD systems, especially when there are QoS and power budget requirements. Interestingly, the SE algorithm achieves a higher gain when higher power budgets are available while the EE does not. Finally, the results show that when SI has small values, the impaired FD communications outperform ideal HD communications, which relaxes the design constraints of FD systems. Multi-user, imperfect channel conditions and other fading channel models will be considered in future works.

Chapter 5

Towards a Practical FD MU-MIMO System: Performance Analysis Considering Imperfect CSI and Non-ideal Transceivers

5.1 Introduction and Related Works

WIRELESS communication technologies have seeped into every aspect of our day-to-day lives. Such growth can only be supported by higher data rates, lower latency, and greater reliability. However, the SE of wireless connections is hindered by many factors, including low SNR decreased transceiver and RF chain quality, as well as channel estimation and digital signal processing errors [23, 129–132].

The combination of SDMA and MIMO techniques allows for efficient utilization of the frequency spectrum. For SDMA transmission, it has been proven that the total SE increases proportionally to the number of users. This is achieved by serving multiple users simultaneously, and by increasing the number of BS antennas in a way that achieves an array gain counteracting the increased interference [1]. The FD system can theoretically double the SE because signals can be transmitted and received at the same time-frequency resource.

However, the major challenge for FD is the SI at the BS, created by the transmitted DL signals to the received UL signals. The interference signal can be 50–100 dB stronger than the desired one at the receiver [20]. As a result, appropriate SI suppression and cancellation are critical factors to consider during system implementation [20,21]. In [85,96], the achievable rate of FD massive MIMO relay systems over Rician fading channels was investigated. It was seen that the SI can be effectively canceled by using zero-forcing (ZF) processing at the decode-and-forward relay when the number of antennas is increased to infinity. The same findings were obtained in [97] for the multi-cell FD MU-MIMO system. The authors in [133] studied the effects of channel estimation errors and HWIs on the secrecy performance of NOMA systems.

In practice, the physical transceivers experience many hardware imperfections, such as power amplifier nonlinearities, in-phase quadrature-phase (I/Q) imbalance, analog imperfectness, phase noise, time and frequency synchronization errors, etc. While these impairments are generally mitigated in existing communication systems, HWIs may cause major issues for FD systems because the degradation caused is accumulated, and even made worse, in the presence of the SI and IUI [101,102,111,134]. In this chapter, the residual HWIs after appropriate compensation has been performed for each transceiver hardware component are considered. Motivated by the promising nature of FD MU-MIMO, the contribution of this chapter can be summarized as

- Studies the joint impact of the channel estimation errors and HWIs on the system performance when using MRC/MRT and zero-forcing reception/zero-forcing transmission (ZFR/ZFT) linear detectors/precoders. Using the ZF technique, the IUI can be eliminated and considerable improvements in the performance of the FD MU-MIMO can be achieved compared to the MRC one.

- Derives mathematical frameworks for the lower bounds of the average FD DL/UL SE under imperfect channel state information (CSI) in the presence of HWIs at all system terminals (i.e., DL users, UL users, transmit and receive antenna array at the BS) and IUI.

- Designs linear minimum mean square error (LMMSE) and least square (LS) estima-
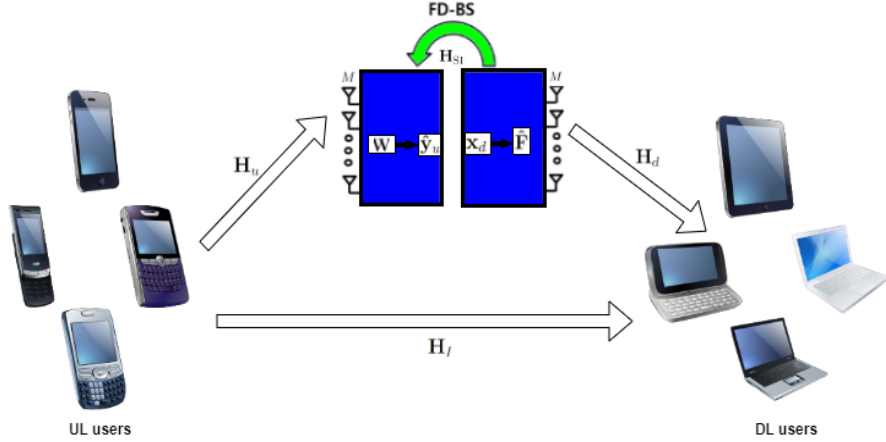
Figure 5.1: Full-duplex multi-user MIMO system model.

tors for the impaired FD MU-MIMO system. At high transmission power, there is an error floor in the channel estimation, which depends on the hardware quality. On the other hand, this estimation error tends to be zero in the case of ideal hardware. Increasing the number of pilots can eliminate the estimation error for both ideal and impaired systems.

5.2   System and Channel Models

5.2.1   System and Signal Model

This work considers a single-cell FD MU-MIMO system as illustrated in Fig. 5.1. There are M transmit and M receive antennas at the BS. This BS serves K_d DL and K_u UL users, each equipped with one antenna. IUI between the UL and DL users is assumed. SI exists at the BS, as well, which is the interference from the transmit antenna array to the receive antenna array. Interference cancellation is conducted to reduce the SI [93,94]. $\mathbf{H}_{\mathrm{SI}} \in C^{M \times M}$ is used to represent the residual SI channel matrix, whose entries can be modeled as independent and identically distributed (i.i.d.), each following $\mathcal{CN} \sim (0, \sigma_s^2)$ [14–19]. Here, σ_s^2 represents the residual SI power and is modeled by a Rayleigh distribution [12–14, 18] [1]. The UL

---

[1]Before active cancellation, the SI can be modeled as a Rician distribution with a large K-factor because it has a strong line-of-sight (LOS) component before the active cancellation. The work in [12,118] showed that the analog cancellation attenuates the strong LOS component of the SI channel and the residual SI channel follows a Rician distribution with a small K-factor or a Rayleigh distribution.

channel matrix, from the K_u UL users to the BS, is denoted as $\mathbf{H}_u \in C^{M \times K_u}$, and the DL channel matrix, from the BS to the K_d DL users, is denoted as $\mathbf{H}_d \in C^{M \times K_d}$. The channel matrices can be modeled as [4, 13, 85]

$$\mathbf{H}_x = \mathbf{G}_x \mathbf{D}_x^{\frac{1}{2}}, \quad \text{for} \quad x \in \{u, d\}, \tag{5.1}$$

where $\mathbf{G}_x \in C^{M \times K_x}$ denotes the small-scale fading channel matrix and $\mathbf{D}_x = \text{diag}\{[\beta_{x,1}, \ldots, \beta_{x,K_x}]\}$. In this case, $\beta_{x,i}$ is the large-scale fading coefficient between the BS and the ith user. It is assumed that $\mathbf{G}_u$ and $\mathbf{G}_d$ channels are Rayleigh channels, the elements of which are i.i.d. complex Gaussian random variables with zero mean and unit variance. Furthermore, $\mathbf{H}_I \in C^{K_d \times K_u}$ represents the channel between the set of UL users and the set of DL users. The elements of $\mathbf{H}_I$ are assumed to be independent with the $(i, j)^{th}$ entry following $\mathcal{CN} \sim (0, \sigma_{I_{i,j}}^2)$ [15, 17, 19].

5.2.2 Hardware Impairment Model

Physical transceiver implementations include various electronic circuits, each circuit distorting the signal in different ways. In practice, compensation algorithms are considered for each impaired component; however, after the compensation, some residual impairments linger. Analytically and experimentally, the aggregate residual hardware impairments are modeled as independent additive Gaussian distortion noise with zero-mean and a variance proportional to the average transmitted signal power [1, 135–138]. Using the HWI model in (2.1) and assuming that all the UL users have the same HWI factor κ^u and additive distortion noise η_u. Similarly, the DL users have the same HWI factor κ^d and additive distortion noise η_d. For the coming discussion, κ_t^{BS}, η_{BS}^t, and κ_r^{BS}, η_{BS}^r are used to represent the transmitter and receiver HWI factors and additive distortion noises at the BS, respectively. Moreover, since the BS consists of a homogeneous and identical set of antennas, the hardware factors are considered to be the same.

Uplink scenario in FD MU-MIMO systems: The transmitted signal of the kth UL user follows $x_{u,k} \sim \mathcal{CN}(0, 1) \ \forall k \in [1, 2, \ldots, K_u]$. This complex Gaussian signal is distorted by the transmitter hardware. From (2.1), $\tilde{x}_{u,k} = \sqrt{\kappa^u P_u} x_{u,k} + \eta_u$, will be sent over the channel instead of $x_{u,k}$. The transmitted power is P_u. The factor $\kappa^u \in (0, 1]$ determines the
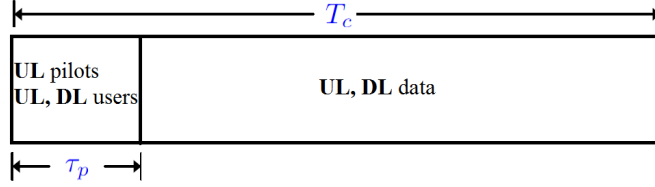
Figure 5.2: Channel estimation.

quality of the UL user's transmitter hardware, and $\eta_u \sim \mathcal{CN}(0, (1-\kappa^u)P_u)$ is the hardware additive distortion term.

Downlink scenario in FD MU-MIMO systems: The BS is supposed to transmit the signal vector $\mathbf{x}_d = [x_{d,1}, x_{d,2}, \ldots, x_{d,K_d}]^{\mathrm{T}}$, where $x_{d,j}$ is the signal intended to the jth DL user, $\forall j \in [1, 2, \ldots, K_d]$, and $\mathbf{x}_d$ is normalized as $\mathbb{E}\{\mathbf{x}_d\mathbf{x}_d^H\} = \mathbf{I}_{K_d}$. The BS applies a precoding vector $\hat{\mathbf{f}}_{d,j}$ depending on the current channel realizations. As such, the transmitted vector over the channel becomes $\mathbf{s}_d = \sum_{j=1}^{K_d} \sqrt{\frac{P_d}{K_d}}\hat{\mathbf{f}}_{d,j}x_{d,j}$ instead of $\mathbf{x}_d$. From (2.1), $\tilde{\mathbf{s}}_d = \sqrt{\kappa_t^{\mathrm{BS}}}\mathbf{s}_d + \boldsymbol{\eta}_{\mathrm{BS}}^t$. The factor $\kappa_t^{\mathrm{BS}} \in (0, 1]$ determines the quality of the hardware at each BS transmitter antenna, and the hardware additive distortion term $\boldsymbol{\eta}_{\mathrm{BS}}^t \sim \mathcal{CN}(\mathbf{0}_M, \mathbf{C}_{\boldsymbol{\eta}_{\mathrm{BS}}}^t) \in \mathbb{C}^M$. The covariance matrix $\mathbf{C}_{\boldsymbol{\eta}_{\mathrm{BS}}}^t \in \mathbb{C}^{M \times M}$ can be given as

$$\mathbf{C}_{\boldsymbol{\eta}_{\mathrm{BS}}}^t = (1 - \kappa_t^{\mathrm{BS}})\frac{P_d}{K_d} \operatorname{diag}\left(\sum_{i=1}^{K_d} |\hat{f}_{d,i}^{(1)}|^2, \sum_{i=1}^{K_d} |\hat{f}_{d,i}^{(2)}|^2, \cdots, \sum_{i=1}^{K_d} |\hat{f}_{d,i}^{(M)}|^2\right), \qquad (5.2)$$

where $\hat{f}_d^{(i)}$ denotes the ith element of $\hat{\mathbf{f}}_d$.

5.3 Channel Estimation

In practice, the channel matrix $\mathbf{H}$ has to be estimated at the BS. The standard way of doing this is to use UL pilots, with a part of the coherence interval of the channel used for UL training. Let T_c be the coherence time interval and let τ_p be the number of symbols used for pilots. During the training part of the coherence interval, all users simultaneously transmit mutually orthogonal pilot sequences of length τ_p symbols. The pilot sequences used by the $K = K_d + K_u$ users can be represented by the $\mathbf{X}^p \in \mathbb{C}^{\tau_p \times K}$ matrix with $(\tau_p \geq K)$. Here, orthogonal pilots are assumed, $(\mathbf{X}^p)^H \mathbf{X}^p = \tau_p \mathbf{I}_K$. The received pilot signal from the kth

user $\mathbf{Y}_k^p \in \mathbb{C}^{M \times \tau_p}$ at the BS can be given as

$$\mathbf{Y}_k^p = \sqrt{P_u \kappa_r^{\mathrm{BS}} \kappa^u} \mathbf{h}_k (\mathbf{x}_k^p)^T + \sqrt{\kappa_r^{\mathrm{BS}}} \mathbf{h}_k \boldsymbol{\eta}_k^T + \boldsymbol{\eta}_{\mathrm{BS}}^r + \mathbf{N}_u, \tag{5.3}$$

where $\boldsymbol{\eta}_k$ and $\boldsymbol{\eta}_{\mathrm{BS}}^r$ represent the user's transmitter Gaussian distortion and the receiver Gaussian distortion at the BS, respectively. $\mathbf{N}_u$ is the additive white Gaussian noise (AWGN) at the BS receive antenna array with each element following $\mathcal{CN}(0, \sigma_u^2)$. The BS estimates the channel $\mathbf{h}_k$ from the kth user by correlating the received pilot signal $\mathbf{Y}_k^p$ with the pilot sequence $(\mathbf{x}_k^p)^*$ employed by this user. Then, $\mathbf{y}_k^p = \mathbf{Y}_k^p (\mathbf{x}_k^p)^*$ can be given as

$$\mathbf{y}_k^p = \tau_p \sqrt{P_u \kappa_r^{\mathrm{BS}} \kappa^u} \mathbf{h}_k + \sqrt{\kappa_r^{\mathrm{BS}}} \mathbf{h}_k \boldsymbol{\eta}_k^T (\mathbf{x}_k^p)^* + \boldsymbol{\eta}_{\mathrm{BS}}^r (\mathbf{x}_k^p)^* + \mathbf{N}_u (\mathbf{x}_k^p)^*. \tag{5.4}$$

It is assumed that all channels are independent so that each channel can be estimated separately. The elements of $\mathbf{y}_k^p$ can be averaged over τ_p, resulting in

$$y_{k,i}^p = \sqrt{P_u \kappa_r^{\mathrm{BS}} \kappa^u} h_{k,i} + \frac{1}{\tau_p} \sqrt{\kappa_r^{\mathrm{BS}}} h_{k,i} \sum_{l=1}^{\tau_p} \eta_{k,l} x_{k,l}^{p*} + \frac{1}{\tau_p} \sum_{l=1}^{\tau_p} \eta_{\mathrm{BS},l}^r x_{k,l}^{p*} + \frac{1}{\tau_p} \sum_{l=1}^{\tau_p} n_u x_{k,l}^{p*}, \tag{5.5}$$

where $v_{k,i}$ denotes the ith element in $\mathbf{v}_k$.

- Using the LMMSE estimator, the estimated channel $\hat{h}_{k,i}$ can be given as [1,75]

$$\hat{h}_{k,i}^{\mathrm{LMMSE}} = \frac{\tau_p \sqrt{P_u \kappa_r^{\mathrm{BS}} \kappa^u} \beta_k}{P_u \kappa_r^{\mathrm{BS}} \kappa^u (\tau_p - 1)\beta_k + P_u \beta_k + \sigma_u^2} y_{k,i}^p, \tag{5.6}$$

where $\hat{h}_{k,i}$ is the estimated channel between the ith BS antenna and the kth user. The large-scale fading coefficient between the BS and the kth user is denoted by β_k. The variance of the estimated channel $\mathbb{E}\{\hat{h}_{k,i} \hat{h}_{k,i}^*\}$ can be given as

$$\sigma_{\hat{h}_{k,i}}^{2,\mathrm{LMMSE}} = \frac{\tau_p P_u \kappa_r^{\mathrm{BS}} \kappa^u \beta_k^2}{P_u \kappa_r^{\mathrm{BS}} \kappa^u (\tau_p - 1)\beta_k + P_u \beta_k + \sigma_u^2}. \tag{5.7}$$

The MSE in the presence of the HWIs can be given as

$$\mathrm{MSE}^{\mathrm{LMMSE}} = \sigma_{e_{k,i}}^{2,\mathrm{LMMSE}} = \beta_k \left(1 - \frac{\tau_p P_u \kappa_r^{\mathrm{BS}} \kappa^u \beta_k}{P_u \kappa_r^{\mathrm{BS}} \kappa^u (\tau_p - 1)\beta_k + P_u \beta_k + \sigma_u^2} \right). \tag{5.8}$$

- Using the LS estimator, the estimated channel $\hat{h}_{k,i}$ can be given as [73]

$$\hat{h}_{k,i}^{\mathrm{LS}} = \frac{y_{k,i}^p}{\sqrt{P_u \kappa_r^{\mathrm{BS}} \kappa^u}}. \tag{5.9}$$

(a) LMMSE with ideal hardware. (b) LMMSE with HWIs, $\kappa_r^{\text{BS}} = \kappa^u = 0.95$.
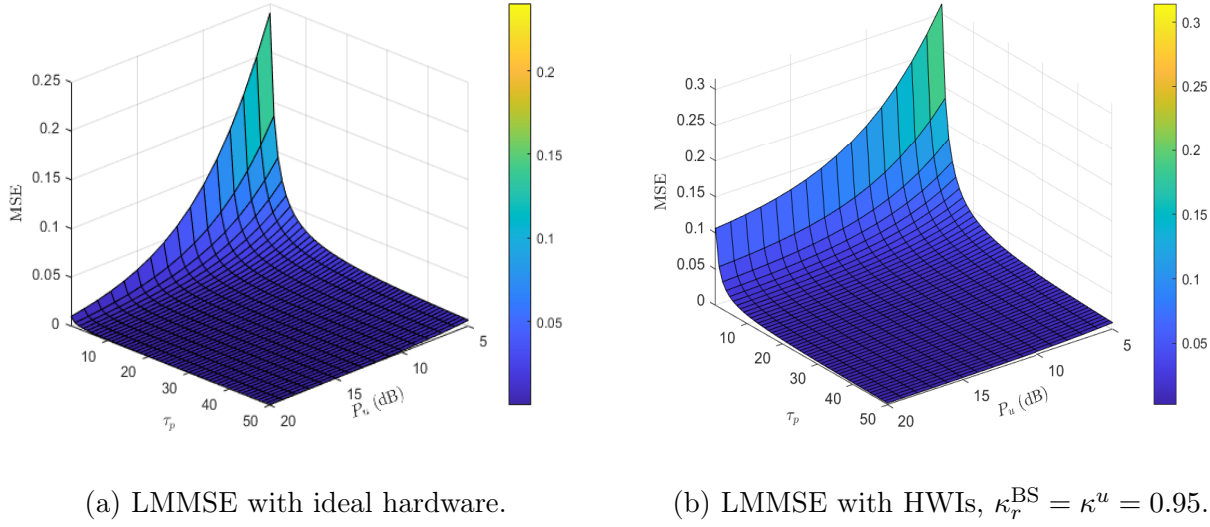
Figure 5.3: The MSE of LMMSE estimation with a different number of pilots and transmit power for the ideal hardware and in presence of HWIs.

The variance of the estimated channel, $\mathbb{E}\{\hat{h}_{k,i}\hat{h}_{k,i}^*\}$ can be given as

$$\sigma_{\hat{h}_{k,i}}^{2,\text{LS}} = \beta_k - \frac{(1 - \kappa_r^{\text{BS}}\kappa^u)P_u\beta_k + \sigma_u^2}{\tau_p P_u \kappa_r^{\text{BS}}\kappa^u}. \tag{5.10}$$

Consequently, the MSE in the presence of the HWIs can be given as

$$\text{MSE}^{\text{LS}} = \sigma_{e_{k,i}}^{2,\text{LS}} = \frac{(1 - \kappa_r^{\text{BS}}\kappa^u)P_u\beta_k + \sigma_u^2}{\tau_p P_u \kappa_r^{\text{BS}}\kappa^u}. \tag{5.11}$$

In Fig. 5.3, the performance of the LMMSE estimator is illustrated. As the figure shows, in the ideal case (i.e., $\kappa_r^{\text{BS}} = \kappa^u = 1$), the estimation error goes to zero when either $\tau_p \to \infty$ or $P_u \to \infty$. This gives us the flexibility to choose between using a large transmission power or a large number of pilots to achieve better channel estimation. This tradeoff is practical in that it depends on applications and budgets. For example, if we are concerned about improving the SE, we will use one pilot $\tau_p = 1$ with a large transmission power because τ_p is a pre-log factor when calculating the SE.

The results are not the same in the presence of HWIs, as the MSE has an error floor even when P_u increases. Fortunately, the figure shows that when τ_p is increased, $\text{MSE}^{\text{LMMSE}}$ approaches zero. As such, it can be concluded that increasing the number of pilots can

86
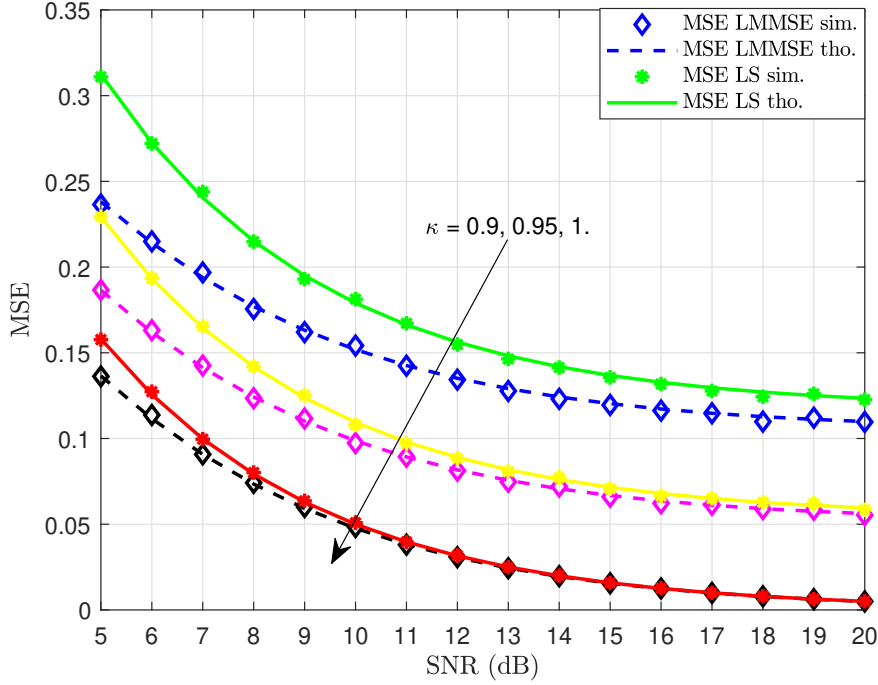
Figure 5.4: The LMMSE and LS with HWIs.

efficiently mitigate the effects of the HWIs. LS performance shows the same trend as LMMSE, and to avoid unnecessary repetition the results are not shown.

The asymptotic MSEs when $P_u \to \infty$ and $\tau_p \to \infty$, are

$$
\begin{aligned}
\lim_{P_u \to \infty} \mathrm{MSE}^{\mathrm{LMMSE}} &= \frac{(1 - \kappa_r^{\mathrm{BS}} \kappa^u) \beta_k}{\tau_p \kappa_r^{\mathrm{BS}} \kappa^u + (1 - \kappa_r^{\mathrm{BS}} \kappa^u)}, \\
\lim_{P_u \to \infty} \mathrm{MSE}^{\mathrm{LS}} &= \frac{(1 - \kappa_r^{\mathrm{BS}} \kappa^u) \beta_k}{\tau_p \kappa_r^{\mathrm{BS}} \kappa^u}, \\
\lim_{\tau_p \to \infty} \mathrm{MSE}^{\mathrm{LMMSE}} &= \lim_{\tau_p \to \infty} \mathrm{MSE}^{\mathrm{LS}} = 0.
\end{aligned}
\tag{5.12}
$$

In Fig. 5.4, the performance of the LMMSE and LS estimators are compared. Apparently, LMMSE estimation is outperforming LS even for imperfect hardware conditions.

5.4 Performance Analysis of Uplink Spectral Efficiency with HWIs and Imperfect Channel State Information

This section discusses the UL SE performance of the studied FD MU-MIMO system. It first derives the signal-to-interference plus noise ratio (SINR) at the BS. Then it derives the lower bound achievable rate for both detection techniques (i.e., MRC and the ZFR). Moreover, it discusses the SE for each detection technique when using the LMMSE and LS estimators.

Considering the transceiver HWIs, the received UL signals vector at the BS can be written as

$$\mathbf{y}_u = \sqrt{\kappa_r^{\text{BS}}}\mathbf{H}_u\tilde{\mathbf{x}}_u + \sqrt{\kappa_r^{\text{BS}}}\mathbf{H}_{\text{SI}}\tilde{\mathbf{s}}_d + \boldsymbol{\eta}_{\text{BS}}^r + \mathbf{n}_u \quad \in \mathbb{C}^M, \tag{5.13}$$

where the elements of the transmitted vector $\tilde{\mathbf{x}}_u$ are $\tilde{x}_{u,k} = \sqrt{\kappa^u P_u}x_{u,k} + \eta_u$, $\forall k \in [1, 2, \ldots, K_u]$. Now, if the system has imperfect channel state conditions, the received signal becomes

$$\hat{\mathbf{y}}_u = \underbrace{\sqrt{\kappa_r^{\text{BS}}\kappa^u P_u}\,\hat{\mathbf{h}}_{u,k}x_{u,k}}_{\text{Desired signal}} + \underbrace{\sqrt{\kappa_r^{\text{BS}}\kappa^u P_u}\sum_{i=1,i\neq k}^{K_u}\hat{\mathbf{h}}_{u,i}x_{u,i}}_{\text{UL-UL interference signals}} + \underbrace{\sqrt{\kappa_r^{\text{BS}}\kappa_t^{\text{BS}}}\left(\sum_{j=1}^{K_d}\sqrt{\frac{P_d}{K_d}}\mathbf{H}_{\text{SI}}\hat{\mathbf{f}}_{d,j}x_{d,j}\right)}_{\text{SI interference signals}}$$

$$+ \underbrace{\sqrt{\kappa_r^{\text{BS}}}\sum_{i=1}^{K_u}\hat{\mathbf{h}}_{u,i}\eta_u - \sqrt{\kappa_r^{\text{BS}}}\sum_{i=1}^{K_u}\mathbf{e}_{u,i}\eta_u + \sqrt{\kappa_r^{\text{BS}}}\mathbf{H}_{\text{SI}}\boldsymbol{\eta}_{\text{BS}}^t + \boldsymbol{\eta}_{\text{BS}}^r}_{\text{Distortion noise}=\boldsymbol{\eta}} - \underbrace{\sqrt{\kappa_r^{\text{BS}}\kappa^u P_u}\sum_{i=1}^{K_u}\mathbf{e}_{u,i}x_{u,i}}_{\text{Estimation error}}$$

$$+ \underbrace{\mathbf{n}_u}_{\text{AWGN}}, \tag{5.14}$$

where $\mathbf{n}_u \sim \mathcal{CN}(0, \sigma_u^2\mathbf{I}_M)$ is AWGN at the BS receive array. The channel estimation errors vector is denoted by $\mathbf{e}_u \triangleq \hat{\mathbf{h}}_u - \mathbf{h}_u$. The UL signals from the desired user and the interfering user are denoted by $x_{u,k}, x_{u,i}$, respectively. The DL signal is denoted by $x_{d,j}$. The complex transmitter additive distortion noise of the UL users and BS is denoted by η_u and $\boldsymbol{\eta}_{\text{BS}}^t$, respectively. The receiver Gaussian distortion noise at the BS is denoted by

$\boldsymbol{\eta}_{\mathrm{BS}}^r \sim \mathcal{CN}(\mathbf{0}_M, \mathbf{C}_{\boldsymbol{\eta}_{\mathrm{BS}}}^r)$, where $\mathbf{C}_{\boldsymbol{\eta}_{\mathrm{BS}}}^r$ is given as

$$\mathbf{C}_{\boldsymbol{\eta}_{\mathrm{BS}}}^r = (1 - \kappa_r^{\mathrm{BS}})\big[\mathbf{A} + \mathbf{B}\big],$$

$$\mathbf{A} = P_u \mathrm{diag}\left(\sum_{k=1}^{K_u} |\hat{h}_{u,k}^{(1)}|^2 + |e_{u,k}^{(1)}|^2, \sum_{k=1}^{K_u} |\hat{h}_{u,k}^{(2)}|^2 + |e_{u,k}^{(2)}|^2, \cdots, \sum_{k=1}^{K_u} |\hat{h}_{u,k}^{(M)}|^2 + |e_{u,k}^{(M)}|^2\right),$$

$$\mathbf{B} = \frac{P_d}{K_d}\mathrm{diag}\left(\sum_{j=1}^{K_d}\sum_{i=1}^{\mathrm{M}}\left|\mathbf{H}_{\mathrm{SI}}^{1,i}\hat{f}_{d,j}^{(i)}\right|^2, \sum_{j=1}^{K_d}\sum_{i=1}^{\mathrm{M}}\left|\mathbf{H}_{\mathrm{SI}}^{2,i}\hat{f}_{d,j}^{(i)}\right|^2, \cdots, \sum_{j=1}^{K_d}\sum_{i=1}^{\mathrm{M}}\left|\mathbf{H}_{\mathrm{SI}}^{M,i}\hat{f}_{d,j}^{(i)}\right|^2\right). \quad (5.15)$$

Here, $\hat{h}_{u,k}^{(i)}$ denotes the ith element of $\hat{\mathbf{h}}_{u,k}$ and $\mathbf{H}_{\mathrm{SI}}^{k,i}$ is the ith element of the kth row of $\mathbf{H}_{\mathrm{SI}}$. All the additive distortions in (5.14) can be combined to an $\boldsymbol{\eta} \sim \mathcal{CN}(\mathbf{0}_M, \mathbf{C}_{\boldsymbol{\eta}})$ and $\mathbf{C}_{\boldsymbol{\eta}}$ can be written as

$$\mathbf{C}_{\boldsymbol{\eta}} = (1 - \kappa_r^{\mathrm{BS}}\kappa^u)\mathbf{A} + (1 - \kappa_r^{\mathrm{BS}}\kappa_t^{\mathrm{BS}})\mathbf{B}. \quad (5.16)$$

Let $\mathbf{W} \in \mathbb{C}^{M \times K_u}$ be a linear combining matrix that depends on the estimated channel $\hat{\mathbf{H}}_u$. By using the linear combining technique, the received signal is separated into streams as it is multiplied by $\mathbf{W}^H$. In this work, MRC and ZF are considered as [4]

$$\mathbf{W} = \begin{cases} \hat{\mathbf{H}}_u & \text{for MRC,} \\ \hat{\mathbf{H}}_u \left(\hat{\mathbf{H}}_u^H \hat{\mathbf{H}}_u\right)^{-1} & \text{for ZF.} \end{cases} \quad (5.17)$$

The BS applies $\mathbf{W}^H$ to the received signal in (5.14). After that, the received signal of the kth user can be calculated as

$$\mathbf{w}_{u,k}^H \hat{\mathbf{y}}_u = \underbrace{\sqrt{\kappa_r^{\mathrm{BS}}\kappa^u P_u}\, \mathbf{w}_{u,k}^H \hat{\mathbf{h}}_{u,k} x_{u,k}}_{\text{Desired signal}} + \underbrace{\sqrt{\kappa_r^{\mathrm{BS}}\kappa^u P_u}\sum_{i=1,i\neq k}^{K_u} \mathbf{w}_{u,k}^H \hat{\mathbf{h}}_{u,i} x_{u,i} +}_{\text{UL-UL interference signals}}$$

$$\underbrace{\sqrt{\kappa_r^{\mathrm{BS}}\kappa_t^{\mathrm{BS}}}\left(\sum_{j=1}^{K_d}\sqrt{\frac{P_d}{K_d}}\mathbf{w}_{u,k}^H \mathbf{H}_{\mathrm{SI}}\hat{\mathbf{f}}_{d,j} x_{d,j}\right)}_{\text{SI signals}} - \underbrace{\sqrt{\kappa_r^{\mathrm{BS}}\kappa^u P_u}\sum_{i=1}^{K_u} \mathbf{w}_{u,k}^H \mathbf{e}_{u,i} x_{u,i} +}_{\text{Estimation error}}$$

$$\underbrace{\sqrt{\kappa_r^{\mathrm{BS}}}\sum_{i=1}^{K_u} \mathbf{w}_{u,k}^H \hat{\mathbf{h}}_{u,i}\eta_{u,i} - \sqrt{\kappa_r^{\mathrm{BS}}}\sum_{i=1}^{K_u} \mathbf{w}_{u,k}^H \mathbf{e}_{u,i}\eta_{u,i} + \sqrt{\kappa_r^{\mathrm{BS}}}\mathbf{w}_{u,k}^H \mathbf{H}_{\mathrm{SI}}\boldsymbol{\eta}_{\mathrm{BS}}^t + \mathbf{w}_{u,k}^H \boldsymbol{\eta}_{\mathrm{BS}}^r}_{\text{Distortion noise}=\boldsymbol{\eta}} + \underbrace{\mathbf{w}_{u,k}^H \mathbf{n}_u}_{\text{AWGN}},$$

$$(5.18)$$

where $\mathbf{w}_{u,k}$ and $\hat{\mathbf{h}}_{u,k}$ are the kth columns of the matrices $\mathbf{W}$ and $\hat{\mathbf{H}}_u$, respectively. Therefore, the SINR of the kth user can be given as

$$\gamma_{u,k} = \frac{\kappa_r^{\mathrm{BS}} \kappa^u P_u |\mathbf{w}_{u,k}^H \hat{\mathbf{h}}_{u,k}|^2}{\left(\begin{array}{c} \kappa_r^{\mathrm{BS}} \kappa^u P_u \sum_{i=1,i\neq k}^{K_u} |\mathbf{w}_{u,k}^H \hat{\mathbf{h}}_{u,i}|^2 + \kappa_r^{\mathrm{BS}} \kappa_t^{\mathrm{BS}} \frac{P_d}{K_d} \sum_{j=1}^{K_d} \left| \mathbf{w}_{u,k}^H \mathbf{H}_{\mathrm{SI}} \hat{\mathbf{f}}_{d,j} \right|^2 \\ + \mathbf{w}_{u,k}^H \mathbf{C}_{\boldsymbol{\eta}} \mathbf{w}_{u,k} + \|\mathbf{w}_{u,k}\|^2 \left(\kappa_r^{\mathrm{BS}} \kappa^u P_u \sum_{i=1}^{K_u} \sigma_{e_{u,i}}^2 + \sigma_u^2 \right) \end{array} \right)}. \tag{5.19}$$

This is valid for any linear detectors such as MRC, ZF and MMSE. This work concentrates on MRC and ZF.

5.4.1 Uplink Spectral Efficiency When Using MRC/MRT

MRC is a diversity-combining technique that aims to combat multi-path fading and maximize the SNR at the combiner output. For MRC linear detector, $\mathbf{W} = \hat{\mathbf{H}}_u$ is used, and the SINR of the kth user can be calculated as

$$\gamma_{u,k}^{\mathrm{mrc}} = \frac{\kappa_r^{\mathrm{BS}} \kappa^u P_u}{\left(\begin{array}{c} \left(\kappa_r^{\mathrm{BS}} \kappa^u P_u \sum_{i=1,i\neq k}^{K_u} \left| \frac{\hat{\mathbf{h}}_{u,k}^H \hat{\mathbf{h}}_{u,i}}{\|\hat{\mathbf{h}}_{u,k}\|} \right|^2 + \kappa_r^{\mathrm{BS}} \kappa_t^{\mathrm{BS}} \frac{P_d}{K_d} \sum_{j=1}^{K_d} \left| \frac{\hat{\mathbf{h}}_{u,k}^H \mathbf{H}_{\mathrm{SI}} \hat{\mathbf{h}}_{d,j}}{\|\hat{\mathbf{h}}_{u,k}\| \|\hat{\mathbf{h}}_{d,j}\|} \right|^2 \right) \frac{1}{\|\hat{\mathbf{h}}_{u,k}\|^2} \\ + \left(\kappa_r^{\mathrm{BS}} \kappa^u P_u \sum_{i=1}^{K_u} \sigma_{e_{u,i}}^2 + \sigma_u^2 \right) \frac{1}{\|\hat{\mathbf{h}}_{u,k}\|^2} + \frac{\hat{\mathbf{h}}_{u,k}^H \mathbf{C}_{\boldsymbol{\eta}} \hat{\mathbf{h}}_{u,k}}{\|\hat{\mathbf{h}}_{u,k}\|^4} \end{array} \right)}. \tag{5.20}$$

The Jensen lower bound achievable sum rate for the kth user can be calculated as

$$\mathbb{E}\left\{ \log_2 \left(1 + \gamma_{u,k}^{\mathrm{mrc}} \right) \right\} \geq \log_2 \left(1 + \left(\mathbb{E}\left\{ \frac{1}{\gamma_{u,k}^{\mathrm{mrc}}} \right\} \right)^{-1} \right). \tag{5.21}$$

Lemma 5.4.1 *The average UL achievable sum rate of FD MU-MIMO systems in the presence of HWIs and imperfect CSI conditions when using MRC/MRT linear detector/precoder[2] can be lower bounded as*

$$\bar{\mathcal{R}}_{\mathrm{mrc,HWIs}}^{u,\,\mathrm{imp}} \geq \frac{T_c - \tau_p}{T_c} \sum_{k=1}^{K_u} \log_2 \left(1 + \frac{\kappa_r^{\mathrm{BS}} \kappa^u (M-1) \sigma_{\hat{h},k}^2}{2(1 - \kappa_r^{\mathrm{BS}} \kappa^u) \frac{M-1}{M+1} \sigma_{\hat{h},k}^2 + \sum_{i=1,i\neq k}^{K_u} \beta_{u,i} + \frac{P_d \sigma_s^2 + \sigma_u^2}{P_u} + \sigma_{e,k}^2} \right). \tag{5.22}$$

Proof: See Appendix B.1.

---

[2]This is the precoding technique used in the DL transmission. In FD mode, the DL transmission affects the UL achievable sum rate. So it should be considered in the UL analysis.

Lemma 5.4.1 shows that HWIs and channel estimation errors degrade the FD MU-MIMO systems. Furthermore, increasing the number of transmit antennas can alleviate the impact of the HWIs and the estimation errors. Following the same logic, the SE is obtained when using the ZFR/ZFT detector in the next section.

5.4.2 Uplink Spectral Efficiency When Using ZFR/ZFT

ZFR/ZFT are linear detecting/precoding techniques of spatial signal processing by which a multiple antenna receiver/transmitter can nullify the multi-user interference in an MU-MIMO wireless communication system. For ZFR/ZFT linear detector/precoder, $\mathbf{W} = \hat{\mathbf{H}}_u \left(\hat{\mathbf{H}}_u^H \hat{\mathbf{H}}_u \right)^{-1}$ is used. Then, the SINR of the kth user can be calculated as

$$
\gamma_{u,k}^{\text{ZF}} = \frac{\kappa_r^{\text{BS}} \kappa^u P_u}{\kappa_r^{\text{BS}} \kappa_t^{\text{BS}} \frac{P_d}{K_d} \sum_{j=1}^{K_d} \left| \mathbf{w}_{u,k}^H \mathbf{H}_{\text{SI}} \hat{\mathbf{f}}_{d,j} \right|^2 + \mathbf{w}_{u,k}^H \mathbf{C}_{\boldsymbol{\eta}} \mathbf{w}_{u,k} + \|\mathbf{w}_{u,k}\|^2 \left(\kappa_r^{\text{BS}} \kappa^u P_u \sum_{i=1}^{K_u} \sigma_{e_{u,i}}^2 + \sigma_u^2 \right)}.
$$

(5.23)

From (5.21), the Jensen lower bound achievable sum rate can be derived as

Lemma 5.4.2 *The average UL achievable sum rate of FD MU-MIMO systems in the presence of HWIs and imperfect CSI conditions when using ZFR/ZFT linear detector/precoder can be lower bounded as*

$$
\bar{\mathcal{R}}_{\text{ZF,HWIs}}^{u,\,\text{imp}} \geq \frac{T_c - \tau_p}{T_c} \sum_{k=1}^{K_u} \log_2 \left(1 + \frac{\kappa_r^{\text{BS}} \kappa^u P_u (M - K_u) \sigma_{\hat{h},k}^2}{P_u (1 - \kappa_r^{\text{BS}} \kappa^u) \sum_{i=1}^{K_u} \beta_{u,i} + P_u \kappa_r^{\text{BS}} \kappa^u \sum_{i=1}^{K_u} \sigma_{e,i}^2 + P_d \sigma_s^2 + \sigma_u^2} \right).
$$

(5.24)

Proof: See Appendix B.2.

Lemma 5.4.2 shows that ZF processing can successfully mitigate the IUI; however, it can eliminate neither the effects of HWIs nor those of channel estimation errors. Hence, it is valuable to study their impact on the performance of FD MU-MIMO systems.

Remark 1: The UL achievable sum rates of MRC/MRT and ZFR/ZFT when using LMMSE and LS estimators can be obtained by substituting (5.7), (5.10), in (5.22) and (5.24), respectively. Moreover, many special cases can be found in Tables 5.1 and 5.2.

- Lemmas 5.4.1 and 5.4.2 show that the HWIs and the channel estimation errors have a negative impact on the FD MU-MIMO system's performance. Moreover, the SE is saturated due to the HWIs when the transmit power grows to a very large value for both the MRC/MRT and ZFR/ZFT techniques.

- The hardware imperfection at the DL side does not affect the UL SE as no DL HWI terms can be seen in (5.22) and (5.24).

- The performance of the FD MU-MIMO system increases linearly when increasing the number of users and increases logarithmically when increasing the number of BS antennas.

5.5   Performance Analysis

This section discusses the DL SE performance of the studied FD MU-MIMO systems. As it has been done for the UL scenario, it first derives the SINR at the user. It then derives the lower bound achievable sum rate of the MRT and ZFT precoders. Moreover, it discusses the SE when using the LMMSE and LS channel estimators.

Considering the transceiver hardware impairment, the received signal at the jth DL user can be written as

$$r_{d,j} = \sqrt{\kappa^d}\mathbf{h}_{d,j}^H\tilde{\mathbf{s}}_d + \sqrt{\kappa^d}\mathbf{h}_{I,j}^H\tilde{\mathbf{x}}_u + \eta_{d,j} + n_{d,j}, \tag{5.25}$$

where $n_{d,j}$ is the AWGN at the jth DL user with zero mean and $\sigma_{d,j}^2$ variance. It is assumed that all the DL users have the same noise variance σ_d^2. Moreover, $\eta_{d,j}$ is the complex Gaussian receiver additive distortion noise at the jth DL user, where $\eta_{d,j} \sim \mathcal{CN}\left(0, (1-\kappa^d)(a+b)\right)$, in which a and b are given as

$$a = P_u \sum_{k=1}^{K_u} |h_{I,jk}|^2.$$

$$b = \frac{P_d}{K_d} \sum_{i=1}^{K_d} \sum_{l=1}^{M} \left|\hat{f}_{d,i}^{(l)}\right|^2 \left|h_{d,j}^{(l)}\right|^2. \tag{5.26}$$

Now, considering the imperfect CSI and by substituting the values of $\tilde{\mathbf{s}}_d$ and $\tilde{\mathbf{x}}_u$ in (5.25), the received signal can be written as

$$
\hat{r}_{d,j} = \underbrace{\sqrt{\kappa^d \kappa_t^{\mathrm{BS}} \frac{P_d}{K_d}} \hat{\mathbf{h}}_{d,j}^H \hat{\mathbf{f}}_{d,j} x_{d,j}}_{\text{Desired signal}} + \underbrace{\sqrt{\kappa^d} \sum_{k=1}^{K_u} \sqrt{\kappa^u P_u}\, h_{I,jk}\, x_{u,k}}_{\text{UL-DL interference signals}} + \underbrace{\sqrt{\kappa^d \kappa_t^{\mathrm{BS}} \frac{P_d}{K_d}} \sum_{i=1,i\neq j}^{K_d} \hat{\mathbf{h}}_{d,j}^H \hat{\mathbf{f}}_{d,i} x_{d,i}}_{\text{DL-DL interference signals}}
$$

$$
+ \underbrace{\sqrt{\kappa^d} \sum_{k=1}^{K_u} h_{I,jk}\, \eta_{u,k} + \sqrt{\kappa^d} \hat{\mathbf{h}}_{d,j}^H \boldsymbol{\eta}_{\mathrm{BS}}^t - \sqrt{\kappa^d} \mathbf{e}_{d,j}^H \boldsymbol{\eta}_{\mathrm{BS}}^t + \eta_{d,j}}_{\text{Distortion noise} = \eta_{d,j}^c} - \underbrace{\sqrt{\kappa^d \kappa_t^{\mathrm{BS}} \frac{P_d}{K_d}} \sum_{i=1}^{K_d} \mathbf{e}_{d,j}^H \hat{\mathbf{f}}_{d,i} x_{d,i}}_{\text{Estimation error}} + \underbrace{n_{d,j}}_{\text{AWGN}} .
$$

(5.27)

All the additive distortions in (5.27) can be combined as $\eta_{d,j}^c \sim \mathcal{CN}(0, \sigma_{\eta_{d,j}^c}^2)$, where $\sigma_{\eta_{d,j}^c}^2$ can be given as

$$
\sigma_{\eta_{d,j}^c}^2 = (1 - \kappa^d \kappa^u) a + (1 - \kappa^d \kappa_t^{\mathrm{BS}}) b. \tag{5.28}
$$

Consequently, the SINR of the jth user can be obtained from (5.27) as in (5.29), and it is applicable for any linear precoder, such as MRC, ZF and MMSE:

$$
\gamma_{d,j} = \frac{\frac{P_d}{K_d} \kappa^d \kappa_t^{\mathrm{BS}} |\hat{\mathbf{h}}_{d,j}^H \hat{\mathbf{f}}_{d,j}|^2}{\frac{P_d}{K_d} \kappa^d \kappa_t^{\mathrm{BS}} \sum_{i=1,i\neq j}^{K_d} |\hat{\mathbf{h}}_{d,j}^H \hat{\mathbf{f}}_{d,i}|^2 + \kappa^d \kappa^u P_u \sum_{k=1}^{K_u} |h_{I,jk}|^2 + \kappa^d \kappa_t^{\mathrm{BS}} P_d \sigma_{e_{d,j}}^2 + \sigma_d^2 + \sigma_{\eta_{d,j}^c}^2}. \tag{5.29}
$$

This will be discussed in detail for MRT and ZFT precoders.

5.5.1 Downlink Spectral Efficiency When Using MRT

For MRT linear precoder, the transmitted signals are multiplied by $\hat{\mathbf{F}}$, where $\hat{\mathbf{f}}_{d,j} = \frac{\hat{\mathbf{h}}_{d,j}}{\|\hat{\mathbf{h}}_{d,j}\|}$ is the jth column of $\hat{\mathbf{F}}$. Then, the SINR of the jth user ($\gamma_{d,j}^{\mathrm{mrt}}$) can be calculated as

$$
\gamma_{d,j}^{\mathrm{mrt}} = \frac{\frac{P_d}{K_d} \kappa^d \kappa_t^{\mathrm{BS}}}{\left(\left(\kappa^d \kappa^u P_u \sum_{k=1}^{K_u} |h_{I,jk}|^2 + \kappa^d \kappa_t^{\mathrm{BS}} P_d \sigma_{e_{d,j}}^2 + \sigma_d^2 + \sigma_{\eta_{d,j}^c}^2 \right) \frac{1}{\|\hat{\mathbf{h}}_{d,j}\|^2} \right. }{ \left. + \frac{P_d}{K_d} \kappa^d \kappa_t^{\mathrm{BS}} \sum_{i=1,i\neq j}^{K_d} \left| \frac{\hat{\mathbf{h}}_{d,j}^H}{\|\hat{\mathbf{h}}_{d,j}\|} \frac{\hat{\mathbf{h}}_{d,i}}{\|\hat{\mathbf{h}}_{d,i}\|} \right|^2 \right) }. \tag{5.30}
$$

The Jensen lower bound SE for the jth user can then be calculated as

$$
\mathbb{E}\left\{ \log_2 \left(1 + \gamma_{d,j}^{\mathrm{mrt}} \right) \right\} \geq \log_2 \left(1 + \left(\mathbb{E}\left\{ \frac{1}{\gamma_{d,j}^{\mathrm{mrt}}} \right\} \right)^{-1} \right). \tag{5.31}
$$

Lemma 5.5.1 *The average DL achievable sum rate of FD MU-MIMO systems in the presence of HWIs and imperfect CSI conditions when using MRT linear precoder can be lower bounded as*

$$\bar{\mathcal{R}}_{\text{mrt,HWIs}}^{d,\text{ imp}} \geq \frac{T_c - \tau_p}{T_c} \sum_{j=1}^{K_d} \log_2 \left(1 + \frac{\kappa^d \kappa_t^{\text{BS}} P_d (M-1) \sigma_{\hat{h},j}^2}{\left(\begin{array}{c} P_d(K_d-1)\frac{M-1}{M}\sigma_{\hat{h},j}^2 + 2P_d(1-\kappa^d\kappa_t^{\text{BS}})\left(\frac{M-1}{M+1}\right)\sigma_{\hat{h},j}^2 \\ + K_d\left(P_u \sum_{k=1}^{K_u} \sigma_{I,jk}^2 + P_d \sigma_{e,j}^2 + \sigma_d^2 \right) \end{array} \right)} \right).$$

(5.32)

Proof: See Appendix B.3.

5.5.2   Downlink Spectral Efficiency When Using ZFT

For ZFT linear precoder, the transmitted signals are multiplied by $\hat{\mathbf{F}}$, where $\hat{\mathbf{f}}_{d,j} = \frac{\mathbf{a}_{d,j}}{\|\mathbf{a}_{d,j}\|}$ is the jth normalized column of $\mathbf{A} = \hat{\mathbf{H}}_d \left(\hat{\mathbf{H}}_d^H \hat{\mathbf{H}}_d \right)^{-1}$, and the SINR of the jth user $(\gamma_{d,j}^{\text{ZF}})$ can be calculated as

$$\gamma_{d,j}^{\text{ZF}} = \frac{\frac{P_d}{K_d}\kappa^d\kappa_t^{\text{BS}}|\hat{\mathbf{h}}_{d,j}^H \hat{\mathbf{f}}_{d,j}|^2}{\frac{P_d}{K_d}\kappa^d\kappa_t^{\text{BS}} \sum_{i=1,i\neq j}^{K_d} |\hat{\mathbf{h}}_{d,j}^H \hat{\mathbf{f}}_{d,i}|^2 + \kappa^d\kappa^u P_u \sum_{k=1}^{K_u} |h_{I,jk}|^2 + \kappa^d\kappa_t^{\text{BS}} P_d \sigma_{e,d,j}^2 + \sigma_d^2 + \sigma_{\eta_{d,j}^c}^2}.$$

(5.33)

Lemma 5.5.2 *The average DL achievable sum rate of FD MU-MIMO systems in the presence of HWIs and imperfect CSI conditions when using ZFT linear precoder can be lower bounded as*

$$\bar{\mathcal{R}}_{\text{ZF,HWIs}}^{d,\text{ imp}} \geq \frac{T_c - \tau_p}{T_c} \sum_{j=1}^{K_d} \log_2 \left(1 + \frac{(P_d/K_d)\kappa_t^{\text{BS}}\kappa^d(M-K_d)\sigma_{\hat{h},j}^2}{\left(\begin{array}{c} (P_d/K_d)(1-\kappa^d\kappa_t^{\text{BS}})\beta_{d,j}\sigma_{\hat{h},j}^2 \sum_{i=1}^{K_d}\frac{1}{\sigma_{\hat{h},i}^2} \\ + (P_d/K_d)\kappa_t^{\text{BS}}\kappa^d \sum_{i=1}^{K_d}\sigma_{e,i}^2 + P_u \sum_{i=1}^{K_u}\sigma_{I,jk}^2 + \sigma_d^2 \end{array} \right)} \right).$$

(5.34)

Proof: See Appendix B.4.

Remark 2: The DL achievable rates of MRT and ZFT when using LMMSE and LS estimators can be obtained by substituting (5.7), (5.10), in (5.32) and (5.34), respectively. Also, many special cases can be found in Tables 5.3 and 5.4.

The results in Lemmas 5.5.1 and 5.5.2 in the DL scenario agree with the one obtained in Lemmas 5.4.1 and 5.4.2 in the UL scenario. Also, the hardware imperfection at the UL side does not affect the DL SE, as no UL HWI terms can be seen in (5.32) and (5.34).

As it is expected that future wireless communication systems have to support a large number of devices. In this context, it is worth mentioning that the presented findings can support the FD MU-MIMO system scalability and expansion. The results provided in Lemmas 5.4.1, 5.4.2, 5.5.1 and 5.5.2, and Tables 5.1, 5.2, 5.3 and 5.4 are valid for any number of users and antennas.

Table 5.1: Lower bounds of the uplink achievable sum rates when using MRC/MRT.

Scenario	Mathematical expression
Imperfect CSI and HWIs	$\bar{\mathcal{R}}^{u,\text{imp}}_{\text{mrc,HWIs}} \geq \frac{T_c-\tau_p}{T_c}\sum_{k=1}^{K_u}\log_2\left(1+\frac{\kappa_r^{\text{BS}}\kappa^u(M-1)\sigma_{\hat{h},k}^2}{2(1-\kappa_r^{\text{BS}}\kappa^u)\frac{M-1}{M+1}\sigma_{\hat{h},k}^2+\sum_{i=1,i\neq k}^{K_u}\beta_{u,i}+\frac{P_d\sigma_s^2+\sigma_u^2}{P_u}+\sigma_{e,k}^2}\right).$
Perfect CSI and Hardware	$\bar{\mathcal{R}}^{u,\text{per}}_{\text{mrc,ideal}} \geq \sum_{k=1}^{K_u}\log_2\left(1+\frac{P_u(M-1)\beta_{u,k}}{P_u\sum_{i=1,i\neq k}^{K_u}\beta_{u,i}+P_d\sigma_s^2+\sigma_u^2}\right).$
Perfect CSI with HWIs	$\bar{\mathcal{R}}^{u,\text{per}}_{\text{mrc,HWIs}} \geq \sum_{k=1}^{K_u}\log_2\left(1+\frac{\kappa_r^{\text{BS}}\kappa^u P_u(M-1)\beta_{u,k}}{P_u\sum_{i=1,i\neq k}^{K_u}\beta_{u,i}+2P_u(1-\kappa_r^{\text{BS}}\kappa^u)\frac{M-1}{M+1}\beta_{u,k}+P_d\sigma_s^2+\sigma_u^2}\right).$
Imperfect CSI, LMMSE estimation and perfect hardware	$\bar{\mathcal{R}}^{u,\text{imp,LMMSE}}_{\text{mrc,ideal}} \geq \frac{T_c-\tau_p}{T_c}\sum_{k=1}^{K_u}\log_2\left(1+\frac{\tau_p P_u(M-1)\beta_{u,k}^2}{(\tau_p P_u\beta_{u,k}+\sigma_u^2)\left(\sum_{i=1,i\neq k}^{K_u}\beta_{u,i}+\frac{P_d\sigma_s^2}{P_u}\right)+\beta_{u,k}(\tau_p+1)\sigma_u^2+\frac{\sigma_u^4}{P_u}}\right).$
Imperfect CSI, LS estimation and perfect hardware	$\mathcal{R}^{u,\text{imp,LS}}_{\text{mrc,ideal}} \geq \frac{T_c-\tau_p}{T_c}\sum_{k=1}^{K_u}\log_2\left(1+\frac{(M-1)(\tau_p P_u\beta_k-\sigma_u^2)}{\tau_p P_u\sum_{i=1,i\neq k}^{K_u}\beta_i+\tau_p P_d\sigma_s^2+(\tau_p+1)\sigma_u^2}\right).$

Table 5.2: Lower bounds of the uplink achievable sum rates when using ZFR/ZFT.

Scenario	Mathematical expression
Imperfect CSI and HWIs	$\bar{\mathcal{R}}_{\text{ZF,HWIs}}^{u,\,\text{imp}} \geq \frac{T_c-\tau_p}{T_c} \sum_{k=1}^{K_u} \log_2\left(1 + \frac{\kappa_r^{\text{BS}}\kappa^u P_u (M-K_u)\sigma_{\hat{h},k}^2}{P_u(1-\kappa_r^{\text{BS}}\kappa^u)\sum_{i=1}^{K_u}\beta_{u,i}+P_u\kappa_r^{\text{BS}}\kappa^u\sum_{i=1}^{K_u}\sigma_{e,i}^2+P_d\sigma_s^2+\sigma_u^2}\right).$
Perfect CSI and Hardware	$\bar{\mathcal{R}}_{\text{ZF,ideal}}^{u,\,\text{per}} \geq \sum_{k=1}^{K_u} \log_2\left(1 + \frac{P_u(M-K_u)\beta_{u,k}}{P_d\sigma_s^2+\sigma_u^2}\right).$
Perfect CSI with HWIs	$\bar{\mathcal{R}}_{\text{ZF,HWIs}}^{u,\,\text{per}} \geq \sum_{k=1}^{K_u} \log_2\left(1 + \frac{\kappa_r^{\text{BS}}\kappa^u P_u(M-K_u)\beta_{u,k}}{P_u(1-\kappa_r^{\text{BS}}\kappa^u)\sum_{i=1}^{K_u}\beta_{u,i}+P_d\sigma_s^2+\sigma_u^2}\right).$
Imperfect CSI, LMMSE estimation and perfect hardware	$\bar{\mathcal{R}}_{\text{ZF,ideal}}^{u,\,\text{imp,LMMSE}} \geq \frac{T_c-\tau_p}{T_c} \sum_{k=1}^{K_u} \log_2\left(1 + \frac{\tau_p P_u(M-K_u)\beta_{u,k}^2}{(\tau_p P_u\beta_{u,k}+\sigma_u^2)\left(\sum_{i=1,i\neq k}^{K_u}\frac{\beta_{u,i}\sigma_u^2}{\tau_p P_u\beta_{u,i}+\sigma_u^2}+\frac{P_d\sigma_s^2}{P_u}\right)+\beta_{u,k}(\tau_p\sigma_u^2+1)+\frac{\sigma_u^4}{P_u}}\right).$
Imperfect CSI, LS estimation and perfect hardware	$\bar{\mathcal{R}}_{\text{ZF,ideal}}^{u,\,\text{imp,LS}} \geq \frac{T_c-\tau_p}{T_c} \sum_{k=1}^{K_u} \log_2\left(1 + \frac{(M-K_u)(\tau_p P_u\beta_k+\sigma_u^2)}{\tau_p P_d\sigma_s^2+(\tau_p+K_u)\sigma_u^2}\right).$

Table 5.3: Lower bounds of the downlink achievable sum rates when using MRT.

Scenario	Mathematical expression
Imperfect CSI and HWIs	$\bar{\mathcal{R}}^{d,\,\mathrm{imp}}_{\mathrm{mrt,HWIs}} \geq \frac{T_c-\tau_p}{T_c}\sum_{j=1}^{K_d}\log_2\left(1+\frac{\kappa_t^d\kappa_t^{\mathrm{BS}}P_d(M-1)\sigma_{\hat{h},j}^2}{P_d(K_d-1)\frac{M-1}{M}\sigma_{\hat{h},j}^2+2P_d(1-\kappa_t^d\kappa_t^{\mathrm{BS}})\left(\frac{M-1}{M+1}\right)\sigma_{\hat{h},j}^2+K_d\left(P_u\sum_{k=1}^{K_u}\sigma_{I,jk}^2+P_d\sigma_{e,j}^2+\sigma_d^2\right)}\right).$
Perfect CSI and Hardware	$\bar{\mathcal{R}}^{d,\,\mathrm{per}}_{\mathrm{mrt,ideal}} \geq \sum_{j=1}^{K_d}\log_2\left(1+\frac{P_d(M-1)\beta_{d,j}}{P_d(K_d-1)\frac{M-1}{M}\beta_{d,j}+K_d\left(P_u\sum_{k=1}^{K_u}\sigma_{I,jk}^2+\sigma_d^2\right)}\right).$
Perfect CSI with HWIs	$\bar{\mathcal{R}}^{d,\,\mathrm{per}}_{\mathrm{mrt,HWIs}} \geq \sum_{j=1}^{K_d}\log_2\left(1+\frac{\kappa_t^d\kappa_t^{\mathrm{BS}}P_d(M-1)\beta_{d,j}}{\frac{P_d(K_d-1)(M-1)\beta_{d,j}}{M}+2P_d\frac{M-1}{M+1}(1-\kappa_t^d\kappa_t^{\mathrm{BS}})\beta_{d,j}+K_d\left(P_u\sum_{k=1}^{K_u}\sigma_{I,jk}^2+\sigma_d^2\right)}\right).$
Imperfect CSI, LMMSE estimation and perfect hardware	$\bar{\mathcal{R}}^{d,\,\mathrm{imp,LMMSE}}_{\mathrm{mrt,ideal}} \geq \frac{T_c-\tau_p}{T_c}\sum_{j=1}^{K_d}\log_2\left(1+\frac{\tau_pP_d(M-1)\beta_{d,j}^2}{\tau_pP_d(K_d-1)\frac{M-1}{M}\beta_{d,j}^2+K_d(\tau_pP_u\beta_{d,j}+\sigma_u^2)\left(\sum_{k=1}^{K_u}\sigma_{I,jk}^2+\frac{\sigma_d^2}{P_u}\right)+\frac{K_dP_d\sigma_u^2\beta_{d,j}}{P_u}}\right).$
Imperfect CSI, LS estimation and perfect hardware	$\bar{\mathcal{R}}^{d,\,\mathrm{imp,LS}}_{\mathrm{mrt,ideal}} \geq \frac{T_c-\tau_p}{T_c}\sum_{j=1}^{K_d}\log_2\left(1+\frac{P_d(M-1)(\tau_pP_u\beta_{d,j}-\sigma_u^2)}{P_d(K_d-1)\frac{M-1}{M}(\tau_pP_u\beta_{d,j}-\sigma_u^2)+K_d\left(\tau_pP_u^2\sum_{k=1}^{K_u}\sigma_{I,jk}^2+\tau_pP_u\sigma_d^2+P_d\sigma_u^2\right)}\right).$

Table 5.4: Lower bounds of the downlink achievable sum rates when using ZFT.

Scenario	Mathematical expression
Imperfect CSI and HWIs	$\bar{\mathcal{R}}^{d,\,\text{imp}}_{\text{ZF,HWIs}} \geq \frac{T_c-\tau_p}{T_c}\sum_{j=1}^{K_d}\log_2\left(1+\frac{(P_d/K_d)\kappa_t^{\text{BS}}\kappa^d(M-K_d)\sigma_{\hat{h},j}^2}{(P_d/K_d)(1-\kappa^d\kappa_t^{\text{BS}})\beta_{d,j}\sigma_{\hat{h},j}^2\sum_{i=1}^{K_d}\frac{1}{\sigma_{\hat{h},i}^2}+(P_d/K_d)\kappa_t^{\text{BS}}\kappa^d\sum_{i=1}^{K_d}\sigma_{e,i}^2+P_u\sum_{i=1}^{K_u}\sigma_{I,jk}^2+\sigma_d^2}\right).$
Perfect CSI and Hardware	$\bar{\mathcal{R}}^{d,\,\text{per}}_{\text{ZF,ideal}} \geq \sum_{j=1}^{K_d}\log_2\left(1+\frac{P_d(M-K_d)\beta_{d,j}}{K_d P_u\sum_{k=1}^{K_u}\sigma_{I,jk}^2+K_d\sigma_d^2}\right).$
Perfect CSI with HWIs	$\bar{\mathcal{R}}^{d,\,\text{per}}_{\text{ZF,HWIs}} \geq \sum_{j=1}^{K_d}\log_2\left(1+\frac{(P_d/K_d)\kappa_t^{\text{BS}}\kappa^d(M-K_d)\beta_{d,j}}{(P_d/K_d)(1-\kappa^d\kappa_t^{\text{BS}})\beta_{d,j}^2\sum_{i=1}^{K_d}\frac{1}{\beta_{d,i}}+P_u\sum_{i=1}^{K_u}\sigma_{I,jk}^2+\sigma_d^2}\right).$
Imperfect CSI, LMMSE estimation and perfect hardware	$\bar{\mathcal{R}}^{d,\,\text{imp,LMMSE}}_{\text{ZF,ideal}} \geq \frac{T_c-\tau_p}{T_c}\sum_{j=1}^{K_d}\log_2\left(1+\frac{\tau_p P_d(M-K_d)\beta_{d,j}^2}{K_d(\tau_p P_u\beta_{d,j}+\sigma_u^2)\left(\sum_{k=1}^{K_u}\sigma_{I,jk}^2+\sigma_u^2\right)\left(\frac{\sigma_d^2}{P_u}\right)+\tau_p P_d(\beta_{d,j}+\frac{\sigma_u^2}{\tau_p P_u})\sum_{i=1}^{K_d}\frac{\beta_{d,i}\sigma_u^2}{\tau_p P_u\beta_{d,i}+\sigma_u^2}}\right).$
Imperfect CSI, LS estimation and perfect hardware	$\bar{\mathcal{R}}^{d,\,\text{imp,LS}}_{\text{ZF,ideal}} \geq \frac{T_c-\tau_p}{T_c}\sum_{j=1}^{K_d}\log_2\left(1+\frac{P_d(M-K_d)(\tau_p P_u\beta_{d,j}+\sigma_u^2)}{K_d(\tau_p P_u^2\sum_{k=1}^{K_u}\sigma_{I,jk}^2+\tau_p P_u\sigma_d^2+P_d\sigma_u^2)}\right).$
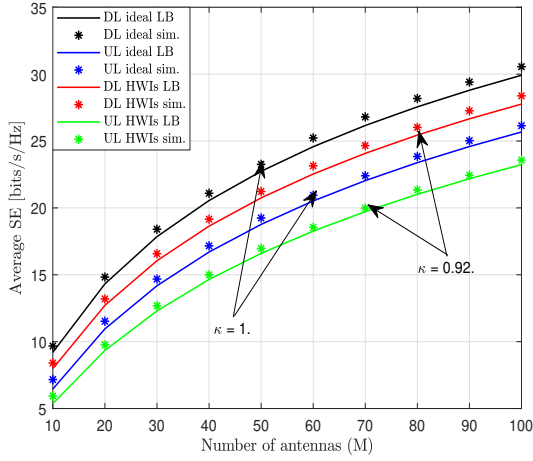
(a) MRC with perfect CSI.
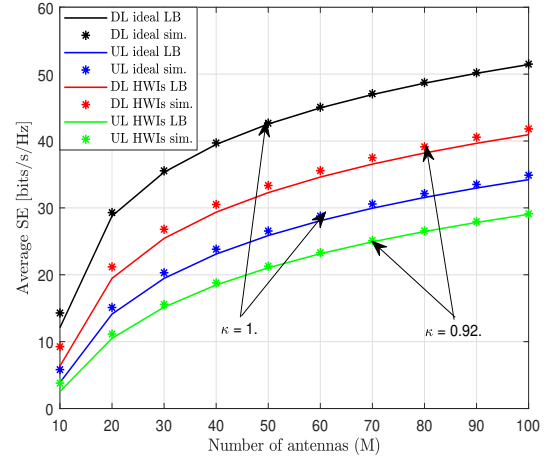
(b) ZF with perfect CSI.

Figure 5.5: Average SE of DL/UL FD MU-MIMO when $M = [10 - 100]$, $K_d = K_u = 8$, $\kappa = 1, 0.92$, and $P_d = P_u = 0$ dB.
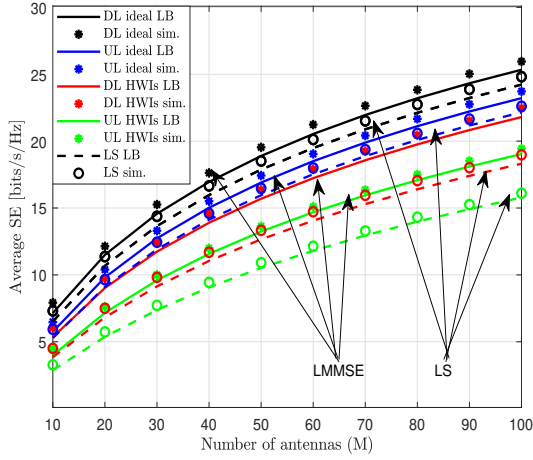
(a) MRC with imperfect CSI.
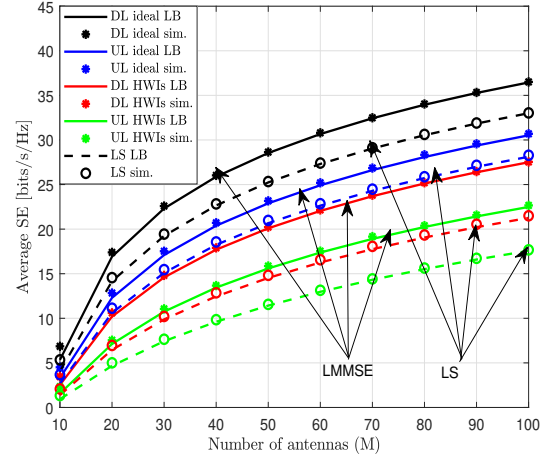
(b) ZF with imperfect CSI.

Figure 5.6: Average SE of DL/UL FD MU-MIMO when $M = [10 - 100]$, $K_d = K_u = 8$, $\kappa = 1, 0.92$, and $P_d = P_u = 5$ dB.

5.6 Simulation Results and Discussion

In this section, computer simulations were conducted to validate the theoretical derivations presented in this work. Without loss of generality and unless otherwise specified, it is
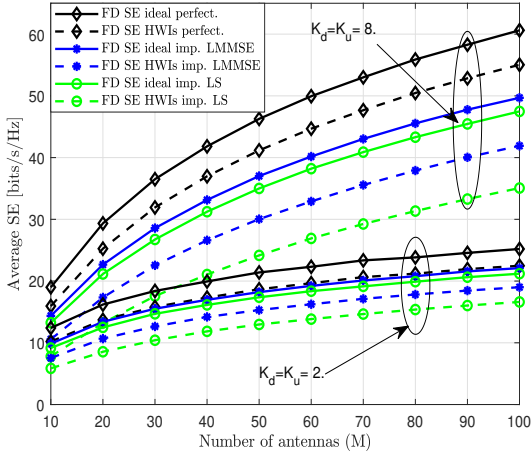
(a) MRC with perfect/imperfect CSI.
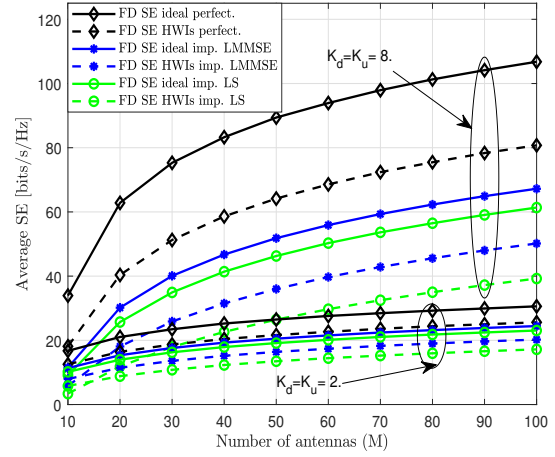
(b) ZF with perfect/imperfect CSI.

Figure 5.7: Average SE of FD MU-MIMO for a different number of users considering perfect/imperfect CSI and ideal/impaired hardware. Here, $M = [10 - 100]$, $\kappa = 1, 0.92$, and $P_d = P_u = 5$ dB.

assumed that $\kappa = \kappa_t^{BS} = \kappa_r^{BS} = \kappa^u = \kappa^d$, $\sigma_d^2 = \sigma_u^2 = 1$, and $\sigma_{I_{j,k}}^2 = 0.01$, $\beta_{u,k} = \beta_{d,j} = 1$, $\forall k \in [1, 2, \cdots K_u]$ and $\forall j \in [1, 2, \cdots K_d]$. Pilot sequences of length $\tau_p = K_d + K_u$ (the minimum training for orthogonal pilots) are used for CSI estimation from UL pilots and $T_c = 196$ as in [4]. $\sigma_s^2(P_d, \kappa_r^{BS}, \kappa_t^{BS})^3$. The ideal hardware is denoted by $\kappa = 1$. It is important to mention that the analysis is general and not restricted to these values.

Different sets of system parameters are used in Figs. 5.5 and 5.6 to verify the analytical results. As can be seen from these simulations, the obtained bounds closely resemble the exact ones for all studied cases (i.e., perfect and imperfect CSI with ideal and impaired hardware). Fig. 5.5 shows that when using a large number of antennas (e.g., $M = 100$), ZFR/ZFT technique achieves significant improvements compared to MRC/MRT because of its ability to eliminate the interference. On the other hand, when using a small number of antennas (e.g., $M = 10$) and serving a relatively large number of users (e.g., $K_d = K_u = 8$), both techniques achieve comparable performance. This can be explained from (5.22), (5.32),

---

[3]The residual SI power depends on the transmitted power and the BS transceiver hardware quality [139]. $\sigma_s^2 = \left(1 - \frac{P_d \kappa_r^{BS} \kappa_t^{BS}}{P_d + \sigma_u^2}\right)$. In this analysis, a very long coherence time and minimum pilot symbols are assumed, making the overhead required for CSI exchange negligible.
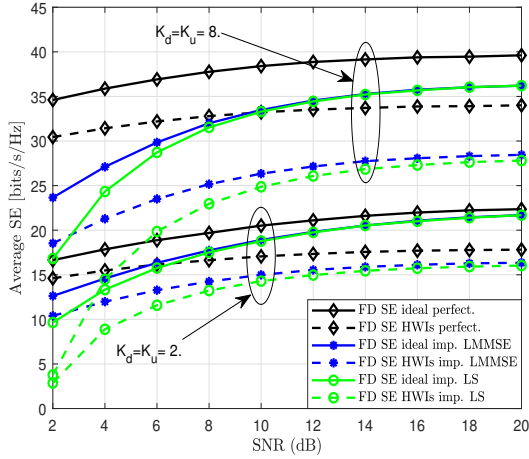
(a) MRC with perfect/imperfect CSI.
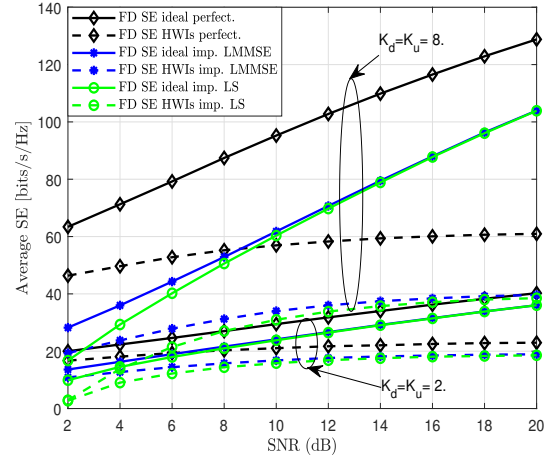
(b) ZF with perfect/imperfect CSI.

Figure 5.8: Average SE of FD MU-MIMO for a different number of users considering perfect/imperfect CSI and ideal/impaired hardware. Here, SNR $= \frac{P_u}{\sigma_u^2} = \frac{P_d}{\sigma_d^2}$, $M = 30$, and $\kappa = 1, 0.92$.

(5.24) and (5.34). In (5.24) and (5.34) the ZFR/ZFT has $(M - K_u)$ and $(M - K_d)$ factors in the numerator which decreases its performance when increasing the number of users. In contrast, K_u and K_d do not appear in the numerator of MRC/MRT as it can be seen in (5.22) and (5.32). Fig. 5.6 confirms the previous results. Additionally, the performance is worsened due to channel estimation errors. It also shows that as expected from the analytical results, LMMSE estimation outperforms LS one. Finally, all the simulation results agree with the theoretical one.

Fig. 5.7 plots the SE against the number of transmit antennas, considering a different number of DL/UL users for both ideal and impaired systems when the system has perfect and imperfect CSI. The performance of FD MU-MIMO is significantly improved by increasing the number of BS antennas and when serving more users. It also shows that the HWIs have detrimental effects on the system performance, which worsen in the case of imperfect CSI. Moreover, the ZF (illustrated in Fig. 5.7b) outperforms the MRC (illustrated in Fig. 5.7a) because it mitigates the interference.

Fig. 5.8 plots the SE against the transmit power considering MRC and ZR scenarios
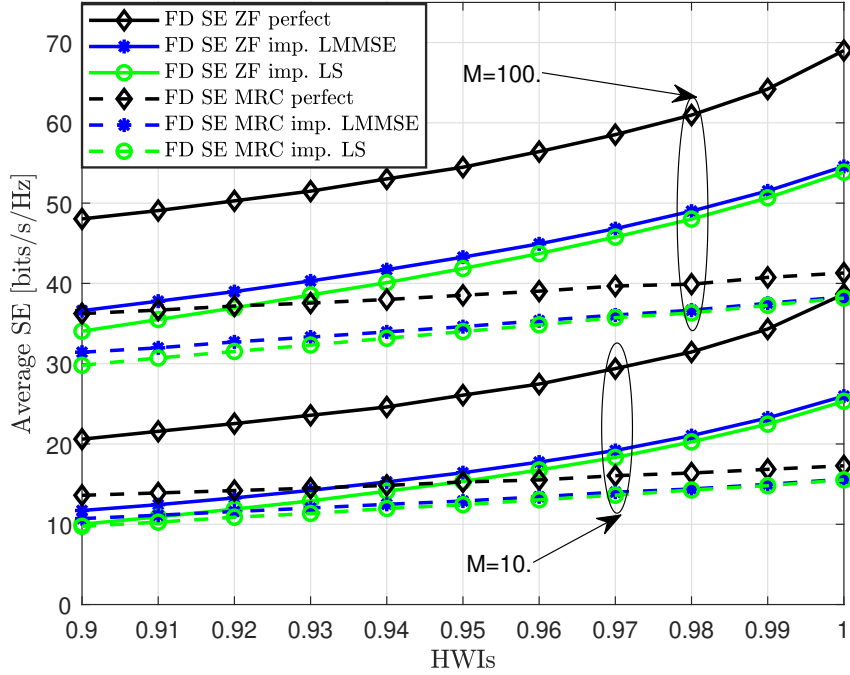
Figure 5.9: Average SE of FD MU-MIMO vs. HWIs levels when $P_d = P_u = 10$ dB, $K_d = K_u = 4$, and at different number of BS antennas.

for both ideal and impaired systems while assuming perfect and imperfect CSI. This figure shows that at the high SNR region, the performance is saturated for both MRC and ZF due to the HWIs. Furthermore, in the case of ideal hardware, the performance of the MRC is upper-bounded due to interference. In contrast, the ZF is able to tackle this thanks to its interference mitigation capability. Interestingly, increasing the number of users enhances the performance while, at the same time, it speeds up the system saturation for MRC (since the interference also increases). Focusing on the power budget, it can be seen that there is no noticeable improvement in the SE for the ideal MRC system when the SNR reaches 16 dB. This value shifts left, to 10 dB, for the impaired system when $K_d = K_u = 8$ users.

Fig. 5.9 shows the system performance when $K_d = K_u = 4$ users, the number of transmit antennas $M = [10, 100]$, and the HWIs levels $\kappa = [0.9 - 1]$. This figure confirms that the HWIs have a negative impact on the performance of MRC and ZF under perfect and imperfect CSI. ZF achieves a considerable gain compared to MRC, but its performance degrades faster. This figure also illustrates that, for the ideal hardware, when using a high

103
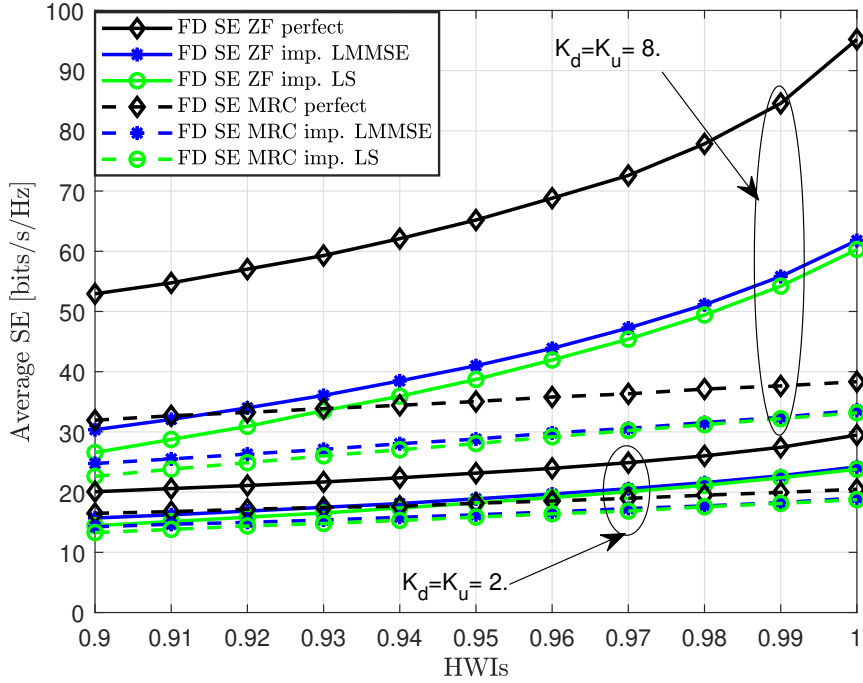
Figure 5.10: Average SE of FD MU-MIMO vs. HWIs levels when $P_d = P_u = 10$ dB, $M = 30$, and at different number of DL/UL users.

transmit power, both estimations (LMMSE and LS) achieve comparable performance. In contrast, the HWIs affect both estimators, having more of an impact on the LS estimator.

Fig. 5.10 shows that the system performance can be dramatically increased by serving more users for both MRC and ZF scenarios. Two important things affect the obtained gain, the channel estimation errors and the HWIs. In the case of ideal hardware and perfect CSI, increasing the number of DL/UL users from 2 to 8 increases the performance from 29.5 to 95.2 bits/s/Hz for the ZF scenario. However, the performance decreases to 52.93 from 95.2 bits/s/Hz when $\kappa = 0.9$ (with perfect CSI). In addition, the performance decreases to 30.36 and 26.57 bits/s/Hz when $\kappa = 0.9$ (with imperfect CSI and using LMMSE and LS estimation, respectively). The same trends can be seen in the MRC scenario.

5.7 Conclusion

This work discussed the lower-bound spectral efficiency of the FD MU-MIMO system under practical operating conditions. It studied the effects of the residual hardware impairments and the channel estimation errors. Mathematical frameworks for the average lower bound DL/UL spectral efficiencies are obtained for MRC/MRT and ZFR/ZFT schemes when using LMMSE/LS estimators. Comprehensive analyses were conducted to validate the presented findings. The performance analysis section presented the spectral efficiency expressions for all special cases when the system is affected/non-affected by hardware impairments or/and the channel estimation errors. The results showed that the performance of the FD MU-MIMO systems can be significantly improved by serving more users and by increasing the number of transmit antennas as well. ZF scenario can efficiently remove the inter-user-interference but cannot eliminate the impact of the hardware impairments. Moreover, the hardware quality causes an error floor in the channel estimation even at high transmission power, which can be mitigated by increasing the number of pilots.

Chapter 6

Conclusions and Future Work

6.1 Conclusions

This thesis investigates the potential of promising technology of FD systems for next-generation wireless communication networks. It studies many aspects that affect the system performance in terms of SE and EE. More precisely, it analyzes the performance of FD systems in presence of HWIs under different scenarios. Furthermore, the fading channels are modeled by Nakagami-m and Rayleigh distributions. The analyses have been done assuming perfect and imperfect CSI. Moreover, MRC/MRT and ZFR/ZFT linear detectors/precoders are used at the BS. For the channel estimation, the LMMSE and LS estimations are used.

In the first scenario, this thesis studies the performance of FD SISO communication systems when all system terminals have non-ideal transceivers. The average UL and DL lower bounds of the achievable rates assuming all fading channels follow Nakagami-m distribution are derived and verified by the simulations. The results show that the analytical and the simulation match. They also show that the HWIs degrade the performance and the SE is upper-bounded due to the HWIs even if the transmit powers grow boundlessly. Then a power allocation optimization problem that maximizes the average FD SE and EE considering QoS and power budget constraints is formulated. Next, the optimization problem is solved by using the fractional programming theory and the KKT conditions technique

and a novel algorithm is proposed. The proposed solution exploits the channels' statistics rather than the instantaneous channels' states which reduces the system's complexity. The results show that considerable improvements are obtained in SE and EE system performance when using the proposed solution. In addition, it is important to employ proper power allocation to keep the FD systems spectrum and energy efficient.

In the second scenario, this thesis studies the performance of FD MIMO communication systems under non-ideal transceivers. Closed-form expressions for the lower bounds of the FD UL and DL achievable rates are obtained and compared with the HD ones. Next, many power allocation optimization problems are formulated that aim to achieve different objectives, such as maximizing the average FD SE, max-min SE, EE and max-min EE while fulfilling the QoS and power budget constraints. The max-min objective functions are formulated to assure fairness between users. Then these problems are solved by proposing different algorithms to find the optimal UL and DL transmit powers. A combination of optimization techniques is used in solving these optimization problems such as the Dinkelbach approach, transformation, and the KKT conditions. Moreover, an easier solution is proposed for maximizing the SE. The proposed solutions are compared with the exhaustive search ones and the results show a match in performance. The results also show that the average FD SE saturates due to the HWIs and the interference. Moreover, transmitting the maximum power is not the optimal solution for FD systems, especially when there are QoS and power budget requirements. Importantly, the SE algorithm achieves a higher gain when higher power budgets are available while the EE does not. The proposed algorithms achieve a significant gain. Interestingly, the impaired FD systems are superior to the ideal HD systems when there is an excellent SI cancellation.

In the third scenario, this thesis studies the performance of FD MU-MIMO communication systems considering practical operation conditions. Besides non-ideal transceivers and the multiple antennas, it considers multiple UL and DL users and imperfect CSI. It studies the impact of the residual HWIs and the channel estimation error on the average UL and DL achievable sum rates of FD MU-MIMO systems. In the same context, it discusses the effects of HWIs on the MSE of channel estimation. It uses MRC/MRT and ZFR/ZFT linear detectors/precoders at the BS while it uses LMMSE and LS estimations to estimate the

channel at the BS from UL pilots. Mathematical frameworks for the average UL and DL SE lower bounds under the considered conditions are presented. Moreover, closed-form expressions for all special cases including ideal/impaired systems assuming perfect/imperfect CSI when using LMMSE and LS estimations are provided. The results show that the FD MU-MIMO systems are efficient and can be improved when increasing the number of BS antennas alongside serving more users. The results also show that the IUI can be efficiently eliminated when using the ZF technique and a significant improvement can be obtained in the performance compared with the MRC technique. Regarding the MSE of the estimated channel, the analysis proved that there is an error floor in the channel estimation even if the transmit power grows boundlessly due to the HWIs. Fortunately, it can be mitigated by increasing the number of training pilot symbols. Finally, LMMSE and LS estimators for the FD MU-MIMO systems considering non-ideal transceivers are designed.

6.2 Future Work

There are still several opportunities and challenges related to the FD communication systems. New wireless technologies have been emerged recently. For example, the RIS technology has been proposed as a game player in wireless communications to provide an affordable and spectral-energy efficient system. The potential of FD alongside RIS is still an open area to explore. By exploiting the benefits of RIS technology, the proposed work presented in the thesis can be further enhanced to improve the performance of FD SE and EE systems. Another promising technology is massive cell-free MIMO, in which multiple wireless APs cooperate to jointly serve the users by exploiting coherent signal processing. Studying the benefits and feasibility of combining the FD and massive cell-free MIMO technologies is still an attractive topic among researchers. The unmanned aerial vehicle (UAV)s also have emerged as promising solutions to overcome the challenges that face traditional terrestrial communication. They are reliable and cost-effective with inherent benefits such as diversity, flexibility, and altitude adaptability. Applying FD technology on the UAV is a hot topic to investigate. Studying machine-to-machine and internet-of-things applications with FD technology can also be considered another new research topic.

A good starting point to enhance the current work and achieve considerable improvements in the FD systems is suggested by studying additional precoding and decoding techniques such as MMSE and regularized zero-forcing (RZF). In addition, finding optimal precoders and decoders that can cancel all the interference (i.e., SI, IUI and the interference among the UL users as well as the DL users) and applying them on FD MU-MIMO systems is expected to achieve remarkable improvements in the performance.

Proposing power allocation optimization solutions for FD MU-MIMO systems to maximize both the SE and EE simultaneously which can be viewed as a multi-objective optimization is an interesting point to study. Moreover, formulating an optimization problem to maximize the performance for all users in the FD MU-MIMO systems and proposing novel algorithms is also another good starting point. Using machine learning and deep learning are also can be considered as future work. These techniques can be used in developing the proposed algorithms and provide intelligent and smart systems with less complexity which contribute to improving the performance of the FD MU-MIMO systems.

Bibliography

[1] E. Björnson, J. Hoydis, and L. Sanguinetti, "Massive MIMO networks: Spectral, energy, and hardware efficiency," *Foundations and Trends in Signal Processing*, vol. 11, no. 3-4, pp. 154–655, 2017.

[2] Cisco, "Cisco annual internet report (2018–2023)," https://www.cisco.com/c/en/us/solutions/collateral/executive-perspectives/annual-internet-report/white-paper-c11-741490.pdf, 2020.

[3] Ericsson, "Ericsson mobility report," https://www.ericsson.com/4ae28d/assets/local/reports-papers/mobility-report/documents/2022/ericsson-mobility-report-november-2022.pdf, 2022.

[4] H. Q. Ngo, E. G. Larsson, and T. L. Marzetta, "Energy and spectral efficiency of very large multiuser MIMO systems," *IEEE Transactions on Communications*, vol. 61, no. 4, pp. 1436–1449, 2013.

[5] C. Kong, A. Mezghani, C. Zhong, A. L. Swindlehurst, and Z. Zhang, "Multipair massive MIMO relaying systems with one-bit ADCs and DACs," *IEEE Transactions on Signal Processing*, vol. 66, no. 11, pp. 2984–2997, 2018.

[6] F. Boccardi, R. W. Heath, A. Lozano, T. L. Marzetta, and P. Popovski, "Five disruptive technology directions for 5G," *IEEE Communications Magazine*, vol. 52, no. 2, pp. 74–80, 2014.

[7] A. E. Canbilen, S. S. Ikki, E. Basar, S. S. Gultekin, and I. Develi, "Joint impact of I/Q imbalance and imperfect CSI on SM-MIMO systems over generalized beckmann

fading channels: Optimal detection and cramer-rao bound," *IEEE Trans. Wireless Commun.*, vol. 19, no. 5, pp. 3034–3046, 2020.

[8] Q. Wu and R. Zhang, "Intelligent reflecting surface enhanced wireless network via joint active and passive beamforming," *IEEE Transactions on Wireless Communications*, vol. 18, no. 11, pp. 5394–5409, 2019.

[9] S. Zhang, Q. Wu, S. Xu, and G. Y. Li, "Fundamental green tradeoffs: Progresses, challenges, and impacts on 5G networks," *IEEE Commun. Surveys Tutorials*, vol. 19, no. 1, pp. 33–56, 2017.

[10] Q. Wu, G. Y. Li, W. Chen, D. W. K. Ng, and R. Schober, "An overview of sustainable green 5G networks," *IEEE Wireless Commun.*, vol. 24, no. 4, pp. 72–80, 2017.

[11] W. Saad, M. Bennis, and M. Chen, "A vision of 6G wireless systems: Applications, trends, technologies, and open research problems," *IEEE Network*, vol. 34, no. 3, pp. 134–142, 2020.

[12] E. Park, J. Bae, H. Ju, and Y. Han, "Resource allocation for full-duplex systems with imperfect co-channel interference estimation," *IEEE Transactions on Wireless Communications*, vol. 18, no. 4, pp. 2388–2400, 2019.

[13] Q. Ding, Y. Lian, and Y. Jing, "Performance analysis of full-duplex massive MIMO systems with low-resolution ADCs/DACs over Rician fading channels," *IEEE Transactions on Vehicular Technology*, vol. 69, no. 7, pp. 7389–7403, 2020.

[14] J. Zhang, L. Dai, Z. He, B. Ai, and O. A. Dobre, "Mixed-ADC/DAC multipair massive MIMO relaying systems: Performance analysis and power optimization," *IEEE Transactions on Communications*, vol. 67, no. 1, pp. 140–153, 2018.

[15] C. Kong, C. Zhong, S. Jin, S. Yang, H. Lin, and Z. Zhang, "Full-duplex massive MIMO relaying systems with low-resolution ADCs," *IEEE Transactions on Wireless Communications*, vol. 16, no. 8, pp. 5033–5047, 2017.

[16] X. Jia, M. Zhou, M. Xie, L. Yang, and H. Zhu, "Effect of low-resolution ADCs and loop interference on multi-user full-duplex massive MIMO amplify-and-forward relaying systems," *IET Communications*, vol. 11, no. 5, pp. 687–695, 2017.

[17] P. Anokye, R. K. Ahiadormey, C. Song, and K.-J. Lee, "On the sum-rate of heterogeneous networks with low-resolution ADC quantized full-duplex massive MIMO-enabled backhaul," *IEEE Wireless Communications Letters*, vol. 8, no. 2, pp. 452–455, 2018.

[18] J. Dai, J. Liu, J. Wang, J. Zhao, C. Cheng, and J.-Y. Wang, "Achievable rates for full-duplex massive MIMO systems with low-resolution ADCs/DACs," *IEEE Access*, vol. 7, pp. 24 343–24 353, 2019.

[19] X. Wang, D. Zhang, K. Xu, and W. Ma, "On the energy/spectral efficiency of multi-user full-duplex massive MIMO systems with power control," *EURASIP Journal on Wireless Communications and Networking*, vol. 2017, no. 1, pp. 1–17, 2017.

[20] Z. Zhang, K. Long, A. V. Vasilakos, and L. Hanzo, "Full-duplex wireless communications: Challenges, solutions, and future research directions," *Proceedings of the IEEE*, vol. 104, no. 7, pp. 1369–1409, 2016.

[21] Z. Zhang, X. Chai, K. Long, A. V. Vasilakos, and L. Hanzo, "Full duplex techniques for 5G networks: self-interference cancellation, protocol design, and relay selection," *IEEE Communications Magazine*, vol. 53, no. 5, pp. 128–137, 2015.

[22] J. Qi and S. Aissa, "Analysis and compensation of power amplifier nonlinearity in MIMO transmit diversity systems," *IEEE Transactions on Vehicular Technology*, vol. 59, no. 6, pp. 2921–2931, 2010.

[23] M. M. Alsmadi, A. E. Canbilen, N. Abu Ali, S. S. Ikki, and E. Basar, "Cognitive networks in the presence of I/Q imbalance and imperfect CSI: Receiver design and performance analysis," *IEEE Access*, vol. 7, pp. 49 765–49 777, 2019.

[24] S. Zhou, W. Xu, K. Wang, M. Di Renzo, and M. Alouini, "Spectral and energy efficiency of IRS-assisted MISO communication with hardware impairments," *IEEE Wireless Communications Letters*, pp. 1–1, 2020.

[25] R. Want, B. N. Schilit, and S. Jenson, "Enabling the internet of things," *Computer*, vol. 48, no. 1, pp. 28–35, 2015.

[26] M. Kim and S. Chang, "A consumer transceiver for long-range IoT communications in emergency environments," *IEEE Transactions on Consumer Electronics*, vol. 62, no. 3, pp. 226–234, 2016.

[27] T. Aulin, "Characteristics of a digital mobile radio channel," *IEEE Transactions on Vehicular Technology*, vol. 30, no. 2, pp. 45–53, 1981.

[28] A. Sabharwal, P. Schniter, D. Guo, D. W. Bliss, S. Rangarajan, and R. Wichman, "In-band full-duplex wireless: Challenges and opportunities," *IEEE Journal on Selected Areas in Communications*, vol. 32, no. 9, pp. 1637–1652, 2014.

[29] G. J. Foschini, M. J. Gans *et al.*, "On limits of wireless communications in a fading environment when using multiple antennas," *Wireless personal communications*, vol. 6, no. 3, pp. 311–336, 1998.

[30] G. J. Foschini, "Layered space-time architecture for wireless communication in a fading environment when using multi-element antennas," *Bell labs technical journal*, vol. 1, no. 2, pp. 41–59, 1996.

[31] E. Telatar, "Capacity of multi-antenna gaussian channels," *European transactions on telecommunications*, vol. 10, no. 6, pp. 585–595, 1999.

[32] N. Bambos, "Toward power-sensitive network architectures in wireless communications: Concepts, issues, and design aspects," *IEEE Personal Communications*, vol. 5, no. 3, pp. 50–59, 1998.

[33] N. Bambos, S. C. Chen, and G. J. Pottie, "Channel access algorithms with active link protection for wireless communication networks with power control," *IEEE/ACM Transactions On Networking*, vol. 8, no. 5, pp. 583–597, 2000.

[34] R. D. Yates, "A framework for uplink power control in cellular radio systems," *IEEE Journal on selected areas in communications*, vol. 13, no. 7, pp. 1341–1347, 1995.

[35] J. Price and T. Javidi, "Decentralized rate assignments in a multi-sector CDMA network," *IEEE transactions on wireless communications*, vol. 5, no. 12, pp. 3537–3547, 2006.

[36] M. Chiang and J. Bell, "Balancing supply and demand of bandwidth in wireless cellular networks: utility maximization over powers and rates," in *IEEE INFOCOM 2004*, vol. 4. IEEE, 2004, pp. 2800–2811.

[37] D. C. ONeill, D. Julian, and S. Boyd, "Adaptive management of network resources," in *2003 IEEE 58th Vehicular Technology Conference. VTC 2003-Fall (IEEE Cat. No. 03CH37484)*, vol. 3. IEEE, 2003, pp. 1929–1933.

[38] K.-K. Leung and C. W. Sung, "An opportunistic power control algorithm for cellular network," *IEEE/ACM Transactions on Networking*, vol. 14, no. 3, pp. 470–478, 2006.

[39] R. Knopp and P. A. Humblet, "Information capacity and power control in single-cell multiuser communications," in *Proceedings IEEE International Conference on Communications ICC'95*, vol. 1. IEEE, 1995, pp. 331–335.

[40] D. Tse and P. Viswanath, *Fundamentals of wireless communication.* Cambridge university press, 2005.

[41] M. Chiang, P. Hande, T. Lan, C. W. Tan *et al.*, "Power control in wireless cellular networks," *Foundations and Trends® in Networking*, vol. 2, no. 4, pp. 381–533, 2008.

[42] M. H. N. Shaikh, V. A. Bohara, A. Srivastava, and G. Ghatak, "Performance analysis of intelligent reflecting surface-assisted wireless system with non-ideal transceiver," *IEEE Open Journal of the Communications Society*, vol. 2, pp. 671–686, 2021.

[43] H. E. Rowe, "Memoryless nonlinearities with gaussian inputs: Elementary results," *The Bell System Technical Journal*, vol. 61, no. 7, pp. 1519–1525, 1982.

[44] O. T. Demir and E. Bjornson, "The Bussgang decomposition of nonlinear systems: Basic theory and MIMO extensions [lecture notes]," *IEEE Signal Processing Magazine*, vol. 38, no. 1, pp. 131–136, 2021.

[45] G. T. Specification, "LTE; evolved universal terrestrial radio access (E-UTRA); base station (BS) radio transmission and reception," 2017.

[46] H. Holma and A. Toskala, *LTE for UMTS: Evolution to LTE-Advanced*. John Wiley & Sons, 2011.

[47] E. TS, "5G; NR; base station (BS) radio transmission and reception (3GPP TS 38.104 version 16.4.0 release 16)," *URL: https://www.etsi.org/deliver/etsi_ts/138100_138199/138104/16.04.00_60/ts_138104v160400p.pdf*, 2020.

[48] H. Suzuki, "A statistical model for urban radio propogation," *IEEE Transactions on Communications*, vol. 25, no. 7, pp. 673–680, 1977.

[49] M. Nakagami, "The m-distribution: a general formula of intensity distribution of rapid fading," in *Statistical methods in radio wave propagation*. Elsevier, 1960, pp. 3–36.

[50] Nakagami, "Some considerations on random phase problems from the standpoint of fading," *The Institute of Electrical and Communication Engineers Proceedings*, vol. 36, no. 11, pp. 595–602, 1953.

[51] M. A. Taneda, J.-I. Takada, and K. Araki, "The problem of the fading model selection," *IEICE Transactions on Communications*, vol. 84, no. 3, pp. 660–666, 2001.

[52] M. Yacoub, G. Fraidenraich, and J. Santos Filho, "Nakagami-m phase-envelope joint distribution," *Electronics Letters*, vol. 41, no. 5, pp. 259–261, 2005.

[53] M. D. Yacoub, "Nakagami-m phase-envelope joint distribution: A new model," *IEEE Transactions on Vehicular Technology*, vol. 59, no. 3, pp. 1552–1557, 2010.

[54] N. C. Sagias and G. K. Karagiannidis, "Effects of carrier phase error on EGC receivers in correlated Nakagami-m fading," *IEEE Communications Letters*, vol. 9, no. 7, pp. 580–582, 2005.

[55] R. K. Mallik, "A new statistical model of the complex Nakagami-m fading gain," *IEEE Transactions on Communications*, vol. 58, no. 9, pp. 2611–2620, 2010.

[56] L. Rayleigh, "XII. on the resultant of a large number of vibrations of the same pitch and of arbitrary phase," *The London, Edinburgh, and Dublin Philosophical Magazine and Journal of Science*, vol. 10, no. 60, pp. 73–78, 1880.

[57] S. Rice and N. Wax, "Statistical properties of random noise currents," pp. 52–114, 1954.

[58] M. K. Simon and M. Alouini, *Digital communication over fading channels: A Unified Approach to Performance Analysis.* New York: Wiley, 2001.

[59] J. Liu, J. Dai, J.-Y. Wang, J. Zhao, and C. Cheng, "Achievable rates for full-duplex massive MIMO systems over Rician fading channels," *IEEE Access*, vol. 6, pp. 30 208–30 216, 2018.

[60] Q. Zhang, S. Jin, K.-K. Wong, H. Zhu, and M. Matthaiou, "Power scaling of uplink massive MIMO systems with arbitrary-rank channel means," *IEEE Journal of Selected Topics in Signal Processing*, vol. 8, no. 5, pp. 966–981, 2014.

[61] W. Wongtrairat and P. Supnithi, "New simple form for pdf and mgf of rician fading distribution," in *2011 International Symposium on Intelligent Signal Processing and Communications Systems (ISPACS)*, 2011, pp. 1–4.

[62] R. Mesleh and O. S. Badarneh, "Quadrature spatial modulation in correlated η - μ fading channels with imperfect channel state information," in *2017 int. Conf. on Wireless Commun., Sig. Proc. and Net. (WiSPNET)*, March 2017, pp. 887–892.

[63] E. Basar, U. Aygolu, E. Panayirci, and H. V. Poor, "Performance of spatial modulation in the presence of channel estimation errors," *IEEE Commun. Lett.*, vol. 16, no. 2, pp. 176–179, February 2012.

[64] A. Afana, T. M. N. Ngatched, O. A. Dobre, and S. Ikki, "Spatial modulation in MIMO spectrum-sharing systems with imperfect channel estimation and multiple primary users," in *2015 IEEE Glob. Commun. Conf. (GLOBECOM)*, Dec 2015, pp. 1–5.

[65] A. Afana, T. M. N. Ngatched, and O. A. Dobre, "Spatial modulation in MIMO limited-feedback spectrum-sharing sys. with mutual interference and channel estimation errors," *IEEE Commun. Lett.*, vol. 19, no. 10, pp. 1754–1757, Oct 2015.

[66] R. Mesleh and S. S. Ikki, "On the effect of Gaussian imperfect channel estimations on the performance of space modulation techniques," in *2012 IEEE 75th Veh. Tech. Conf. (VTC Spring)*, May 2012, pp. 1–5.

[67] A. Afana, I. A. Mahady, and S. Ikki, "Quadrature spatial modulation in MIMO cognitive radio systems with imperfect channel estimation and limited feedback," *IEEE Tran. on Commun.*, vol. 65, no. 3, pp. 981–991, March 2017.

[68] S. S. Ikki and R. Mesleh, "A general framework for performance analysis of space shift keying (SSK) modulation in the presence of Gaussian imperfect estimations," *IEEE Commun. Letters*, vol. 16, no. 2, pp. 228–230, Feb. 2012.

[69] T. E. Bogale and L. B. Le, "Pilot optimization and channel estimation for multiuser massive mimo systems," in *2014 48th Annual Conference on Information Sciences and Systems (CISS)*. IEEE, 2014, pp. 1–6.

[70] T. X. Vu, T. A. Vu, and T. Q. Quek, "Successive pilot contamination elimination in multiantenna multicell networks," *IEEE Wireless Communications Letters*, vol. 3, no. 6, pp. 617–620, 2014.

[71] F. Fernandes, A. Ashikhmin, and T. L. Marzetta, "Inter-cell interference in non-cooperative TDD large scale antenna systems," *IEEE Journal on Selected Areas in Communications*, vol. 31, no. 2, pp. 192–201, 2013.

[72] W. A. Mahyiddin, P. A. Martin, and P. J. Smith, "Pilot contamination reduction using time-shifted pilots in finite massive mimo systems," in *2014 IEEE 80th Vehicular Technology Conference (VTC2014-Fall)*. IEEE, 2014, pp. 1–5.

[73] M. Biguesh and A. Gershman, "Training-based MIMO channel estimation: a study of estimator tradeoffs and optimal training signals," *IEEE Transactions on Signal Processing*, vol. 54, no. 3, pp. 884–893, 2006.

[74] M. Biguesh and A. B. Gershman, "Downlink channel estimation in cellular systems with antenna arrays at base stations using channel probing with feedback," *EURASIP Journal on Advances in Signal Processing*, vol. 2004, no. 9, pp. 1–10, 2004.

[75] S. M. Kay, *Fundamentals of statistical signal processing: estimation theory.* Prentice-Hall, Inc., 1993.

[76] J. Mirzaei, *Channel Estimation in TDD and FDD-Based Massive MIMO Systems.* University of Toronto (Canada), 2021.

[77] M. Alsmadi, "The effects of I/Q imbalance and improper gaussian noise on different wireless communication systems," Ph.D. dissertation, Lakehead University, 2020.

[78] P. Anokye, D. K. P. Asiedu, and K.-J. Lee, "Power optimization of cell-free massive MIMO with full-duplex and low-resolution ADCs," *IEEE Transactions on Wireless Communications*, pp. 1–1, 2023.

[79] A. Bazrafkan, M. Poposka, Z. Hadzi-Velkov, P. Popovski, and N. Zlatanov, "Performance comparison between a simple full-duplex multi-antenna relay and a passive reflecting intelligent surface," *IEEE Transactions on Wireless Communications*, 2023.

[80] P. Guan, Y. Wang, H. Yu, and Y. Zhao, "Energy efficiency maximisation for STAR-RIS assisted full-duplex communications," *IET Communications*, 2023.

[81] Y. Wang, P. Guan, H. Yu, and Y. Zhao, "Energy efficiency of full-duplex communication system assisted by reconfigurable intelligent surface," *IET Communications*, 2022.

[82] E. Balti and B. L. Evans, "A unified framework for full-duplex massive MIMO cellular networks with low resolution data converters," *IEEE Open Journal of the Communications Society*, 2022.

[83] A. J. Fernandes and I. Psaromiligkos, "Channel estimation for reconfigurable intelligent surface-assisted full-duplex MIMO with hardware impairments," *arXiv preprint arXiv:2301.05263*, 2023.

[84] T.-H. Vu and S. Kim, "Performance analysis of full-duplex two-way RIS-based systems with imperfect CSI and discrete phase-shift design," *IEEE Communications Letters*, 2022.

[85] S. Wang, Y. Liu, W. Zhang, and H. Zhang, "Achievable rates of full-duplex massive MIMO relay systems over Rician fading channels," *IEEE Transactions on Vehicular Technology*, vol. 66, no. 11, pp. 9825–9837, 2017.

[86] J. Zhang, N. Hu, and G. Pan, "Outage performance for full-duplex relaying satellite-terrestrial multi-antenna NOMA systems with imperfect SIC," *Digital Signal Processing*, p. 103909, 2023.

[87] L.-T. Tu, V.-D. Phan, T. N. Nguyen, P. T. Tran, T. T. Duy, Q.-S. Nguyen, N.-T. Nguyen, and M. Voznak, "Performance analysis of multihop full-duplex NOMA systems with imperfect interference cancellation and near-field path-loss," *Sensors*, vol. 23, no. 1, p. 524, 2023.

[88] S. Li, S. Yan, L. Bariah, S. Muhaidat, and A. Wang, "IRS-assisted full duplex systems over Rician and Nakagami fading channels," *IEEE Open Journal of Vehicular Technology*, pp. 1–12, 2023.

[89] K. Pan, B. Zhou, and Z. Bu, "Optimal power allocation with multiple joint associations in multi-user MIMO full-duplex systems," *IEEE Access*, vol. 11, pp. 1175–1192, 2023.

[90] M. Shirzadian Gilan and B. Maham, "Diversity achieving full-duplex DF relaying with joint relay-antenna selection under Nakagami-m fading environment," *International Journal of Communication Systems*, p. e5427, 2023.

[91] N. Nayak, S. Kalyani, and H. A. Suraweera, "A DRL approach for RIS-assisted full-duplex UL and DL transmission: Beamforming, phase shift and power optimization," *arXiv preprint arXiv:2212.13854*, 2022.

[92] N. N. Tan, P. Fazio, and M. Voznak, "Capacity maximizing adaptive time-switching protocol for energy harvesting full-duplex relaying network over Rayleigh fading channel," *Journal of Advanced Engineering and Computation*, vol. 6, no. 4, pp. 282–290, 2022.

[93] T. Riihonen, S. Werner, and R. Wichman, "Mitigation of loopback self-interference in full-duplex MIMO relays," *IEEE Transactions on Signal Processing*, vol. 59, no. 12, pp. 5983–5993, 2011.

[94] J. I. Choi, M. Jain, K. Srinivasan, P. Levis, and S. Katti, "Achieving single channel, full duplex wireless communication," in *Proceedings of the sixteenth annual international conference on Mobile computing and networking*, 2010, pp. 1–12.

[95] P. Anokye, R. K. Ahiadormey, and K.-J. Lee, "Full-duplex cell-free massive MIMO with low-resolution ADCs," *IEEE Transactions on Vehicular Technology*, pp. 1–1, 2021.

[96] J. Liu, J. Dai, J.-Y. Wang, J. Zhao, and C. Cheng, "Achievable rates for full-duplex massive MIMO systems over Rician fading channels," *IEEE Access*, vol. 6, pp. 30 208–30 216, 2018.

[97] J. Bai and A. Sabharwal, "Asymptotic analysis of MIMO multi-cell full-duplex networks," *IEEE Transactions on Wireless Communications*, vol. 16, no. 4, pp. 2168–2180, 2017.

[98] C. B. Barneto, S. D. Liyanaarachchi, M. Heino, T. Riihonen, and M. Valkama, "Full duplex radio/radar technology: The enabler for advanced joint communication and sensing," *IEEE Wireless Communications*, vol. 28, no. 1, pp. 82–88, 2021.

[99] M. Mohammadi, B. K. Chalise, H. A. Suraweera, H. Q. Ngo, and Z. Ding, "Design and analysis of full-duplex massive antenna array systems based on wireless power

transfer," *IEEE Transactions on Communications*, vol. 69, no. 2, pp. 1302–1316, 2021.

[100] M. A. Saeidi, M. J. Emadi, H. Masoumi, M. R. Mili, D. W. K. Ng, and I. Krikidis, "Weighted sum-rate maximization for multi-IRS-assisted full-duplex systems with hardware impairments," *IEEE Transactions on Cognitive Communications and Networking*, vol. 7, no. 2, pp. 466–481, 2021.

[101] C. Deng, M. Liu, X. Li, and Y. Liu, "Hardware impairments aware full-duplex NOMA networks over Rician fading channels," *IEEE Systems Journal*, vol. 15, no. 2, pp. 2515–2518, 2021.

[102] B. C. Nguyen, X. N. Tran, D. T. Tran, X. N. Pham, and L. T. Dung, "Impact of hardware impairments on the outage probability and ergodic capacity of one-way and two-way full-duplex relaying systems," *IEEE Transactions on Vehicular Technology*, vol. 69, no. 8, pp. 8555–8567, 2020.

[103] X. N. Tran, B. C. Nguyen, and D. T. Tran, "Outage probability of two-way full-duplex relay system with hardware impairments," in *2019 3rd International Conference on Recent Advances in Signal Processing, Telecommunications Computing (SigTelCom)*, 2019, pp. 135–139.

[104] S. Dey, E. Sharma, and R. Budhiraja, "Scaling analysis of hardware-impaired two-way full-duplex massive MIMO relay," *IEEE Communications Letters*, vol. 23, no. 7, pp. 1249–1253, 2019.

[105] S.-N. Jin, D.-W. Yue, and H. H. Nguyen, "Power scaling laws of massive MIMO full-duplex relaying with hardware impairments," *IEEE Access*, vol. 6, pp. 40 860–40 882, 2018.

[106] G. DONG, Z. YANG, Y. FENG, and B. LYU, "Exploiting RIS-aided cooperative non-orthogonal multiple access with full-duplex relaying," *IEICE Transactions on Fundamentals of Electronics, Communications and Computer Sciences*, p. 2022EAL2067, 2023.

[107] T. T. H. Nguyen, X. N. Tran, and T. H. H. Hoang, "Full-duplex relaying multi-user NOMA system under impacts of realistic conditions," *Journal of Science and Technique-Section on Information and Communication Technology*, vol. 11, no. 02, 2022.

[108] L. D. Le *et al.*, "Compensation of physical impairments in multi-carrier communications," Ph.D. dissertation, University of Saskatchewan, 2021.

[109] L. D. Le and H. H. Nguyen, "Compensation of phase noise and IQ imbalance in multi-carrier systems," *IEEE Access*, vol. 8, pp. 191 263–191 277, 2020.

[110] A. Bouhlel, , M. Alsmadi, E. Saleh, and S. Ikki, "Performance analysis of RIS-SSK in the presence of hardware impairments," in *2021 IEEE PIMRC Commun. Conf.*, 2021, pp. 1–6.

[111] E. Saleh, M. M. Alsmadi, A. Bouhlel, A. E. Canbilen, N. A. Ali, and S. Ikki, "Impact of channel correlation and hardware impairments on large intelligent surfaces-aided communication systems," in *2021 IEEE 32nd Annual International Symposium on Personal, Indoor and Mobile Radio Communications (PIMRC)*, 2021, pp. 805–810.

[112] S. Zhang, Q. Wu, S. Xu, and G. Y. Li, "Fundamental green tradeoffs: Progresses, challenges, and impacts on 5G networks," *IEEE Commun. Surveys Tutorials*, vol. 19, no. 1, pp. 33–56, 2017.

[113] Q. Wu, G. Y. Li, W. Chen, D. W. K. Ng, and R. Schober, "An overview of sustainable green 5G networks," *IEEE Wireless Commun.*, vol. 24, no. 4, pp. 72–80, 2017.

[114] Z. Zhang, X. Chai, K. Long, A. V. Vasilakos, and L. Hanzo, "Full duplex techniques for 5G networks: self-interference cancellation, protocol design, and relay selection," *IEEE Communications Magazine*, vol. 53, no. 5, pp. 128–137, 2015.

[115] A. M. M. Chandran, L. Wang, and M. Zawodniok, "Channel estimators for full-duplex communication using orthogonal pilot sequences," *IEEE Access*, vol. 8, pp. 117 706–117 713, 2020.

[116] F. Ghaseminajm, E. Saleh, M. Alsmadi, and S. S. Ikki, "Localization error bounds for 5G mmWave systems under hardware impairments," in *2021 IEEE 32nd Annual International Symposium on Personal, Indoor and Mobile Radio Communications (PIMRC)*, 2021, pp. 1228–1233.

[117] J. Zhao, M. Chen, M. Chen, Z. Yang, Y. Wang, B. Cao, and M. Shikh-Bahaei, "Energy efficient full-duplex communication systems with reconfigurable intelligent surface," in *2020 IEEE 92nd Vehicular Technology Conference (VTC2020-Fall)*, 2020, pp. 1–5.

[118] M. Duarte, C. Dick, and A. Sabharwal, "Experiment-driven characterization of full-duplex wireless systems," *IEEE Transactions on Wireless Communications*, vol. 11, no. 12, pp. 4296–4307, 2012.

[119] R. K. Mallik, "A new statistical model of the complex Nakagami-m fading gain," *IEEE Transactions on Communications*, vol. 58, no. 9, pp. 2611–2620, 2010.

[120] F. Louzada, P. L. Ramos, and D. Nascimento, "The inverse Nakagami-m distribution: A novel approach in reliability," *IEEE Transactions on Reliability*, vol. 67, no. 3, pp. 1030–1042, 2018.

[121] W. Dinkelbach, "On nonlinear fractional programming," *Management science*, vol. 13, no. 7, pp. 492–498, 1967.

[122] S. Boyd, S. P. Boyd, and L. Vandenberghe, *Convex optimization.* Cambridge university press, 2004.

[123] F. Tariq, M. R. A. Khandaker, K.-K. Wong, M. A. Imran, M. Bennis, and M. Debbah, "A speculative study on 6G," *IEEE Wireless Communications*, vol. 27, no. 4, pp. 118–125, 2020.

[124] Y. Li, M. Sheng, X. Wang, Y. Zhang, and J. Wen, "Max–min energy-efficient power allocation in interference-limited wireless networks," *IEEE Transactions on Vehicular Technology*, vol. 64, no. 9, pp. 4321–4326, 2015.

[125] S. Schaible, "Fractional programming. II, on dinkelbach's algorithm," *Management science*, vol. 22, no. 8, pp. 868–873, 1976.

[126] K. Shen and W. Yu, "Fractional programming for communication systems—part I: Power control and beamforming," *IEEE Transactions on Signal Processing*, vol. 66, no. 10, pp. 2616–2630, 2018.

[127] A. Zappone and E. Jorswieck, "Energy efficiency in wireless networks via fractional programming theory," *Foundations and Trends in Communications and Information Theory*, vol. 11, no. 3-4, pp. 185–396, 2015.

[128] L. Shi, Y. Ye, R. Q. Hu, and H. Zhang, "Energy efficiency maximization for SWIPT enabled two-way DF relaying," *IEEE Signal Processing Letters*, vol. 26, no. 5, pp. 755–759, Mar. 2019.

[129] E. Bjornson, P. Zetterberg, M. Bengtsson, and B. Ottersten, "Capacity limits and multiplexing gains of MIMO channels with transceiver impairments," *IEEE Communications Letters*, vol. 17, no. 1, pp. 91–94, 2012.

[130] E. Saleh, M. M. Alsmadi, and S. Ikki, "Spectral-energy efficiency and power allocation in full-duplex networks: the effects of hardware impairment and Nakagami-m fading channels," *IEEE Transactions on Vehicular Technology*, pp. 1–16, 2022.

[131] M. Medard, "The effect upon channel capacity in wireless communications of perfect and imperfect knowledge of the channel," *IEEE Transactions on Information Theory*, vol. 46, no. 3, pp. 933–946, 2000.

[132] F. Rusek, D. Persson, B. K. Lau, E. G. Larsson, T. L. Marzetta, O. Edfors, and F. Tufvesson, "Scaling up MIMO: Opportunities and challenges with very large arrays," *IEEE Signal Processing Magazine*, vol. 30, no. 1, pp. 40–60, 2013.

[133] K. Guo, C. Dong, and K. An, "NOMA-based cognitive satellite terrestrial relay network: Secrecy performance under channel estimation errors and hardware impairments," *IEEE Internet of Things Journal*, vol. 9, no. 18, pp. 17 334–17 347, 2022.

[134] E. Saleh, M. M. Alsmadi, and S. Ikki, "Spectral efficiency of full-duplex MIMO systems under the effects of hardware impairments," in *2022 IEEE 95th Vehicular Technology Conference: (VTC2022-Spring)*, 2022, pp. 1–7.

[135] T. Schenk, *RF imperfections in high-rate wireless systems: impact and digital compensation.* Springer Science & Business Media, 2008.

[136] P. Zetterberg, "Experimental investigation of TDD reciprocity-based zero-forcing transmit precoding," *EURASIP Journal on Advances in Signal Processing*, vol. 2011, pp. 1–10, 2011.

[137] M. Wenk, "MIMO-OFDM-testbed: challenges, implementations, and measurement results: challenges, implementations, and measurement results," Ph.D. dissertation, ETH Zurich, 2010.

[138] C. Studer, M. Wenk, and A. Burg, "MIMO transmission with residual transmit-RF impairments," in *2010 International ITG Workshop on Smart Antennas (WSA)*, 2010, pp. 189–196.

[139] A. C. Cirik, Y. Rong, and Y. Hua, "Achievable rates of full-duplex MIMO radios in fast fading channels with imperfect channel estimation," *IEEE Transactions on Signal Processing*, vol. 62, no. 15, pp. 3874–3886, 2014.

[140] N. Jindal, "MIMO broadcast channels with finite-rate feedback," *IEEE Transactions on information theory*, vol. 52, no. 11, pp. 5045–5060, 2006.

Appendix A

Proofs of Lemmas in Chapter 4

A.1 Proof of Lemma 4.3.1

Using Jensen's inequality, we can get the following bounds:

$$\mathbb{E}\left\{\log_2\left(1+\gamma_u\right)\right\} \geq \log_2\left(1+\left(\mathbb{E}\left\{\frac{1}{\gamma_u}\right\}\right)^{-1}\right). \tag{A.1}$$

Here, from (4.8), the term $\mathbb{E}\left\{\frac{1}{\gamma_u}\right\}$ can be calculated as

$$\mathbb{E}\left\{\frac{P_d}{P_u}\frac{\kappa_t^{\mathrm{BS}}}{\kappa^{\mathrm{u}}}\left|\frac{\mathbf{h}_u^{\mathrm{H}}\mathbf{H}_{\mathrm{SI}}\mathbf{h}_d}{\|\mathbf{h}_u\|^2\,\|\mathbf{h}_d\|}\right|^2 + \frac{\sigma_u^2}{\kappa_r^{\mathrm{BS}}\kappa^{\mathrm{u}}P_u\|\mathbf{h}_u\|^2}\right\} + \mathbb{E}\left\{\frac{\mathbf{h}_u^{\mathrm{H}}\mathbf{C}_{\boldsymbol{\eta}}\mathbf{h}_u}{\kappa_r^{\mathrm{BS}}\kappa^{\mathrm{u}}P_u\|\mathbf{h}_u\|^4}\right\}. \tag{A.2}$$

The first term can be calculated as

$$\mathbb{E}\left\{\frac{P_d}{P_u}\frac{\kappa_t^{\mathrm{BS}}}{\kappa^{\mathrm{u}}}\left|\frac{\mathbf{h}_u^{\mathrm{H}}\mathbf{H}_{\mathrm{SI}}\mathbf{h}_d}{\|\mathbf{h}_u\|^2\,\|\mathbf{h}_d\|}\right|^2\right\} + \frac{\sigma_u^2}{\kappa_r^{\mathrm{BS}}\kappa^{\mathrm{u}}P_u}\mathbb{E}\left\{\frac{1}{\|\mathbf{h}_u\|^2}\right\}$$

$$= \left(\frac{P_d}{P_u}\frac{\kappa_t^{\mathrm{BS}}}{\kappa^{\mathrm{u}}}\Omega_s + \frac{\sigma_u^2}{\kappa_r^{\mathrm{BS}}\kappa^{\mathrm{u}}P_u}\right)\frac{m_u}{(Mm_u-1)\Omega_u}, \tag{A.3}$$

where, $\mathbb{E}\left\{\frac{1}{\|\mathbf{h}_u\|^2}\right\} = \frac{m_u}{(Mm_u-1)\Omega_u}$, for $Mm_u \geq 2$. Because $\frac{1}{\|\mathbf{h}_u\|^2}$ follows inverse of sum of Gamma distribution.

The second term can be obtained by calculating

$$\mathbb{E}\left\{\frac{\mathbf{h}_u^{\mathrm{H}}\mathbf{C}_{\boldsymbol{\eta}}\mathbf{h}_u}{\|\mathbf{h}_u\|^4}\right\} = \mathbb{E}\left\{\frac{\mathbf{h}_u^{\mathrm{H}}\left(\left(1-\kappa_r^{\mathrm{BS}}\kappa^u\right)\mathbf{A} + (1-\kappa_r^{\mathrm{BS}}\kappa_t^{\mathrm{BS}})\mathbf{B}\right)\mathbf{h}_u}{\|\mathbf{h}_u\|^4}\right\}$$

$$= \mathbb{E}\left\{\frac{\left(1-\kappa_r^{\mathrm{BS}}\kappa^u\right)\mathbf{h}_u^{\mathrm{H}}\mathbf{A}\mathbf{h}_u}{\|\mathbf{h}_u\|^4} + \frac{(1-\kappa_r^{\mathrm{BS}}\kappa_t^{\mathrm{BS}})\mathbf{h}_u^{\mathrm{H}}\mathbf{B}\mathbf{h}_u}{\|\mathbf{h}_u\|^4}\right\}. \tag{A.4}$$

Here, $\mathbf{A}$ is correlated with $\|\mathbf{h}_u\|^4$ but $\mathbf{B}$ is independent of $\|\mathbf{h}_u\|^4$. Hence, (A.4) can be separated into two parts, where the first part can be calculated as

$$\mathbb{E}\left\{\frac{\left(1-\kappa_r^{\mathrm{BS}}\kappa^u\right)\mathbf{h}_u^{\mathrm{H}}\mathbf{A}\mathbf{h}_u}{\|\mathbf{h}_u\|^4}\right\} = \left(1-\kappa_r^{\mathrm{BS}}\kappa^u\right)P_u\,\mathbb{E}\left\{\frac{\sum_{l=1}^{\mathrm{M}}|h_u^{(l)}|^4}{\|\mathbf{h}_u\|^4}\right\}$$

$$= \frac{(m_u+1)\left(1-\kappa_r^{\mathrm{BS}}\kappa^u\right)P_u}{(Mm_u+1)}. \tag{A.5}$$

The second part can be calculated using the following equality

$$\mathbb{E}\left\{\frac{|h_u^{(l)}|^2}{\|\mathbf{h}_u\|^4}\right\} = \frac{m_u}{M(Mm_u-1)\Omega_u} \quad \forall l \in \{1,\cdots,M\}. \tag{A.6}$$

$$\mathbb{E}\left\{\frac{(1-\kappa_r^{\mathrm{BS}}\kappa_t^{\mathrm{BS}})\mathbf{h}_u^{\mathrm{H}}\mathbf{B}\mathbf{h}_u}{\|\mathbf{h}_u\|^4}\right\} = P_d\left(1-\kappa_r^{\mathrm{BS}}\kappa_t^{\mathrm{BS}}\right)\mathbb{E}\left\{\sum_{l=1}^{\mathrm{M}}\frac{|h_u^{(l)}|^2}{\|\mathbf{h}_u\|^4}\sum_{i=1}^{\mathrm{M}}\left|\mathbf{H}_{\mathrm{SI}}^{l,i}\frac{h_d^{(i)}}{\|\mathbf{h}_d\|}\right|^2\right\}$$

$$= P_d(1-\kappa_r^{\mathrm{BS}}\kappa_t^{\mathrm{BS}})\left(\frac{m_u\Omega_s}{(Mm_u-1)\Omega_u}\right). \tag{A.7}$$

By combining the two parts in (A.5) and (A.7) we obtain

$$\mathbb{E}\left\{\frac{\mathbf{h}_u^{\mathrm{H}}\mathbf{C}_{\boldsymbol{\eta}}\mathbf{h}_u}{\|\mathbf{h}_u\|^4}\right\} = \frac{(m_u+1)\left(1-\kappa_r^{\mathrm{BS}}\kappa^u\right)P_u}{(Mm_u+1)} + \frac{(1-\kappa_r^{\mathrm{BS}}\kappa_t^{\mathrm{BS}})P_dm_u\Omega_s}{(Mm_u-1)\Omega_u}. \tag{A.8}$$

Using (A.8), the second term can be given as

$$\mathbb{E}\left\{\frac{\mathbf{h}_u^{\mathrm{H}}\mathbf{C}_{\boldsymbol{\eta}}\mathbf{h}_u}{\kappa_r^{\mathrm{BS}}\kappa^u P_u\|\mathbf{h}_u\|^4}\right\} = \frac{\frac{\Omega_u(Mm_u-1)(m_u+1)\left(1-\kappa_r^{\mathrm{BS}}\kappa^u\right)P_u}{(Mm_u+1)} + (1-\kappa_r^{\mathrm{BS}}\kappa_t^{\mathrm{BS}})P_dm_u\Omega_s}{\kappa_r^{\mathrm{BS}}\kappa^u P_u(Mm_u-1)\Omega_u}. \tag{A.9}$$

Consequently, Combining (A.3) and (A.9) we obtain

$$\mathbb{E}\left\{\frac{1}{\gamma_u}\right\} = \frac{P_dm_u\Omega_s + m_u\sigma_u^2 + \frac{\Omega_u(Mm_u-1)(m_u+1)\left(1-\kappa_r^{\mathrm{BS}}\kappa^u\right)P_u}{(Mm_u+1)}}{\kappa_r^{\mathrm{BS}}\kappa^u P_u(Mm_u-1)\Omega_u}. \tag{A.10}$$

Substituting (A.10) in (A.1) ends up with the result in (4.9).

A.2 Proof of Lemma 4.3.2

Using Jensen's inequality, we can get the following bounds:

$$\mathbb{E}\left\{\log_2\left(1+\gamma_d\right)\right\} \geq \log_2\left(1+\left(\mathbb{E}\left\{\frac{1}{\gamma_d}\right\}\right)^{-1}\right). \tag{A.11}$$

Notice that h_I and $\mathbf{h}_d$ are independent. Then, from (4.14), the term $\mathbb{E}\left\{\frac{1}{\gamma_d}\right\}$ can be calculated as

$$\mathbb{E}\left\{\frac{1}{\gamma_d}\right\} = \mathbb{E}\left\{\frac{P_u\kappa^u|h_I|^2}{P_d\kappa_t^{\mathrm{BS}}} + \frac{\sigma_d^2}{P_d\kappa^d\kappa_t^{\mathrm{BS}}}\right\}\mathbb{E}\left\{\frac{1}{\|\mathbf{h}_d\|^2}\right\} + \mathbb{E}\left\{\frac{\sigma_{\eta_d^c}^2}{P_d\kappa^d\kappa_t^{\mathrm{BS}}\|\mathbf{h}_d\|^2}\right\}. \qquad (A.12)$$

The first term can be calculated as

$$\mathbb{E}\left\{\frac{P_u\kappa^u|h_I|^2}{P_d\kappa_t^{\mathrm{BS}}} + \frac{\sigma_d^2}{P_d\kappa^d\kappa_t^{\mathrm{BS}}}\right\}\mathbb{E}\left\{\frac{1}{\|\mathbf{h}_d\|^2}\right\} = \left(\frac{P_u\ \kappa^u\Omega_I}{P_d\kappa_t^{\mathrm{BS}}} + \frac{\sigma_d^2}{P_d\kappa^d\kappa_t^{\mathrm{BS}}}\right)\frac{m_d}{(Mm_d-1)\Omega_d}. \qquad (A.13)$$

The second term is given as

$$\mathbb{E}\left\{\frac{\sigma_{\eta_d^c}^2}{P_d\kappa^d\kappa_t^{\mathrm{BS}}\|\mathbf{h}_d\|^2}\right\} = \mathbb{E}\left\{\frac{P_u(1-\kappa^d\kappa^u)|h_I|^2 + P_d(1-\kappa^d\kappa_t^{\mathrm{BS}})\sum_{l=1}^M\frac{\left|h_d^{(l)}\right|^4}{\|\mathbf{h}_d\|^2}}{P_d\kappa^d\kappa_t^{\mathrm{BS}}\|\mathbf{h}_d\|^2}\right\}$$

$$= \frac{(1-\kappa^d\kappa^u)P_u m_d\Omega_I}{P_d\kappa^d\kappa_t^{\mathrm{BS}}(Mm_d-1)\Omega_d} + \frac{(m_d+1)(1-\kappa^d\kappa_t^{\mathrm{BS}})}{\kappa^d\kappa_t^{\mathrm{BS}}(Mm_d+1)}, \qquad (A.14)$$

where $\sum_{l=1}^M\mathbb{E}\left\{\frac{\left|h_d^{(l)}\right|^4}{\|\mathbf{h}_d\|^4}\right\} = \frac{m_d+1}{Mm_d+1}$. Because $\frac{\left|h_d^{(l)}\right|^2}{\|\mathbf{h}_d\|^2}$ follows Beta distribution. Now, combining (A.13) and (A.14) we get

$$\mathbb{E}\left\{\frac{1}{\gamma_d}\right\} = \frac{P_u m_d\Omega_I + m_d\sigma_d^2}{P_d\kappa^d\kappa_t^{\mathrm{BS}}(Mm_d-1)\Omega_d} + \frac{(m_d+1)(1-\kappa^d\kappa_t^{\mathrm{BS}})}{\kappa^d\kappa_t^{\mathrm{BS}}(Mm_d+1)}$$

$$= \frac{P_u m_d\Omega_I + m_d\sigma_d^2 + \frac{P_d(Mm_d-1)\Omega_d(m_d+1)(1-\kappa^d\kappa_t^{\mathrm{BS}})}{(Mm_d+1)}}{P_d\kappa^d\kappa_t^{\mathrm{BS}}(Mm_d-1)\Omega_d}. \qquad (A.15)$$

Substituting (A.15) in (A.11) ends up with the result in (4.16).

A.3   Proof of Lemma 4.4.1

Here, (4.33a) and (4.33b) are obtained from the fact that as P_d and P_u grow without bound, $\bar{\mathcal{R}}^d$ and $\bar{\mathcal{R}}^u$ are upper bounded as

$$\bar{\mathcal{R}}_d^{\max} \geq \log_2\left(1 + \frac{\kappa^d\kappa_t^{\mathrm{BS}}(Mm_d+1)}{\frac{m_d(Mm_d+1)\Omega_I}{(Mm_d-1)\Omega_d} + (m_d+1)(1-\kappa^d\kappa_t^{\mathrm{BS}})}\right). \qquad (A.16)$$

$$\bar{\mathcal{R}}_u^{\max} \geq \log_2\left(1 + \frac{\kappa_r^{\mathrm{BS}}\kappa^u(Mm_u+1)}{\frac{m_u(Mm_u+1)\Omega_s}{(Mm_u-1)\Omega_u} + (m_u+1)(1-\kappa_r^{\mathrm{BS}}\kappa^u)}\right). \qquad (A.17)$$

Since (A.16) and (A.17) are the maximum system achievable rates, then the required QoS should be less than them. Consequently,

$$\tilde{\mathcal{R}}_{\text{th}}^d \leq \log_2\left(1 + \frac{\kappa^d \kappa_t^{\text{BS}}(Mm_d + 1)}{\frac{m_d(Mm_d+1)\Omega_I}{(Mm_d-1)\Omega_d} + (m_d + 1)(1 - \kappa^d \kappa_t^{\text{BS}})}\right).$$

$$\tilde{\mathcal{R}}_{\text{th}}^u \leq \log_2\left(1 + \frac{\kappa_r^{\text{BS}} \kappa^{\text{u}}(Mm_u + 1)}{\frac{m_u(Mm_u+1)\Omega_s}{(Mm_u-1)\Omega_u} + (m_u + 1)\left(1 - \kappa_r^{\text{BS}} \kappa^{u}\right)}\right).$$

Furthermore, (4.33c) and (4.33d) are obtained from solving (4.29b) and (4.29c), as such

$$2^{\mathcal{R}_{\text{th}}^d} - 1 = \frac{P_d \kappa^d \kappa_t^{\text{BS}}(Mm_d - 1)\Omega_d}{P_u m_d \Omega_I + m_d \sigma_d^2 + \frac{P_d(Mm_d-1)(m_d+1)(1-\kappa^d \kappa_t^{\text{BS}})\Omega_d}{(Mm_d+1)}}. \tag{A.18}$$

$$2^{\mathcal{R}_{\text{th}}^u} - 1 = \frac{P_u \kappa^{\text{u}} \kappa_r^{\text{BS}}(Mm_u - 1)\Omega_u}{P_d m_u \Omega_s + m_u \sigma_u^2 + \frac{P_u(Mm_u-1)(m_u+1)(1-\kappa_r^{\text{BS}} \kappa^u)\Omega_u}{(Mm_u+1)}}. \tag{A.19}$$

After that, we obtained (4.33c) and (4.33d) by solving (A.18) and (A.19) for P_d and P_u. Where the solution can be given as

$$\tilde{P}_d^{\text{th}} = \frac{m_d \Omega_I \tilde{P}_u^{\text{th}} + m_d \sigma_d^2}{\Omega_d(Mm_d - 1)\left(\frac{\kappa^d \kappa_t^{\text{BS}}}{2^{\mathcal{R}_{\text{th}}^d}-1} - \frac{(m_d+1)(1-\kappa^d \kappa_t^{\text{BS}})}{(Mm_d+1)}\right)}, \tag{A.20}$$

$$\tilde{P}_u^{\text{th}} = \frac{m_u \sigma_u^2 \Omega_d(Mm_d - 1)Q + m_u m_d \sigma_d^2 \Omega_s}{(Mm_u - 1)(Mm_d - 1)\Omega_u \Omega_d QT - m_u m_d \Omega_I \Omega_s}, \tag{A.21}$$

where $Q = \frac{\kappa^d \kappa_t^{\text{BS}}}{2^{\mathcal{R}_{\text{th}}^d}-1} - \frac{(m_d+1)(1-\kappa^d \kappa_t^{\text{BS}})}{Mm_d+1}$ and $T = \frac{\kappa^u \kappa_r^{\text{BS}}}{2^{\mathcal{R}_{\text{th}}^u}-1} - \frac{(m_u+1)(1-\kappa^u \kappa_r^{\text{BS}})}{Mm_u+1}$, $\tilde{P}_d^{\text{th}}$ and $\tilde{P}_u^{\text{th}}$ are the power values that achieve the minimum required QoS.

Appendix B

Proofs of Lemmas in Chapter 5

B.1   Proof of Lemma 5.4.1

Using Jensen's inequality, we can get the following bounds

$$\mathbb{E}\left\{\log_2\left(1+\gamma\right)\right\} \geq \log_2\left(1+\left(\mathbb{E}\left\{\frac{1}{\gamma}\right\}\right)^{-1}\right). \tag{B.1}$$

Here, in the UL scenario and considering MRC/MRT linear combining/precoding, from (5.20), the term $\mathbb{E}\left\{\frac{1}{\gamma_{u,k}^{mrc}}\right\}$ can be calculated as

$$\mathbb{E}\left\{\frac{1}{\gamma_{u,k}^{mrc}}\right\} = \left(\mathbb{E}\left\{\sum_{i=1,i\neq k}^{K_u}\left|\frac{\hat{\mathbf{h}}_{u,k}^H\hat{\mathbf{h}}_{u,i}}{\|\hat{\mathbf{h}}_{u,k}\|}\right|^2\right\} + \frac{P_d}{K_d}\frac{\kappa_t^{\mathrm{BS}}}{\kappa^{\mathrm{u}}P_u}\mathbb{E}\left\{\sum_{j=1}^{K_d}\left|\frac{\hat{\mathbf{h}}_{u,k}^H\mathbf{H}_{\mathrm{SI}}\hat{\mathbf{h}}_{d,j}}{\|\hat{\mathbf{h}}_{u,k}\|\|\hat{\mathbf{h}}_{d,j}\|}\right|^2\right\}\right)\mathbb{E}\left\{\frac{1}{\|\hat{\mathbf{h}}_{\hat{u},k}\|^2}\right\}$$

$$+ \left(\sum_{i=1}^{K_u}\sigma_{e_{u,i}}^2 + \frac{\sigma_u^2}{\kappa_r^{\mathrm{BS}}\kappa^{\mathrm{u}}P_u}\right)\mathbb{E}\left\{\frac{1}{\|\hat{\mathbf{h}}_{\hat{u},k}\|^2}\right\} + \frac{1}{\kappa_r^{\mathrm{BS}}\kappa^{\mathrm{u}}P_u}\mathbb{E}\left\{\frac{\hat{\mathbf{h}}_{u,k}^H\mathbf{C}_{\boldsymbol{\eta}}\hat{\mathbf{h}}_{u,k}}{\|\hat{\mathbf{h}}_{u,k}\|^4}\right\}, \tag{B.2}$$

where $\mathbb{E}\left\{\frac{1}{\|\hat{\mathbf{h}}_{u,k}\|^2}\right\} = \frac{1}{(M-1)\sigma_{\hat{h}_{u,k}}^2}$ for $M \geq 2$ [4]. The first term can be calculated as

$$\mathbb{E}\left\{\sum_{i=1,i\neq k}^{K_u}\left|\frac{\hat{\mathbf{h}}_{u,k}^H\hat{\mathbf{h}}_{u,i}}{\|\hat{\mathbf{h}}_{u,k}\|}\right|^2\right\} = \sum_{i=1,i\neq k}^{K_u}\sigma_{\hat{h}_{u,i}}^2.$$

$$\frac{P_d}{K_d}\frac{\kappa_t^{\mathrm{BS}}}{\kappa^{\mathrm{u}}P_u}\mathbb{E}\left\{\sum_{j=1}^{K_d}\left|\frac{\hat{\mathbf{h}}_{u,k}^H\mathbf{H}_{\mathrm{SI}}\hat{\mathbf{h}}_{d,j}}{\|\hat{\mathbf{h}}_{u,k}\|\|\hat{\mathbf{h}}_{d,j}\|}\right|^2\right\} = \frac{\kappa_t^{\mathrm{BS}}P_d}{\kappa^{\mathrm{u}}P_u}\sigma_s^2. \tag{B.3}$$

Using the result in (B.3), the first term can be calculated as

$$\frac{1}{(M-1)\sigma_{\hat{h}_{u,k}}^2}\left[\sum_{i=1,i\neq k}^{K_u}\sigma_{\hat{h}_{u,i}}^2+\frac{\kappa_t^{\mathrm{BS}}P_d}{\kappa^{\mathrm{u}}P_u}\sigma_s^2+\sum_{i=1}^{K_u}\sigma_{e_{u,i}}^2+\frac{\sigma_u^2}{\kappa_r^{\mathrm{BS}}\kappa^{\mathrm{u}}P_u}\right]. \tag{B.4}$$

The second term can be obtained by calculating

$$\mathbb{E}\left\{\frac{\hat{\mathbf{h}}_{u,k}^H\mathbf{C}_{\boldsymbol{\eta}}\hat{\mathbf{h}}_{u,k}}{\|\hat{\mathbf{h}}_{u,k}\|^4}\right\}=\mathbb{E}\left\{\frac{\hat{\mathbf{h}}_{u,k}^{\mathrm{H}}\left(\left(1-\kappa_r^{\mathrm{BS}}\kappa^u\right)\mathbf{A}+(1-\kappa_r^{\mathrm{BS}}\kappa_t^{\mathrm{BS}})\mathbf{B}\right)\hat{\mathbf{h}}_{u,k}}{\|\hat{\mathbf{h}}_{u,k}\|^4}\right\}$$

$$=\mathbb{E}\left\{\frac{\left(1-\kappa_r^{\mathrm{BS}}\kappa^u\right)\hat{\mathbf{h}}_{u,k}^{\mathrm{H}}\mathbf{A}\hat{\mathbf{h}}_{u,k}}{\|\hat{\mathbf{h}}_{u,k}\|^4}+\frac{(1-\kappa_r^{\mathrm{BS}}\kappa_t^{\mathrm{BS}})\hat{\mathbf{h}}_{u,k}^{\mathrm{H}}\mathbf{B}\hat{\mathbf{h}}_{u,k}}{\|\hat{\mathbf{h}}_{u,k}\|^4}\right\}. \tag{B.5}$$

Here, $\mathbf{A}$ is correlated with $\|\hat{\mathbf{h}}_{u,k}\|^4$ but $\mathbf{B}$ is independent of $\|\hat{\mathbf{h}}_{u,k}\|^4$. Hence, (B.5) can be separated into two parts, where the first part can be expressed as

$$\mathbb{E}\left\{\frac{\left(1-\kappa_r^{\mathrm{BS}}\kappa^u\right)\hat{\mathbf{h}}_{u,k}^{\mathrm{H}}\mathbf{A}\hat{\mathbf{h}}_{u,k}}{\|\hat{\mathbf{h}}_{u,k}\|^4}\right\}$$

$$=\left(1-\kappa_r^{\mathrm{BS}}\kappa^u\right)P_u\sum_{i=1}^{K_u}\left(\mathbb{E}\left\{\frac{\sum_{l=1}^{\mathrm{M}}|\hat{h}_{u,k}^l|^2|\hat{h}_{u,i}^l|^2}{\|\hat{\mathbf{h}}_{u,k}\|^4}\right\}+\mathbb{E}\left\{\frac{\sum_{l=1}^{\mathrm{M}}|\hat{h}_{u,k}^l|^2|\hat{h}_{e,i}^l|^2}{\|\hat{\mathbf{h}}_{u,k}\|^4}\right\}\right)$$

$$=\left(1-\kappa_r^{\mathrm{BS}}\kappa^u\right)P_u\left(\frac{2}{M+1}+\sum_{i=1,i\neq k}^{K_u}\frac{\sigma_{\hat{h}_{u,i}}^2}{(M-1)\sigma_{\hat{h}_{u,k}}^2}+\sum_{i=1}^{K_u}\frac{\sigma_{e_{u,i}}^2}{(M-1)\sigma_{\hat{h}_{u,k}}^2}\right), \tag{B.6}$$

where $\sum_{l=1}^{\mathrm{M}}\left|\frac{\hat{h}_{u,k}^l}{\|\hat{\mathbf{h}}_{u,k}\|}\right|^4=\frac{2}{M+1}$ $\forall l\in\{1,\cdots,M\}$. The second part can be calculated using the following equality

$$\mathbb{E}\left\{\frac{|\hat{h}_{u,k}^l|^2}{\|\hat{\mathbf{h}}_{u,k}\|^4}\right\}=\frac{1}{M(M-1)\sigma_{\hat{h}_{u,k}}^2}\quad\forall l\in\{1,\cdots,M\}. \tag{B.7}$$

$$\mathbb{E}\left\{\frac{(1-\kappa_r^{\mathrm{BS}}\kappa_t^{\mathrm{BS}})\hat{\mathbf{h}}_{u,k}^{\mathrm{H}}\mathbf{B}\hat{\mathbf{h}}_{u,k}}{\|\hat{\mathbf{h}}_{u,k}\|^4}\right\}=\left(1-\kappa_r^{\mathrm{BS}}\kappa_t^{\mathrm{BS}}\right)\frac{P_d}{K_d}\sum_{j=1}^{K_d}\mathbb{E}\left\{\sum_{l=1}^{M}\frac{|\hat{h}_{u,k}^l|^2}{\|\hat{\mathbf{h}}_{u,k}\|^4}\sum_{i=1}^{M}\left|\mathbf{H}_{\mathrm{SI}}^{l,i}\frac{\hat{h}_{d,j}^i}{\|\hat{\mathbf{h}}_{d,j}\|}\right|^2\right\}$$

$$=(1-\kappa_r^{\mathrm{BS}}\kappa_t^{\mathrm{BS}})P_d\left(\frac{\sigma_s^2}{(M-1)\sigma_{\hat{h}_{u,k}}^2}\right). \tag{B.8}$$

By combining the two parts in (B.6) and (B.8), the second term can be given as

$$\mathbb{E}\left\{\frac{\hat{\mathbf{h}}_{u,k}^H\mathbf{C}_{\boldsymbol{\eta}}\hat{\mathbf{h}}_{u,k}}{\|\hat{\mathbf{h}}_{u,k}\|^4}\right\}=\left(1-\kappa_r^{\mathrm{BS}}\kappa^u\right)P_u\left(\frac{2}{M+1}+\sum_{i=1,i\neq k}^{K_u}\frac{\sigma_{\hat{h}_{u,i}}^2}{(M-1)\sigma_{\hat{h}_{u,k}}^2}+\sum_{i=1}^{K_u}\frac{\sigma_{e_{u,i}}^2}{(M-1)\sigma_{\hat{h}_{u,k}}^2}\right)$$

$$+\frac{(1-\kappa_r^{\mathrm{BS}}\kappa_t^{\mathrm{BS}})P_d\sigma_s^2}{(M-1)\sigma_{\hat{h}_{u,k}}^2}. \tag{B.9}$$

Now, combining (B.4), (B.9), and substituting them in (B.2), the average SINR can be calculated as

$$\mathbb{E}\left\{\frac{1}{\gamma_{u,k}^{mrc}}\right\} = \frac{2(1-\kappa_r^{\mathrm{BS}}\kappa^{\mathrm{u}})\frac{M-1}{M+1}\sigma_{\hat{h},k}^2 + \sum_{i=1,i\neq k}^{K_u}\beta_{u,i} + \frac{P_d\sigma_s^2+\sigma_u^2}{P_u} + \sigma_{e,k}^2}{\kappa_r^{\mathrm{BS}}\kappa^{\mathrm{u}}(M-1)\sigma_{\hat{h},k}^2} \tag{B.10}$$

Finally, substituting (B.10) in (5.21) ends up with the result in (5.22).

B.2   Proof of Lemma 5.4.2

Using Jensen's inequality in (B.1), we can get the SE lower bound in UL scenario under ZFR/ZFT linear precoding. Then, from (5.23), the term $\mathbb{E}\left\{\frac{1}{\gamma_{u,k}^{\mathrm{ZF}}}\right\}$ can be calculated as

$$\mathbb{E}\left\{\frac{1}{\gamma_{u,k}^{ZF}}\right\} = \frac{P_d}{K_d}\frac{\kappa_t^{\mathrm{BS}}}{\kappa^{\mathrm{u}}P_u}\sum_{j=1}^{K_d}\mathbb{E}\left\{\mathbf{w}_{u,k}^H\mathbf{H}_{\mathrm{SI}}\hat{\mathbf{f}}_{d,j}\hat{\mathbf{f}}_{d,j}^H\mathbf{H}_{\mathrm{SI}}^H\mathbf{w}_{u,k}\right\} + \frac{1}{\kappa_r^{\mathrm{BS}}\kappa^{\mathrm{u}}P_u}\mathbb{E}\left\{\mathbf{w}_{u,k}^H\mathbf{C}_{\boldsymbol{\eta}}\mathbf{w}_{u,k}\right\}$$
$$+ \left(\sum_{i=1}^{K_u}\sigma_{e_u,i}^2 + \frac{\sigma_u^2}{\kappa_r^{\mathrm{BS}}\kappa^{\mathrm{u}}P_u}\right)\mathbb{E}\left\{\|\mathbf{w}_{u,k}\|^2\right\}, \tag{B.11}$$

where $\mathbb{E}\left\{\|\mathbf{w}_{u,k}\|^2\right\} = \frac{1}{(M-K_u)\sigma_{\hat{h}_{u,k}}^2}$, for $M \geq K_u + 1$ [4]. The first term can be obtained by considering the fact that the combining $\mathbf{w}_{u,k}$, precoding $\hat{\mathbf{f}}_{d,j}$ vectors and the residual SI channels are independent [13], and by calculating the following expectation

$$\sum_{j=1}^{K_d}\mathbb{E}\left\{\mathbf{w}_{u,k}^H\mathbf{H}_{\mathrm{SI}}\hat{\mathbf{f}}_{d,j}\hat{\mathbf{f}}_{d,j}^H\mathbf{H}_{\mathrm{SI}}^H\mathbf{w}_{u,k}\right\} = \sigma_s^2 K_d\mathbb{E}\left\{\|\mathbf{w}_{u,k}\|^2\right\}. \tag{B.12}$$

Therefore, the first term can be given as

$$\frac{P_d\kappa_t^{\mathrm{BS}}}{P_u\kappa^{\mathrm{u}}K_d}\sum_{j=1}^{K_d}\mathbb{E}\left\{\mathbf{w}_{u,k}^H\mathbf{H}_{\mathrm{SI}}\hat{\mathbf{f}}_{d,j}\hat{\mathbf{f}}_{d,j}^H\mathbf{H}_{\mathrm{SI}}^H\mathbf{w}_{u,k}\right\} = \frac{P_d\kappa_t^{\mathrm{BS}}\sigma_s^2}{P_u\kappa^{\mathrm{u}}(M-K_u)\sigma_{\hat{h}_{u,k}}^2}. \tag{B.13}$$

The second term can be obtained by calculating the following expectation

$$\mathbb{E}\left\{\mathbf{w}_{u,k}^H\mathbf{C}_{\boldsymbol{\eta}}\mathbf{w}_{u,k}\right\} = \mathbb{E}\left\{\mathbf{w}_{u,k}^{\mathrm{H}}\left(\left(1-\kappa_r^{\mathrm{BS}}\kappa^u\right)\mathbf{A} + (1-\kappa_r^{\mathrm{BS}}\kappa_t^{\mathrm{BS}})\mathbf{B}\right)\mathbf{w}_{u,k}\right\}$$
$$= \left(1-\kappa_r^{\mathrm{BS}}\kappa^u\right)\mathbb{E}\left\{\mathbf{w}_{u,k}^{\mathrm{H}}\mathbf{A}\mathbf{w}_{u,k}\right\} + (1-\kappa_r^{\mathrm{BS}}\kappa_t^{\mathrm{BS}})\mathbb{E}\left\{\mathbf{w}_{u,k}^{\mathrm{H}}\mathbf{B}\mathbf{w}_{u,k}\right\}. \tag{B.14}$$

132

The first part can be calculated as

$$
\begin{aligned}
\left(1 - \kappa_r^{\mathrm{BS}} \kappa^u\right) \mathbb{E}\left\{\mathbf{w}_{u,k}^{\mathrm{H}} \mathbf{A} \mathbf{w}_{u,k}\right\} &= \left(1 - \kappa_r^{\mathrm{BS}} \kappa^u\right) P_u \sum_{i=1}^{K_u} \left(\mathbb{E}\left\{\sum_{l=1}^{M} |w_{u,k}^{(l)}|^2 |h_{u,i}^{(l)}|^2\right\}\right) \\
&\approx \left(1 - \kappa_r^{\mathrm{BS}} \kappa^u\right) P_u \sum_{i=1}^{K_u} \sum_{l=1}^{M} \mathbb{E}\left\{|w_{u,k}^{(l)}|^2\right\} \mathbb{E}\left\{|h_{u,i}^{(l)}|^2\right\} \\
&= \left(1 - \kappa_r^{\mathrm{BS}} \kappa^u\right) P_u \left(\sum_{i=1}^{K_u} \frac{\beta_{u,i}}{(M - K_u)\sigma_{\hat{h}_{u,k}}^2}\right), \quad \text{(B.15)}
\end{aligned}
$$

where $w_{u,k}^{(l)}$ is the lth element of $\mathbf{w}_{u,k}$. We used the approximation $\mathbb{E}\left\{|w_{u,k}^l|^2 |h_{u,i}^l|^2\right\} \approx \mathbb{E}\left\{|w_{u,k}^l|^2\right\} \mathbb{E}\left\{|h_{u,i}^l|^2\right\}$, because it is very difficult to find and it has a very small value compared to the other terms, rendering its effect negligible. We verified this by simulation, where Fig. 5.5b and 5.6b show that both the exact and the approximated match (the green curves) for both the perfect and imperfect CSI.

The second part can be calculated as

$$
\begin{aligned}
(1 - \kappa_r^{\mathrm{BS}} \kappa_t^{\mathrm{BS}}) \mathbb{E}\left\{\mathbf{w}_{u,k}^{\mathrm{H}} \mathbf{B} \mathbf{w}_{u,k}\right\} &= (1 - \kappa_r^{\mathrm{BS}} \kappa_t^{\mathrm{BS}}) \frac{P_d}{K_d} \sum_{j=1}^{K_d} \mathbb{E}\left\{\sum_{l=1}^{M} |w_{u,k}^{(l)}|^2 \sum_{i=1}^{M} \left|\mathbf{H}_{\mathrm{SI}}^{l,i} \hat{f}_{d,j}^{(i)}\right|^2\right\} \\
&= (1 - \kappa_r^{\mathrm{BS}} \kappa_t^{\mathrm{BS}}) P_d \left(\frac{\sigma_s^2}{(M - K_u)\sigma_{\hat{h}_{u,k}}^2}\right). \quad \text{(B.16)}
\end{aligned}
$$

By combining the two parts in (B.15) and (B.16), the second term can be given as

$$
\frac{\mathbb{E}\left\{\mathbf{w}_{u,k}^H \mathbf{C}_{\boldsymbol{\eta}} \mathbf{w}_{u,k}\right\}}{\kappa_r^{\mathrm{BS}} \kappa^{\mathrm{u}} P_u} = \frac{1}{(M - K_u)\sigma_{\hat{h}_{u,k}}^2} \left(\frac{\left(1 - \kappa_r^{\mathrm{BS}} \kappa^u\right)}{\kappa_r^{\mathrm{BS}} \kappa^{\mathrm{u}}} \sum_{i=1}^{K_u} \beta_{u,i} + \frac{(1 - \kappa_r^{\mathrm{BS}} \kappa_t^{\mathrm{BS}}) P_d}{\kappa_r^{\mathrm{BS}} \kappa^u P_u} \sigma_s^2\right). \quad \text{(B.17)}
$$

The third term can be given as

$$
\left(\sum_{i=1}^{K_u} \sigma_{e_{u,i}}^2 + \frac{\sigma_u^2}{\kappa_r^{\mathrm{BS}} \kappa^{\mathrm{u}} P_u}\right) \mathbb{E}\left\{\|\mathbf{w}_{u,k}\|^2\right\} = \left(\sum_{i=1}^{K_u} \sigma_{e_{u,i}}^2 + \frac{\sigma_u^2}{\kappa_r^{\mathrm{BS}} \kappa^{\mathrm{u}} P_u}\right) \frac{1}{(M - K_u)\sigma_{\hat{h}_{u,k}}^2}. \quad \text{(B.18)}
$$

Finally, combining (B.13), (B.17), (B.18), and substituting them into (B.11), the SINR can be calculated as

$$
\mathbb{E}\left\{\frac{1}{\gamma_{u,k}^{ZF}}\right\} = \frac{P_u(1 - \kappa_r^{\mathrm{BS}} \kappa^{\mathrm{u}}) \sum_{i=1}^{K_u} \beta_{u,i} + P_u \kappa_r^{\mathrm{BS}} \kappa^{\mathrm{u}} \sum_{i=1}^{K_u} \sigma_{e,i}^2 + P_d \sigma_s^2 + \sigma_u^2}{\kappa_r^{\mathrm{BS}} \kappa^{\mathrm{u}} P_u (M - K_u)\sigma_{\hat{h},k}^2}. \quad \text{(B.19)}
$$

Finally, using (B.19) ends up with the result in (5.24).

B.3 Proof of Lemma 5.5.1

Using Jensen's inequality in (B.1), we can get the SE lower bound in DL scenario under MRT linear precoding. Then, from (5.30), the term $\mathbb{E}\left\{\frac{1}{\gamma_{d,j}^{mrc}}\right\}$ can be calculated as

$$\mathbb{E}\left\{\frac{1}{\gamma_{d,j}^{mrc}}\right\} = \mathbb{E}\left\{\sum_{i=1,i\neq j}^{K_d}\left|\frac{\hat{\mathbf{h}}_{d,j}^H\,\hat{\mathbf{h}}_{d,i}}{\|\hat{\mathbf{h}}_{d,j}\|\,\|\hat{\mathbf{h}}_{d,i}\|}\right|^2\right\} + K_d\mathbb{E}\left\{\frac{P_u\kappa^u}{P_d\kappa_t^{\mathrm{BS}}}\sum_{k=1}^{K_u}|h_{I,jk}|^2 + \frac{\sigma_d^2}{P_d\kappa^d\kappa_t^{\mathrm{BS}}} + \sigma_{e_{d,j}}^2\right\}\times$$
$$\mathbb{E}\left\{\frac{1}{\|\hat{\mathbf{h}}_{d,j}\|^2}\right\} + \mathbb{E}\left\{\frac{K_d\sigma_{\eta_d^c}^2}{P_d\kappa^d\kappa_t^{\mathrm{BS}}\|\hat{\mathbf{h}}_{d,j}\|^2}\right\}. \tag{B.20}$$

The first term can be calculated by utilizing the fact that $\left|\frac{\hat{\mathbf{h}}_{d,j}^H\,\hat{\mathbf{h}}_{d,i}}{\|\hat{\mathbf{h}}_{d,j}\|\,\|\hat{\mathbf{h}}_{d,i}\|}\right|^2$ is beta-distributed with parameters 1 and $(M-1)$ [140], which implies that the expectation is $\frac{1}{M}$.

$$\mathbb{E}\left\{\sum_{i=1,i\neq j}^{K_d}\left|\frac{\hat{\mathbf{h}}_{d,j}^H\,\hat{\mathbf{h}}_{d,i}}{\|\hat{\mathbf{h}}_{d,j}\|\,\|\hat{\mathbf{h}}_{d,i}\|}\right|^2\right\} = \frac{K_d-1}{M}. \tag{B.21}$$

Notice that h_I and $\hat{\mathbf{h}}_{d,j}$ are independent. Therefore, the second term can be calculated as

$$K_d\mathbb{E}\left\{\frac{P_u\kappa^u\sum_{k=1}^{K_u}|h_{I,jk}|^2}{P_d\kappa_t^{\mathrm{BS}}} + \sigma_{e_{d,j}}^2 + \frac{\sigma_d^2}{P_d\kappa^d\kappa_t^{\mathrm{BS}}}\right\}\mathbb{E}\left\{\frac{1}{\|\hat{\mathbf{h}}_{d,j}\|^2}\right\} =$$
$$\left(\frac{P_u\,\kappa^u\sum_{k=1}^{K_u}\sigma_{I,jk}^2}{P_d\kappa_t^{\mathrm{BS}}} + \frac{\sigma_d^2}{P_d\kappa^d\kappa_t^{\mathrm{BS}}} + \sigma_{e_{d,j}}^2\right)\frac{K_d}{(M-1)\sigma_{\hat{h}_{d,j}}^2}. \tag{B.22}$$

The third term can be calculated as

$$\mathbb{E}\left\{\frac{K_d\sigma_{\eta_d^c}^2}{P_d\kappa^d\kappa_t^{\mathrm{BS}}\|\hat{\mathbf{h}}_{d,j}\|^2}\right\} = \frac{K_dP_u(1-\kappa^d\kappa^u)}{P_d\kappa^d\kappa_t^{\mathrm{BS}}}\mathbb{E}\left\{\frac{\sum_{k=1}^{K_u}|h_{I,jk}|^2}{\|\hat{\mathbf{h}}_{d,j}\|^2}\right\} + \frac{(1-\kappa^d\kappa_t^{\mathrm{BS}})}{\kappa^d\kappa_t^{\mathrm{BS}}}\mathbb{E}\left\{\sum_{l=1}^{\mathrm{M}}\frac{\left|\hat{h}_{d,j}^l\right|^4}{\|\hat{\mathbf{h}}_{d,j}\|^4}\right.$$
$$+\sum_{l=1}^{\mathrm{M}}\left|\frac{\hat{h}_{d,j}^l}{\|\hat{\mathbf{h}}_{d,j}\|}\right|^2\frac{|e_{d,j}^l|^2}{\|\hat{\mathbf{h}}_{d,j}\|^2} + \sum_{i=1,i\neq j}^{K_d}\sum_{l=1}^{\mathrm{M}}\left|\frac{\hat{h}_{d,i}^l}{\|\hat{\mathbf{h}}_{d,i}\|}\right|^2\frac{\left|\hat{h}_{d,j}^l\right|^2}{\|\hat{\mathbf{h}}_{d,j}\|^2} + \sum_{i=1,i\neq j}^{K_d}\sum_{l=1}^{\mathrm{M}}\left|\frac{\hat{h}_{d,i}^l}{\|\hat{\mathbf{h}}_{d,i}\|}\right|^2\frac{|e_{d,j}^l|^2}{\|\hat{\mathbf{h}}_{d,j}\|^2}\right\}.$$
$$= \frac{K_d(1-\kappa^d\kappa^u)P_u\sum_{k=1}^{K_u}\sigma_{I,jk}^2}{P_d\kappa^d\kappa_t^{\mathrm{BS}}(M-1)\sigma_{\hat{h}_{d,j}}^2} + \frac{2(1-\kappa^d\kappa_t^{\mathrm{BS}})}{\kappa^d\kappa_t^{\mathrm{BS}}(M+1)} + \frac{K_d(1-\kappa^d\kappa_t^{\mathrm{BS}})\sigma_{e_{d,j}}^2}{\kappa^d\kappa_t^{\mathrm{BS}}(M-1)\sigma_{\hat{h}_{d,j}}^2} + \frac{(1-\kappa^d\kappa_t^{\mathrm{BS}})(K_d-1)}{\kappa^d\kappa_t^{\mathrm{BS}}M},$$
$$\tag{B.23}$$

where $\sum_{l=1}^{\mathrm{M}}\left|\frac{\hat{h}_{d,j}^l}{\|\hat{\mathbf{h}}_{d,j}\|}\right|^4 = \frac{2}{M+1}$, and $\mathbb{E}\left\{\frac{|\hat{h}_{d,j}^l|^2}{\|\hat{\mathbf{h}}_{d,j}\|^4}\right\} = \frac{1}{M(M-1)\sigma_{\hat{h}_{d,j}}^2}$. $\forall l \in \{1,\cdots,M\}$. Now, combining (B.21), (B.22), (B.23), and substituting them in (B.20), the average SINR can

be calculated as

$$\mathbb{E}\left\{\frac{1}{\gamma_d^{mrc}}\right\} =$$

$$\frac{P_d(K_d-1)\frac{M-1}{M}\sigma_{\hat{h},j}^2 + 2P_d(1-\kappa^d\kappa_t^{\mathrm{BS}})\left(\frac{M-1}{M+1}\right)\sigma_{\hat{h},j}^2 + K_d\left(P_u\sum_{k=1}^{K_u}\sigma_{I,jk}^2 + P_d\sigma_{e,j}^2 + \sigma_d^2\right)}{\kappa^d\kappa_t^{\mathrm{BS}}P_d(M-1)\sigma_{\hat{h},j}^2}.$$

$$(B.24)$$

Finally, substituting (B.24) in (5.31) ends up with the result in (5.32).

B.4   Proof of Lemma 5.5.2

Using Jensen's inequality in (B.1), we can get the SE lower bound in the DL scenario under ZFT linear precoding. Then, from (5.33), the term $\mathbb{E}\left\{\frac{1}{\gamma_{d,j}^{ZF}}\right\}$ can be calculated as

$$\mathbb{E}\left\{\frac{1}{\gamma_{d,j}^{ZF}}\right\} = K_d\mathbb{E}\left\{\frac{P_u\kappa^u}{P_d\kappa_t^{\mathrm{BS}}}\sum_{k=1}^{K_u}|h_{I,jk}|^2 + \frac{\sigma_d^2}{P_d\kappa^d\kappa_t^{\mathrm{BS}}} + \sigma_{e,d,j}^2\right\}\mathbb{E}\left\{\|\mathbf{a}_{d,j}\|^2\right\} + \mathbb{E}\left\{\frac{K_d\mathbf{a}_{d,j}^H\sigma_{\eta_d^c}^2\mathbf{a}_{d,j}}{P_d\kappa^d\kappa_t^{\mathrm{BS}}}\right\}.$$

$$(B.25)$$

By noting that $\hat{\mathbf{f}}_{d,j} = \frac{\mathbf{a}_{d,j}}{\|\mathbf{a}_{d,j}\|}$ is the normalized j^{th} column of $\mathbf{A} = \hat{\mathbf{G}}_d\left(\hat{\mathbf{G}}_d^H\hat{\mathbf{G}}_d\right)^{-1}$ and $\hat{\mathbf{h}}_{d,j}^H\mathbf{a}_{d,j} = 1$ and $\hat{\mathbf{h}}_{d,j}^H\mathbf{a}_{d,i} = 0 \ \ \forall j \neq i$. Utilizing the fact that $\mathbb{E}\left\{\|\mathbf{a}_{d,j}\|^2\right\} = \frac{1}{(M-K_d)\sigma_{\hat{h}_{d,j}}^2}$ and $h_{I,jk}$ and $\mathbf{a}_{d,j}$ are independent. The first term can be given as

$$K_d\mathbb{E}\left\{\frac{P_u\kappa^u}{P_d\kappa_t^{\mathrm{BS}}}\sum_{k=1}^{K_u}|h_{I,jk}|^2 + \frac{\sigma_d^2}{P_d\kappa^d\kappa_t^{\mathrm{BS}}} + \sigma_{e,d,j}^2\right\}\mathbb{E}\left\{\|\mathbf{a}_{d,j}\|^2\right\} =$$

$$\left(\frac{P_u\kappa^u}{P_d\kappa_t^{\mathrm{BS}}}\sum_{k=1}^{K_u}\sigma_{I,jk}^2 + \frac{\sigma_d^2}{P_d\kappa^d\kappa_t^{\mathrm{BS}}} + \sigma_{e,d,j}^2\right)\frac{K_d}{(M-K_d)\sigma_{\hat{h}_{d,j}}^2}. \qquad (B.26)$$

The second term can be calculated as

$$\mathbb{E}\left\{\frac{K_d\sigma_{\eta_d^c}^2\|\mathbf{a}_{d,j}\|^2}{P_d\kappa^d\kappa_t^{\mathrm{BS}}}\right\} = \frac{K_dP_u(1-\kappa^d\kappa^u)}{P_d\kappa^d\kappa_t^{\mathrm{BS}}}\mathbb{E}\left\{\sum_{k=1}^{K_u}|h_{I,jk}|^2\right\}\mathbb{E}\left\{\|\mathbf{a}_{d,j}\|^2\right\} + \frac{(1-\kappa^d\kappa_t^{\mathrm{BS}})}{\kappa^d\kappa_t^{\mathrm{BS}}}\times$$

$$\mathbb{E}\left\{\sum_{l=1}^{M}\left|h_{d,j}^{(l)}\right|^2\left|a_{d,j}^{(l)}\right|^2 + \sum_{i=1,i\neq j}^{K_d}\sum_{l=1}^{M}\frac{\left|a_{d,i}^{(l)}\right|^2}{\|a_{d,i}\|^2}\left|h_{d,j}^{(l)}\right|^2\|a_{d,j}\|^2\right\}$$

$$\approx \frac{K_d(1-\kappa^d\kappa^u)P_u\sum_{k=1}^{K_u}\sigma_{I,jk}^2}{P_d\kappa^d\kappa_t^{\mathrm{BS}}(M-K_d)\sigma_{\hat{h}_{d,j}}^2} + \frac{(1-\kappa^d\kappa_t^{\mathrm{BS}})\beta_{d,j}}{\kappa^d\kappa_t^{\mathrm{BS}}(M-K_d)\sigma_{\hat{h}_{d,j}}^2} + \frac{(1-\kappa^d\kappa_t^{\mathrm{BS}})\beta_{d,j}}{\kappa^d\kappa_t^{\mathrm{BS}}(M-K_d)}\sum_{i=1,i\neq j}^{K_d}\frac{1}{\sigma_{\hat{h}_{d,i}}^2},$$

$$(B.27)$$

where the second and third terms of (B.27) are obtained assuming that $h_{d,i}^{(l)}$ and $h_{d,j}^{(l)}$ are independent $\forall i, j \in [1, \cdots, K_d]$ and $\forall l \in [1, \cdots, M]$, and $\mathbb{E}\left\{\frac{\|a_{d,j}\|^2}{\|a_{d,i}\|^2}\right\} \to 1$. We verified this by simulation, where Fig. 5.5b and 5.6b show that both the exact and the approximated are matched (the red curves) for both perfect and imperfect CSI.

Now, after combining (B.26), (B.27), doing some mathematical manipulations, and substituting them into (B.25), the average SNIR can be given as

$$
\mathbb{E}\left\{\frac{1}{\gamma_{d,j}^{ZF}}\right\} =
$$

$$
\frac{(P_d/K_d)(1 - \kappa^d \kappa_t^{\mathrm{BS}})\beta_{d,j}\sigma_{\hat{h},j}^2 \sum_{i=1}^{K_d}\frac{1}{\sigma_{\hat{h},i}^2} + (P_d/K_d)\kappa_t^{\mathrm{BS}}\kappa^d \sum_{i=1}^{K_d}\sigma_{e,i}^2 + P_u \sum_{i=1}^{K_u}\sigma_{I,jk}^2 + \sigma_d^2}{(P_d/K_d)\kappa_t^{\mathrm{BS}}\kappa^{\mathrm{d}}(M - K_d)\sigma_{\hat{h},j}^2}.
$$

$$
\text{(B.28)}
$$

Finally, using (B.28) results in (5.34).